DURBAN UNIVERSITY OF TECHNOLOGY
INYUVESI YASETHEKWINI YEZOBUCHWEPHESHE

APPLICATION OF SYNTHESIZED MAGNETIC NANOPARTICLES FOR BIOGAS PRODUCTION USING ANAEROBIC DIGESTION

Submitted in fulfilment of the requirements for the degree of:

Master of Engineering in the Department of Chemical Engineering,

Faculty of Engineering
and the Built Environment

at Durban University of Technology

By

Gloria Amo-Duodu (22064692)

Date: July 2022

Supervisor: Prof S. Rathilal

Co-supervisor: Dr. M. N. Chollom

Preface

This research is a collaborative study under Durban University of Technology, Department of Chemical Engineering and Water Research Commission (WRC), under Prof. Sudesh Rathilal and Dr. Martha Noro Chollom supervision. All the analysis which includes the feed characterisation, experimental study and analysis of results obtained were carried out in the Chemical Engineering Department, Faculty of Engineering and the Built Environment, DUT.

Declaration

Gloria Amo-Duodu the undersigned candidate declares that

I. The research reported in this dissertation, except where otherwise indicated, is my original work.

II. This dissertation has not been submitted for any degree or examination at any other university.

III. This dissertation does not contain other persons' data, pictures, graphs or other information, unless specifically acknowledged as being sourced from other persons.

IV. This dissertation does not contain other persons' writing, unless specifically acknowledged as being sourced from other researchers. Where other written sources have been quoted, then:

a) their words have been re-written, but the general information attributed to them has been referenced;

b) where their exact words have been used, their writing has been placed inside quotation marks, and referenced.

V. Where I have reproduced a publication of which I am an author, co-author or editor, I have indicated in detail which part of the publication was actually written by myself alone and have fully referenced such publications.

VI. This dissertation does not contain text, graphics or tables copied and pasted from the Internet, unless specifically acknowledged, and the source being detailed in the dissertation and in the References sections.

Signature: …… Date: 19 - 04 - 2023 ……..

Prof S. Rathilal

Signatur Date: 20 April 2023 ……..

Dr. M. N. Chollom

Signature: Date: 20/04/2023 ……..

Acknowledgements

My gratitude is directed first and foremost to God, for His grace, guidance, providence, and mercy. I am very grateful to the Lord, for providence throughout the journey.

I would like to also express my profound gratitude to my supervisor, Prof. Sudesh Rathilal for his guidance, supports, advice, encouragement, opportunities and all the time he spent to attend to my needs throughout my research studies. His impact has been great, and it had been a great time working with him. I am also grateful to my co-supervisor, Dr. Martha Noro Chollom for her support and guidance during my work.

A special thanks to my brothers from Ghana, Dr. Edward Kwaku Armah, Mr. Elorm Obotey Ezugbe, Mr. Samuel Ofori Frimpong and Dr. Dennis Isaac Amoah for their support, guidance, prayer, and undying love they shown me throughout this period and for always having my back during tough times. I also thank my sisters I met here, Miss. Eugaria Argin (Akua), Miss Nomthandozo Sibiya, Miss Izzi Aigbokhaebho, and Mahle (Mrs. Amoah) for their love, prayers and always helping me through tough times, I am most grateful to them for their support.

I thank Water Research Commission (WRC), Durban University Scholarship Scheme and National Research Funding (NRF) for their financial support.

To the members of the Green Engineering Research Group (GERP), especially Dr. Emmanuel Kweinor Tetteh, I am much grateful for your numerable and valuable contributions to my research.

I say thank you to the technician of the Chemical Engineering Department especially, Mr. Vishnu Krbagaran Moodley, Mr. Mohamed Jaafar Bux and Ms. Seshna Sewsanker, for their assistance and support during my experimental work. I am grateful to you all for your contributions. Again, I am grateful to the postgraduates of Chemical Engineering and entire the department of Chemical Engineering, for creating a serene and conducive environment for me to carry out my research. I especially thank Mr. Jeremiah Adjejeji, Mr. Donald, Dr. Anniette and Dr. Omolara Afolabi Felicia.

Last but not least, I would like to say a very big thank you to the entire Amo-Duodu family for their love, financial support, and prayers, thank you to Bernard Twum Agyeman, Valerie Okoffo Asante, Loretta Oduro, Wasilatu Dometi, Mad. Alice Yaa Asor, Prof. N. Y. Asiedu, Dr. Rockson, Mad. Emmanuella Kwao-Boateng and Mad. Enyonam L. Kpikpitse.

Finally, to the support and efforts of all those whose names were not listed, I greatly appreciated you all. God's blessings be upon you all.

Dedication

I dedicate this dissertation to my parents, Mr. Samuel Amo Duodu, and Mad. Linda Afia Oduraa (Mrs. Amo Duodu), my sisters, Harriet Amo-Duodu (Mrs. Adu-Christain), Florence Amo-Duodu (Mrs. Ofori Korangye), Alice Amo-Duodu (Mrs. Owusu Abrokwa) and my late brother, Mr. Samuel Amo Duodu Jnr. You gave everything to see me get this far and realise this dream.

And to all women out there looking for a sign not to give up, if this thesis finds you remember someone like me never gave up and made it, so can you.

Abstract

South Africa is encountering severe challenges in the areas of energy, water, and wastewater management in recent times. This study addresses both water and energy aspects. It aims at using synthesised magnetic nanoparticles (MNPs) on anaerobic digestion (AD) for biogas production from various wastewater sources in South Africa. The study experimented the feasibility of five different synthesized magnetic nanoparticles, magnetite (Fe_3O_4), copper ferrite ($CuFe_2O_4$), nickel ferrite ($NiFe_2O_4$), magnesium ferrite ($MgFe_2O_4$) and aluminium ferrite ($AlFe_2O_4$) on two different wastewater samples (industrial and municipal wastewater) from three sampling sources, Umbilo water works, Umgeni water and a sugar refinery industry.

Five research objectives were accessed. The first objective was the synthesis and characterisation of MNPs using scanning electron microscopy/energy dispersive x-ray (SEM/EDX), Brunauer-Emmett-Teller (BET), Fourier transform infrared spectroscopy (FTIR) and X-ray diffraction (XRD) analysis. The results showed a surface morphology of face-centred and monoclinic crystal structures with a size less than 20 nm. The nanostructures of ferrimagnetite and magnetite were obtained, and it had an O-H stretching and Fe-O vibration functional groups. The surface area obtained was found to be high for magnetite (Fe_3O_4) which was 27.597 m^2/g.

The second objective was to evaluate the AD performance in terms of water quality and biogas production. This was carried out in two stages. The first was to evaluate the five MNPs with sugar refining wastewater. The second stage was to evaluate the performance of three best performing MNPs on two wastewater samples from Umbilo wastewater. The results for the first stage showed good degradation of organic matter for the bioreactors with MNPs which resulted in a higher yield of biogas and methane as compared to the control as well as good removal of contaminant (chemical oxygen demand (COD), colour and turbidity). Among the five MNPs used, Fe_3O_4, $NiFe_2O_4$ and $CuFe_2O_4$ had a contaminant removal efficiency of 60-70% and a cumulative biogas yield of more than 140 ml/day with more than 85% methane composition, hence these three MNPs were found to be the best performed MNPs. The results obtained from the second stage for the three best performed MNPs indicated a high pollutant removal efficiency of more than 70% for Fe_3O_4, as well as a biogas yield of more than 1100 ml/day and a methane composition of approximately 98%.

The third objective was the evaluation and optimisation of the anaerobic magnetised system for biogas production while the fourth objective involved a comparative study between the

performances of magnetised biochemical methane potential (BMP) to non-magnetised biochemical methane potential. From the optimisation study, the predicted results obtained from the BBD-RSM showed an average contaminant removal of 70% and a biogas yield of 522 ml/day at an optimum MNP load of 0.5 g, retention time of 45 days, inoculum load of 500 ml, and a temperature of 35℃ with a desirability of 96% as the optimum conditions. With less than 2% deviation, the confirmatory test demonstrated equal performance at the optimum conditions.

Findings from the fourth objective indicated that the BMP system with MF exposure exhibited a contaminant removal rate of over 80% and a biogas generation of 1715 ml/day with a 99.94% methane composition. Overall, the system that included both MF and MNP performed better than the other in terms of biogas yield and colour removal. The final objective was the kinetic study of the anaerobic magnetised system using modified Gompertz and first-order kinetic models. The results obtained from the kinetics showed that the modified Gompertz model described the kinetics and dynamics of the anaerobic magnetised system better than the first-order kinetic model with a correlation co-efficient (R^2) over 0.9999 and an error less than 0.0002.

Therefore, the possibility of using MNPs, particularly magnetite (Fe_3O_4), in an AD system for biogas production from wastewater was found to be extremely feasible and without negative environmental consequences. Incorporating both MF and MNP in AD was also beneficial for wastewater treatment because it eliminated the need for post-treatment

Research outputs

Conferences

- ✓ **Amo-Duodu, G.,** Rathilal, S., Chollom, M.N., Mbuyu, M. and Tetteh, E.K., 2020, Biogas Enhancement from Wastewater-Comparing Fe/Cu Nanoparticles Additives. 18th Johannesburg Int'l Conference on Science, Engineering, Technology & Waste Management (SETWM-20) Nov. 16-17, 2020, Johannesburg (SA).
- ✓ **Amo-Duodu, G.,** Rathilal, S., Chollom, M.N. and Tetteh, E.K., 2020, Biogas Enhancement Using Metallic Nanoparticles, 5th Interdisciplinary Research and Innovation Conference 2020, Research and Postgraduate Support Directorate of Durban University of Technology, 16-17 September 2020, Virtual, Durban-SA.
- ✓ **Amo-Duodu, G.,** Rathilal, S., Chollom, M.N. and Kweinor Tetteh, E. 2021. Effects of synthesised AlFe2O4 and MgFe2O4 nanoparticles on biogas production from anaerobic digested sugar refinery wastewater. International Conference on Advances in Sustainable Research for Energy and Environmental Management (ASREEM-2021). 6-8 August 2021. Virtual, Gujarat, India.
- ✓ G **Amo-Duodu,** S Rathilal, M.N. Chollom, EK Tetteh, 2021 Evaluating synthesized magnetic nanoparticles: characterisation and biogas assessment, 7th Southern African Sustainable Energy Conference (SASEC-2021) 17-19 November 2021, Stellenbosch-SA.
- ✓ **G. Amo-Duodu**, E. K. Tetteh, S. Rathilal and M. N. Chollom, 2021 Assessment of magnetic nanomaterials for municipality wastewater treatment via biochemical methane potential (BMP) test, International Conference on Sustainable Development. 7-9 December 2021, Durban-SA.
- ✓ **G. Amo-Duodu**, K. S. Buthelezi, S. Rathilal, T. P. Mahlangu and M. N. Chollom, 2021 Biostimulation of anaerobic digested wastewater using magnetic nanoparticles and an external magnetic field for biogas enhancement, 1st Sustainable Bioenergy and Processes Conference. 13-15 December 2021, Cape Town-SA
- ✓ **Amo-Duodu, G.,** Buthelezi, K. S., Rathilal, S., Mahlangu, T. P., Chollom, N. M., and Tetteh, E.K., 2022, Evaluation of the biostimulation aftereffect of magnetic field and magnetic nanoparticles on biogas production from anaerobic digested wastewater. 33rd JOHANNESBURG Int'l Conference on 'Chemical, Biological and Environmental Engineering (JCBEE-22) March. 17-18, 2022, Johannesburg-SA.

Conferences Proceedings

- ✓ **Amo-Duodu, G.,** Rathilal, S., Chollom, M.N., Mbuyu, M. and Tetteh, E.K., 2020, Biogas Enhancement from Wastewater-Comparing Fe/Cu Nanoparticles Additives. 18th JOHANNESBURG Int'l Conference on Science, Engineering, Technology & Waste Management (SETWM-20) Nov. 16-17, 2020, Johannesburg (SA), http://www.eares.org/siteadmin/upload/2717EAP1120266.pdf
- ✓ **G Amo-Duodu**, S Rathilal, MN Chollom, EK Tetteh, 2021 Evaluating synthesized magnetic nanoparticles: characterization and biogas assessment, 7th Southern African Sustainable Energy Conference (SASEC-2021) 17-19 November 2021, Stellenbosch-SA, https://sasec.org.za/documents/SASEC_2021_Conference_Proceedings.pdf
- ✓ E Kweinor Tetteh, **G Amo-Duodu** and S Rathilal, 2021 Synergistic effect of functionalised Zn-FeTiO2 and Cu-ZnFeTiO2 on biostimulated methanation process, 7th Southern African Sustainable Energy Conference (SASEC-2021) 17-19 November 2021,Stellenbosch-SAs
  https://sasec.org.za/documents/SASEC_2021_Conference_Proceedings.pdf

Publications

- ✓ **Amo-Duodu, G.,** Rathilal, S., Chollom, M.N and Tetteh, E.K. (2021)'Application of metallic nanoparticles for biogas enhancement using the biomethane potential.' Scientific African, 12, e00728: http://dx.doi.org/10.1016/j.sciaf.2021.e00728.
- ✓ Tetteh, E.K**., Amo-Duodu, G.** and Rathilal, S. (2021) 'Synergistic effect of magnetic nanomaterials on post-digestate for biogas production.' Molecules, 26 (21), 6434: http://doi.org/10.3390/molecules26216434
- ✓ **Amo-Duodu, G.,** Tetteh, E.K., Rathilal, S., Armah, E.K., Adedeji, J. and Chetty, M. (2021) 'Effect of engineered materials and magnetite on wastewater treatment: biogas and kinetics evaluations', Polymers, 13 (24), 4323. https://doi.org/10.3390/polym13244323
- ✓ **Amo-Duodu, G.,** Tetteh, E.K., Rathilal, S. and Chollom M. N. (2022) 'Synthesis and characterization of magnetic nanoparticles: biocatalytic effects on wastewater treatment', Materials Today: Proceedings, 62, S79 – S84 : https://doi.org/10.1016/j.matpr.2022.02.091

- ✓ **G. Amo-Duodu**, K. S. Buthelezi, S. Rathilal, T. P. Mahlangu, M. N. Chollom, and Tetteh, E.K, 2022 Biostimulation of anaerobic digested wastewater using magnetic nanoparticles and an external magnetic field for biogas enhancement, Biofuel bioproducts and biorefining, https://doi.org/10.1002/bbb.2409
- ✓ **G. Amo-Duodu**, E. K. Tetteh, S. Rathilal and M. N. Chollom, 2022 Assessment of magnetic nanomaterials for municipality wastewater treatment via biochemical methane potential *(BMP) test*, int. J. Environ. Res. Public Health (IJERPH) *19*(16), 9805; https://doi.org/10.3390/ijerph19169805
- ✓ **Amo-Duodu, G.,** Buthelezi, K. S., Rathilal, S., Mahlangu, T. P., Chollom, N. M., and Tetteh, E.K., 2022, Evaluation of biostimulation on biogas production of anaerobic digested wastewater due to magnetic field and magnetic nanoparticles, Journal of Pharmaceutical Negative Results 13(09) https://doi.org/10.47750/pnr.2022.13.S09.430.
- ✓ Adedeji, J., Tetteh, E.K., **Amo-Duodu, G.,** Armah, E.K., Rathilal, S., and Chetty, M., 2022, Central Composite Design Optimisation of Banana Peels/Magnetite for Anaerobic Biogas Production from Wastewater, Applied Sciences 12(23), 12037, https://doi.org/10.3390/app122312037
- ✓ **Amo-Duodu, G.,** Sibiya, N. P., E. K. Tetteh, S. Rathilal and M. N. Chollom, 2022 Comparison of Response Surface Methodology and Artificial Neural Network to Optimize and Predict Biogas Production from Magnetite-Enhanced Anaerobic Digested Municipal Wastewater, Renewable Energy **(RENE-D-23-01612_Under review).**
- ✓ **G. Amo-Duodu**, E. K. Tetteh, Sibiya, N. P., S. Rathilal and M. N. Chollom, 2022 Synthesis and characterisation of magnetic nanoparticles via co-precipitation: Application and assessment in anaerobic digested wastewater, Biofuels, Bioprod. Bioref. **(BIOFPR-23-0029_Under review).**

Table of contents

List of figures

List of tables

Nomenclature

AD	Anaerobic Digestion
APHA	American Public Health Association
BBD	Box-Behnken Design
BET	Brunauer-Emmett-Teller
BMP	Biochemical Methane Potential
BOD	Biological Oxygen Demand
CCD	Central Composite Design
COD	Chemical Oxygen Demand
CECs	Contaminants of Emerging Concerns
DoE	Design of Experiment
DW	Domestic Wastewater
DWA	Department of Water Affairs
ECs	Emerging Contaminants
EPA	Environmental protection agency
FTIR	Fourier-Transform Infrared Spectroscopy
HRT	Hydraulic Retention Time
MW	Municipal Wastewater
MNPs	Magnetic Nanoparticles
ML	Mega Litre
OFAT	One-Factor-At-a-Time
PCPs	Personal Care Products
RSM	Response Surface Methodology
SANS	Southern African National Standards

SEM/EDX	Scanning Electron Microscopy Coupled with Energy-Dispersive X-ray Spectroscopy
SRW	Sugar Refinery Wastewater
TOCs	Total Organic Compounds
TS	Total Solids
VFAs	Volatile Fatty Acids
VOCs	Volatile Organic Compounds
VS	Volatile Solids
WAS	Waste Activated Sludge
WWTPs	Wastewater Treatment Plants
XRD	X-ray Diffraction Analysis

Chapter One

INTRODUCTION

1.1 Background

The increase in population growth and industrialisation over the years has been the cause of the degradation of the ecosystems that living things rely on. This increase in population has also resulted in a drastic rise in pollution which is caused by human activities (Chan *et al.* 2009; Chen and Lee 2014b; K'Oreje *et al.* 2020). The pollution is from some of these pollutants; emerging contaminants (ECs) such as volatile organic compounds (VOCs), pharmaceutical products, chemical waste, domestic wastes, pesticides, herbicides, food processing waste, etc. When wastewater is improperly handled and released into the environment, it poses a significant threat to the ecosystem (Feng *et al.* 2014). Discharge of such wastes continuously has impacted negatively on the aquatic environment which has led to health-related risks to living organisms (aus der Beek *et al.* 2016; K'Oreje *et al.* 2020). Research has also shown that excessive and continuous exposure of humans to these contaminants and pollutants causes a lot of health implications such as cancer and cognitive effects worldwide (K'Oreje *et al.* 2020).

Because of this, several methods have been employed to treat wastewater before discharge. Wastewater treatment is the process of removing impurities from wastewater before it is discharged directly into the ecosystem or reused (Mitchell *et al.* 2014; Liu *et al.* 2021). Treatment methods used over the years include chlorination, desalination, coagulation, anaerobic and aerobic digestion, advanced oxidation processes, and flocculation. Among these treatment interventions, anaerobic digestion (AD) has piqued the society's curiosity and been widely used for decades (Chum *et al.* 2011; Zamri *et al.* 2021). The discharge of inadequately treated wastewater into the environment reduces the environment's ability to offer advantages, on which society relies. While the case of water scarcity is rising, the contaminants carried from the improperly treated wastewater causes several environmental and health-related issues that affect national productivity (Mitchell *et al.* 2014).

Several investigations have shown that using anaerobic digestion treatment method for wastewater management not only helps to eliminate contaminants from the wastewater but also generates a renewable source of energy (biogas), which helps to relieve the world's energy

crisis. Globally, the over-reliance on fossil fuels as a source of energy has resulted in environmental concerns such as greenhouse gas emissions and climate change, which are generated by the continuous combustion of these fossil fuels (Ghassemi *et al.* 2004; Chen and Lee 2014a; Montwedi *et al.* 2021). The anaerobic digestion of organic waste produces biogas. The biogas produced is less expensive and uses widely available local materials including agricultural residue, food waste, and wastewater (Ajay *et al.* 2020).

The recovery of biogas from wastewater treatment is envisioned as an environmentally beneficial and cost-effective energy source for long-term growth. Because of this, the focus of the study was to enhance biogas production from wastewater via anaerobic digestion using synthesized magnetic nanoparticles.

1.2 Problem statement

Wastewater management and energy demand is a global concern. The world is seeking an alternative to ease the over-dependency on fossil fuels and meet the demand of the consumers of energy (Chum *et al.* 2011; Ajay *et al.* 2020; Montwedi *et al.* 2021). In South Africa, they are faced with similar problems that is wastewater management and energy crisis.

In a 2018 report by Green Drop, it was found that about 6500 ML/day wastewater is produced daily in South Africa (Montwedi *et al.* 2021), This is an increase of over 17% as reported by Rodda (2012) and these wastewaters end up in the wastewater treatment plants (WWTPs) (Adewumi, Ilemobade and Van Zyl 2010; Edokpayi, Odiyo and Durowoju 2017; Montwedi *et al.* 2021). However, the effluent does not meet the discharge limit which in turn poses a threat to the river bodies and the environment at large (Igbinosa and Okoh 2009; Adewumi, Ilemobade and Van Zyl 2010; Edokpayi, Odiyo and Durowoju 2017; Montwedi *et al.* 2021). As such, the need to explore different treatment methods or improve on the existing ones to curb the problem is important.

As the demand for energy increases with the increase in population, there is the need to meet this demand. About 59% of the energy supply comes from coal, 20% from a renewable source, 2% nuclear, 16% from crude oil, and 3% from natural gas (Ratshomo 2018; Motjoadi, Bokoro and Onibonoje 2020). About 88% of the nation's electricity is produced from coal. However, there is a limitation to the use of fossil fuels; this is because it is not renewable, it also contributes to the environmental pollution problem in terms of emitting greenhouse gases.

Biogas as a renewable source of energy can augment or serve as a substitute for coal for electricity production, however, its production is limited (CarbonBrief 2018). In this vein, treatment of wastewater with the concert of energy recovery is gaining attention in recent years.

Anaerobic digestion (AD) as a biological system reduces the organic pollutants to produce energy. Biogas production by AD of waste is an attractive yet challenging task (Ahmed *et al.* 2017; Kweinor Tetteh and Rathilal 2021b). Although AD is the most ideal approach for wastewater treatment and renewable energy generation, the process has drawbacks that impedes the system from performing as expected, resulting in a lower biogas yield and poor water quality (Sreekrishnan, Kohli and Rana 2004; Ajay *et al.* 2020). The limitations include reactor failure, inhibition due to the substrate composition, and bioavailability. This setback that the AD system poses has brought about the need for a strategic way to enhance the performance of the AD system (Ajay *et al.* 2020).

Consequently, this research examined the impact of synthesized magnetic nanoparticles on AD performance for the treatment of wastewater and biogas production. The system was optimised to determine the optimal operating conditions and a comparative study was done to determine which system works better between the magnetised and non-magnetised anaerobic digestion systems. The system was fitted on both modified Gompertz and first-order kinetic models.

1.3 Anaerobic digestion (AD) treatment method

Anaerobic digestion (AD) as a biological treatment method is used for the degradation of organic waste to an energy source (biogas) rich in methane. Methane and carbon dioxide are the main components of the gas produced (Bochmann and Montgomery 2013; Laiq Ur Rehman *et al.* 2019). Due to the environmental impact of AD and its conversion of organic waste to energy-rich methane (55-65% methane and 45-35% carbon dioxide) by microorganisms in the absence of oxygen, it has been used widely for wastewater treatment and other organic waste management (Deublein and Steinhauser 2011; Bachmann *et al.* 2015; Laiq Ur Rehman *et al.* 2019).

AD consists of four main stages. The first stage is hydrolysis which involves the breaking down of complex organic matter (carbohydrate, fats & protein) into smaller units (simple sugar, fatty acids & amino acids) (Ahmed *et al.* 2017; Nzila 2017). These smaller units that are easier to handle go to the next stage which is acidogenesis. During acidogenesis, acidogenic bacteria convert the hydrolysis products (smaller units) to methanogenesis substrate. Simple sugars, fatty acids, and amino acids are broken down by acidogenic bacteria into acetic acid, carbon

dioxide, and hydrogen (70%) as well as volatile fatty acids (VFA) and alcohols (30%) (Merlin Christy, Gopinath and Divya 2014). Acetogenesis is the third stage of AD. Acidogenesis metabolites that cannot be easily converted to methane by methanogenic bacteria are transformed into methanogenic substrates at this stage. Acetogens digest simple molecules generated during the acidogenesis phase to create predominantly methanogenic substrates such as acetic acid, as well as carbon dioxide and hydrogen (Ahmed *et al.* 2017; Nzila 2017).

Methanogenesis, the final stage of AD is a biochemical phenomenon that occurs at the end of the process. Methanogens are microorganisms that employ intermediate products from previous processes, such as acetic acid and hydrogen, to transform them into methane, carbon dioxide, and water. These are the components that constitute the largest portion of biogas. This is an important stage in the AD process, and operational conditions like pH and temperature can have a big impact. The digestate is made up of any dead bacterial leftovers as well as any residual non-digestible debris (Chaudhary *et al.* 2013; Jain *et al.* 2015).

The kinetics of the methanogenic process is very slow, and this can be affected by conditions such as pH, temperature, organic composition, and strength of the wastewater. Researchers have explored several ways to improve the performance of the AD system in terms of its biogas and methane enhancement over the years. While some have studied the domain of pre-treatment of the substrate in co-digestion and adjustment to optimise the operational conditions for selective hydrolysis, others have researched the use of nanoparticles to improve the AD performance (Esakkimuthu, Sivakumar and Akila 2014; Abdelsalam *et al.* 2016; Zaidi *et al.* 2018). Among these, the use of nanoparticles for biogas and methane enhancement has gained the interest of many researchers and is most widely used (Ambashta and Sillanpää 2010; Esakkimuthu, Sivakumar and Akila 2014).

1.4 Synthesized magnetic nanoparticles.

Nanotechnology over the years has gained much global attention. The use of nanoparticles, which is the fundamental component of nanotechnology, has become an interesting research focus (Cho *et al.* 2013; Hasan 2015; Hassanein, Lansing and Tikekar 2019). These nanoparticles range from 1 to 100 nm. They are made up of metal, carbon, organic matter, and metal oxides (Ealias and Saravanakumar 2017; Hassanein, Lansing and Tikekar 2019). The application of nanoparticles has been predominant over its bulk particle because of their distinct chemical, physical and biological properties (Joshi, Bhattacharyya and Ali 2008). Nanoparticles have a large surface area to volume which improves the stability and reactivity

of a process. Nanotechnology is applied in the medical, engineering, chemical, and agricultural field to enhance process systems (Silva 2004; Hasan 2015; Ealias and Saravanakumar 2017).

Magnetic nanoparticles in recent years have been most sought after in the medical field for drug delivery, imaging, biosensing, etc. It is also used in environmental remediation and catalytic processes (Kudr *et al.* 2017). This is due to their physicochemical properties such as smaller size, larger surface area, superparamagnetic property, biodegradability, and they are also environmentally friendly. The unique properties of these magnetic nanoparticles allow their applications in a wide area (Kudr *et al.* 2017). A review by Ajay *et al.* (2020) highlighted on the physicochemical characteristics of nanoparticles, explaining why they are more advantageous in its application in biological systems. The authors reported that, the solubility, catalytic nature, surface structure and area and size etc allows the nanoparticles to influence the direct interspecies electron transfer which enhances biogas production in AD.

Nanoparticles have the capability to increase the rate of methane formation and also reduces the lag phase in AD (Baniamerian *et al.* 2019; Abdelwahab *et al.* 2020; Ajay *et al.* 2020).

To improve the properties of magnetic nanoparticles in terms of size, surface morphology, chemical compositions for wider use etc., several synthesis methods have been developed and applied. These methods include sol-gel, co-precipitation, microwave, thermal decomposition, and electrochemical synthesis (Osaka *et al.* 2006; Elhambakhsh *et al.* 2020). Among these synthesis methods, co-precipitation has been promising because of its low cost of operation, readily available apparatus, and materials, and it is a very simple and precise process that gives good results (Jalilpour and Fathalilou 2012; Mascolo, Pei and Ring 2013; Kandpal *et al.* 2014).

1.5 Research questions

The following research questions will be answered.

- ✓ How does the addition of magnetic nanoparticles affect the AD performance?
- ✓ Is there any significant impact on the biogas and methane yield?
- ✓ Which of the factors have impact on the AD process and how can it be adjusted to suit the process?
- ✓ What will be the optimum conditions to yield a higher biogas and methane?

1.6 Research hypothesis

The addition of magnetic nanoparticles does have a significant impact on the performance of anaerobic digestion process in terms of biogas production, yield and quality of the biogas produced (methane yield) as well as improve the treatability performance of the process.

1.7 Aim and objectives

The main aim of this study is to use synthesized magnetic nanoparticles to enhance biogas production in an anaerobic digestion process. The specific objectives of the study are:

- To synthesize and characterise the magnetised nanoparticles using Scanning electron microscopy coupled with energy-dispersive X-ray spectroscopy (SEM/EDS), X-ray diffraction analysis (XRD), Fourier-transform infrared spectroscopy (FTIR), and Brunauer-Emmett-Teller (BET).
- To evaluate the AD performance in terms of water quality (treatability) and biogas production.
- To evaluate and optimise the anaerobic magnetised system for biogas production.
- To compare the performance of magnetised biochemical methane potential to non-magnetised biochemical methane potential.
- To study the kinetics of the anaerobic magnetised system using modified Gompertz and first-order kinetic models.

1.8 Approach

To ascertain the performance of nanoparticles, a feasibility test was done using metal nanoparticles. From the results of the feasibility study, further studies were carried out to determine the loading of nanoparticles as well as the magnetisation.

The initial stage of the study was to synthesize the magnetic nanoparticles (MNPs) using the co-precipitation synthesis method. The synthesized magnetic nanoparticles were then characterised to determine the surface morphology, elemental composition, crystallinity, surface adsorption properties, and the functional groups using SEM/EDX, XRD, BET, and FTIR.

The synthesized MNPs were then applied on a biochemical methane potential (BMP) test to evaluate the performance of the AD process in terms of its wastewater treatability and biogas

enhancement. The pH, total solids (TS), Volatile solids (VS), chemical oxygen demand (COD), colour, and turbidity of the effluent were analysed using standard methods; the biogas composition was determined by gas chromatography (GC-Solution, Shimadzu 2014, Japan).

Based on the results the system was optimised to obtain the optimal operating conditions (MNPs loading, inoculum to substrate ratio, temperature, and hydraulic retention time) for the best performing MNP.

The second stage of the work was to perform a comparative study for a magnetised biochemical methane potential (BMP) and non-magnetised BMP system for the best performing MNP at the optimum operating conditions. The cumulative daily biogas yield results were then fitted on the modified and first-order kinetic models to ascertain which of the models works best for the system

1.9 Structure of dissertation

The thesis has five chapters as follows;

Chapter one

The introduction presents the background of the study. It also gives the problem statement with the aim and objectives to be achieved.

Chapter two

The second chapter reviewed the literature related to the study, outlining the advantages and disadvantages of the already known methods and options for wastewater treatment. It also reviewed studies of how biogas production from wastewater has been enhanced via anaerobic digestion. Presentation of the limitations of the AD treatment method and why the need for this technology was also outlined.

Chapter three

In chapter three, the research methods, materials, and equipment specifications are described. It also presented the analytical data and tools used. It described the optimisation process and study of the kinetics of the system.

Chapter four

The fourth chapter presented the results and discussion. The discussion was as follows, the characterisation of synthesized MNPs, the effects of the MNPs on the AD performance in terms of water quality, the impact of MNPs on biogas and methane yield. It also discussed the optimisation process and the comparative study of the magnetised and non-magnetised BMP systems. Finally, the chapter presented the kinetics of the system.

Chapter five

Chapter five provided the summary of the study's conclusions and recommendations for future actions.

Chapter Two

LITERATURE REVIEW

This chapter reviews other researchers' works in literature on renewable energy, wastewater contamination, and treatment options before focusing on the anaerobic digestion process. The variables impacting the AD process, its limitations, and how to improve the process are investigated. The chapter also assesses nanotechnology works, with an emphasis on the AD wastewater treatment process. There is also a brief review of the use of computerized design programs to optimise the process. Lastly, a recap of the literature review is given to show the knowledge gaps that served as the foundation for this work.

2.1 Background of the study

Throughout these years, wastewater management and energy crises have remained the world's most challenging concerns. In South Africa, the growth of population and increase in industrialization over the past decades has increased the water demand, as most of their activities use water (Gumbi 2020; Iloms *et al.* 2020). These contribute to the generation of highly contaminated wastewater, which has raised significant environmental concerns regarding its safe disposal into water bodies. Concerns are growing as wastewater contaminated with toxic heavy metal pollutants (lead, cadmium, mercury, nickel, and other metals) as well as emerging contaminants (ECs) or micro-pollutants from pesticides, personal care products (PCPs), pharmaceuticals, and other sources are discharged into aquatic environments, posing health and environmental risks (Sorensen *et al.* 2015; Ololade 2018; Chetty and Pillay 2019; Iloms *et al.* 2020; Oruko *et al.* 2020).

In this vein, monitoring the wastewater treatment plants (WWTPs) to be able to meet discharge standard limits is deemed significant. In a nutshell, WWTPs have made great progress as new technologies have been adapted to add value to them, while addressing the pollution problem they cause. In contrast, the energy world has seen an alternative to its principal source of energy, fossil fuel. It is estimated that approximately three-quarters of worldwide greenhouse gas emissions are attributed to the burning of fossil fuels (Hannah 2020).

Energy derived from the combustion of fossil fuels not only contribute significantly to climate change, but it also has a significant negative impact on human health (Ololade 2018; Hannah

2020). Figure 2-1 shows worldwide energy consumption over the last 55 years (1965-2020), demonstrating how dependent the world is on fossil fuels for energy (Hannah 2020). The source of energy for South Africa as of 2020 is depicted in Figure 2-2, where the major source of energy is coal (Motjoadi, Bokoro and Onibonoje 2020; BP 2021). The energy generated from renewables for the year 2020 was less than 22% (Motjoadi, Bokoro and Onibonoje 2020; BP 2021).

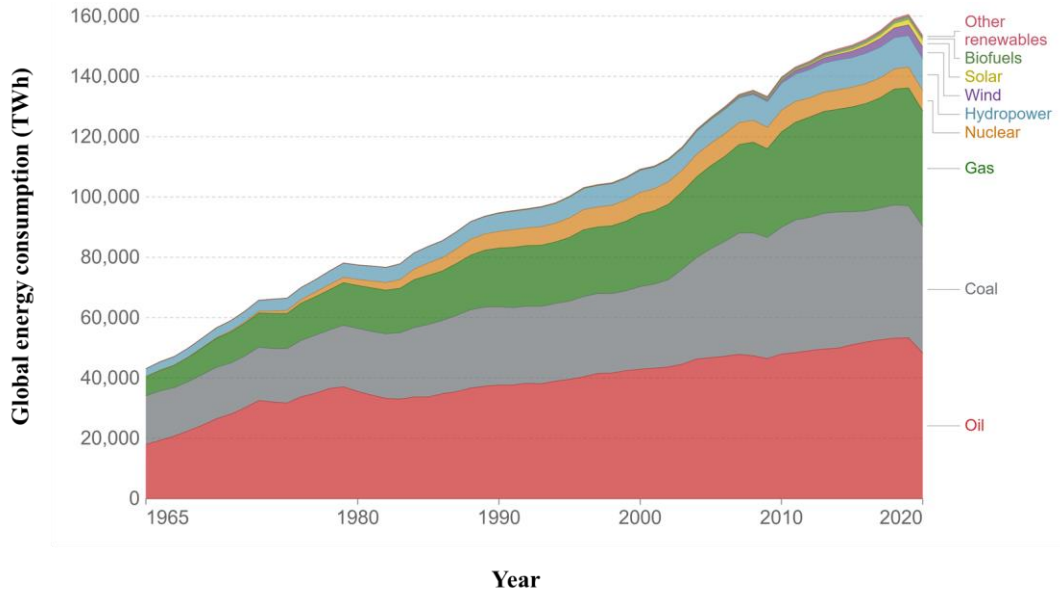

Figure 2-1: Source of global energy consumption (Hannah 2020; BP 2021)

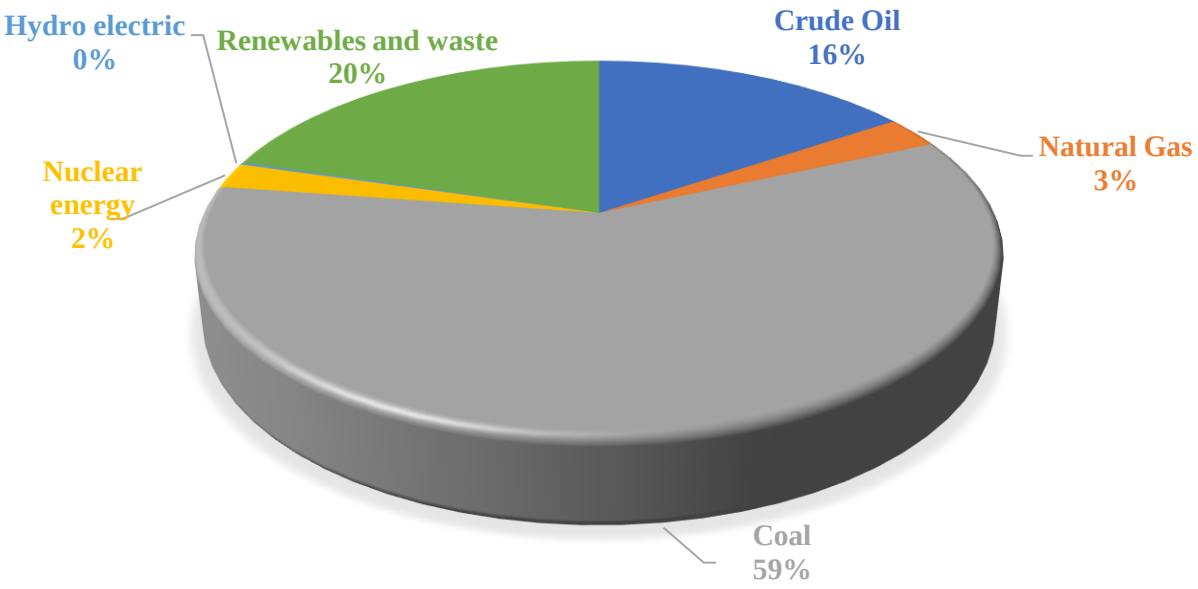

Figure 2-2: South African source of energy for the year 2020 source: (Motjoadi, Bokoro and Onibonoje 2020)

However, the high demand for energy makes this alternate source, renewable energy, difficult to implement. Herein, there is the need to increase the energy generated from renewable sources while reducing the energy generated from fossil fuels (McCarty, Bae and Kim 2011; Zhao and Magoulès 2012; Stafford *et al.* 2013; Paritosh *et al.* 2017; Ololade 2018).

Wastewater with high organic content has been one of the major sources of renewable energy over recent years as the concept of energy-driven WWTPs has gained much attention and mitigation processes have been conducted and researched to improve the WWTPs (Stafford *et al.* 2013; Zaidi *et al.* 2014; Zhou *et al.* 2018; Sikosana *et al.* 2019; Singh *et al.* 2019; Obotey Ezugbe and Rathilal 2020; Ponce-Robles *et al.* 2020; Montwedi *et al.* 2021). In a nutshell, the anaerobic digestion process has emerged as the most suited strategy for both wastewater treatment and renewable energy production, in accordance with the sustainable development goals of inexpensive and clean energy, clean water, and sanitation.

2.2 Energy

Population growth and industrialization are the major cause for the significant increase in energy demand over the last few decades. Increased energy consumption has also generated environmental concerns such as climate change, global warming and ozone depletion (Pérez-Lombard, Ortiz and Pout 2008). This is since most of the energy is derived from fossil fuels. As a result, environmental sustainability has become a global issue. Researchers have spent years examining the impact of energy consumption on economic growth and environmental sustainability (Zhao and Magoulès 2012; Begum *et al.* 2015). The global consumption of energy was estimated to be 0.17 quadrillion kW in 2015, and forecasts show that this amount will shoot up by 2050, with a 50% rise (Kahan 2019).

According to studies by Mohr *et al.* (2015) and Ağbulut and Sarıdemir (2021), fossil fuels account for more than 80% of total energy production. This is due to the fact that they are high in energy and abundant in nature, are easily accessible, provide a large profit from mining, and are simple to store and utilize, among other factors (Adefarati *et al.* 2017; Ololade 2018; BP 2021). However, there are certain drawbacks to using fossil fuels; mining them takes time, they destroy the ozone layer as a result of carbon dioxide and other greenhouse gas emissions, it takes longer to produce and steadily depletes over time (Vaona 2012). Continuous combustion

of fossil fuels releases hazardous gases into the atmosphere, causing global warming and climate change (Ajay *et al.* 2020). Again, the accessing of these resources is in doubt due to the fact that the cost of obtaining/mining them continues to rise, making it harder for both consumers and suppliers. For these constraints, there is a need to seek viable alternatives or substitutes that are less environmentally damaging (Ghassemi *et al.* 2004; Menyah and Wolde-Rufael 2010; Bekun, Alola and Sarkodie 2019). As a result, renewable energy becomes a plausible option for mitigating the situation.

2.2.1 Renewable energy

Renewable energy is energy obtained from renewable resources that regenerate themselves spontaneously on a human time scale. Renewable energy is self-regenerating in nature. The sun, wind, water, and biomass are examples. Biomass comes from crops, agricultural and industrial waste, and municipal trash (Bull 2001). These sources of energy can be utilized to generate power for all economic purposes, transportation fuel, and industrial heat. These sources of energy are plentiful, but, like fossil fuels, they are not evenly distributed over the world. Regardless, every region has a variety of renewable energy options. Renewable energy resources of various forms complement one another and can greatly contribute to energy security (Energy 2020). The most well-known renewable energy sources are hydro energy, solar energy, wind energy, tidal energy, geothermal energy, and biomass energy.

2.2.1.1 Advantages and Disadvantages of Renewable Energy

Renewable energy has numerous amazing advantages; they are simple to maintain because they can be renewed, they never run out, they do not harm the environment, and so on (Afgan and Carvalho 2002; Verbruggen *et al.* 2010; Energy 2020). Although the advantages of renewable energy outweigh the downsides, it is vital to consider its disadvantages. It is difficult to produce the same amount of renewable energy as fossil fuel, and inconsistent weather conditions might limit its availability for the reason that renewable energy production is dependent on particular meteorological conditions (Afgan and Carvalho 2002; Kahan 2019).

2.2.1.2 Biomass Energy

The term "biomass" refers to all organic material derived from plants. They can be utilized as a source of energy (Bar-On, Phillips and Milo 2018). Green plants employ photosynthesis to convert sunlight from plant material, which includes all land-based and water-based vegetation, as well as organic waste, to produce biomass. Historically, biomass has been a more abundant source of energy for humanity (McKendry 2002). Biomass can be utilized to generate methane

(biogas), which is used in furnaces and stoves. Biomass can be divided into two types; biomass derived from lignocellulose and non-lignocellulose. Lignocellulose biomass is the biomass obtained from agricultural waste, energy crops and wood residues while non-lignocellulose biomass consist mainly of animal manure, algae biomass, sewage sludge and municipal solid waste (Mohan, Pittman Jr and Steele 2006; Dhungana, Dutta and Basu 2012; Yu *et al.* 2019; Lu *et al.* 2021).

2.2.1.3 Bioenergy

Bioenergy is energy generated from biological sources; it is an important source of energy that can be used to generate biofuels and electricity for heating and cooking, and so on. As a result of the environmental concern that fossil fuels pose, demand for renewable energy has surged substantially. In this vein, it is crucial to reduce the environmental impact of traditional fuels (fossil fuels) and improve renewable energy source technologies (Verbruggen *et al.* 2010).
Bioenergy has gradually become a viable alternative energy source, resulting in fewer CO_2 emissions because it is economical and safe to use (Mao *et al.* 2015). Bioenergy electricity can be obtained from a variety of sources, including wood residue, sugar cane waste, and animal husbandry. One benefit of biomass-based electricity is that the fuel is typically a by-product, residue, or waste product from the previously mentioned source (Yue, You and Snyder 2014; Owusu and Asumadu-Sarkodie 2016).

Bioenergy has the potential to play a key role in the enhancement of sustainable energy alternatives, and it is projected to become the world's fourth largest energy resource by 2050 (Chum 2011). To reduce pollutant emissions, the econometric indicator suggests that South Africa either sacrifice economic development or reduce energy use per unit of output, or both. Regardless, it is expected to provide the country's energy needs while simultaneously reducing CO_2 emissions through the development of energy alternatives to coal, the largest source of CO_2 emissions (Chum 2011).

2.2.1.4 Forms of bioenergy

Bioenergy comes in three forms: liquid (biofuel), solid (biomass), and gas (biogas). This study will focus on biogas, which is a form of gas.

2.2.2 Biogas

Biogas is a gaseous form of bioenergy produced by anaerobic microbes biologically digesting organic waste (Scarlat, Dallemand and Fahl 2018). Anaerobic digestion is a method of producing biogas by breaking down organic materials such as animal manure, wastewater, and

food scraps in the absence of oxygen. During this breakdown, a combination of gases, primarily methane and carbon dioxide, is emitted. Methane forms around 55-65% of the composition while carbon dioxide is 35-45% (Yadvika *et al.* 2004). Because biogas is a clean, sustainable, and long-term source of baseload power, it can be utilized to supplement fossil fuels (Kalloum *et al.* 2011).

2.3 Wastewater

Wastewater is water that has become contaminated as a result of human activity. Households, business establishments, institutions, and enterprises are all sources of wastewater (Tchobanoglous, Burton and Stensel 1991; Tchobanoglus, Burton and Stensel 2003; Safoniuk 2004; Gumbi 2020). Wastewater is composed of 99.9% water and 0.1% particulates. The two main types of wastewater handled in a wastewater treatment plant are domestic and municipal wastewater (Tebbutt 1997; Templeton and Butler 2011). Figure 2-3 depicts the composition of typical wastewater. Domestic wastewater includes wastewater from businesses, institutions, homes, and some factories, whereas municipal wastewater includes both industrial and domestic wastewater.

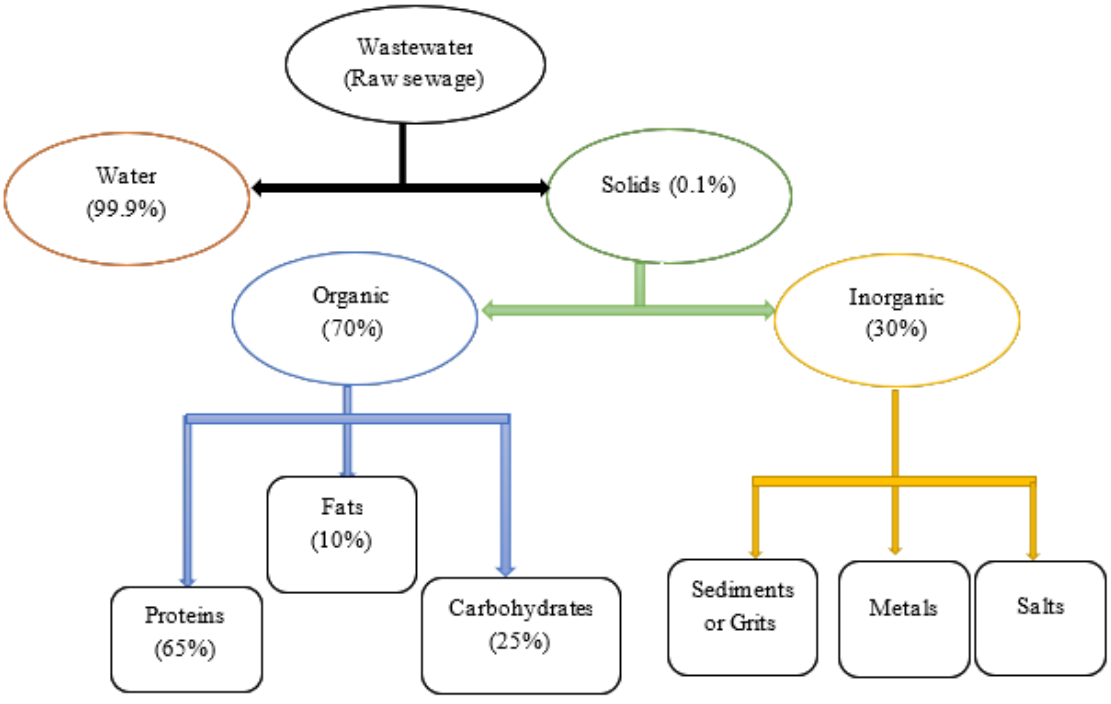

Figure 2-3: Wastewater Physicochemical composition (Tebbutt 1997; Templeton and Butler 2011; Tebbutt 2013).

2.3.1 Characterisation of wastewater

The soluble components of the water supplied to the area, as well as pollutants from the waste production process, are typically found in wastewater. To comprehend the true nature and composition of wastewater, it is necessary to examine its physicochemical and biological components (Muttamara 1996; Tebbutt 2013). Temperature, colour, turbidity, total solids, and conductivity are all common physical characteristics of wastewater. Chemical oxygen demand (COD), alkalinity, pH, biological oxygen demand (BOD), acidity, dissolved oxygen (DO), nitrogen, and trace metals are among the chemical properties. Total organic carbon (TOC), for example, and the biological makeup of wastewater are frequently examined because they play an important role in wastewater treatment (Muttamara 1996; Tebbutt 1997, 2013; Liu *et al.* 2021; Martinez-Burgos *et al.* 2021; Rani *et al.* 2021)

2.3. 2 Sources of wastewater

The generation of wastewater is inevitable as population grows and industrialization increase, among the source of wastewater generation, industrial, domestic and municipal are the major sources of wastewater generation.

2.3.2.1 Sugar refinery wastewater (SRW)

The sugar refinery industry is one of South Africa's largest industries. Because the sugar business utilizes a lot of water in its processes, it generates a lot of wastewater. Sugar cane is refined in numerous phases, including washing, concentration, extraction, clarification, and centrifugation (Fito, Tefera and Van Hulle 2019). Each stage of the method demands the use of water, and the wastewater produced changes in composition based on the chemical or materials used at that stage.

Chemical and biological oxygen demand, as well as total soluble solids, are all high in sugar industry wastewater. Similarly, when wastewater is thrown into rivers without being properly treated, it affects the aquatic ecosystem (Kushwaha 2015; Fito, Tefera and Van Hulle 2019).

2.3.2.2 Domestic wastewater (DW)

Wastewater produced by the community (households, institutions, and some companies) is known as domestic wastewater, and it frequently contains items utilized by the community's residents. Human waste makes up the majority of domestic wastewater (faeces and urine). Water used for cooking, washing, cleaning, bathing, and toilet flushing produces domestic wastewater (Mara 2013). Domestic wastewater composition varies from community to community and country to country.

The biological oxygen and chemical oxygen demand (BOD and COD) content of domestic wastewater determines its strength, as the higher the amount of organic waste, the stronger the wastewater. Domestic wastewater is collected using sewers (underground pipes); gravity is employed in most situations; pumps are only used in a few cases (Mara 2013). Table 2-1 shows the chemical makeup of typical sewage at various levels of treatment.

Residential wastewater is treated in order to reclaim for domestic purposes, and agriculture irrigation. Domestic wastewater has also been used to generate electricity over the years (McCarty, Bae and Kim 2011).

Table 2-1: Characteristics of typical sewage (Tebbutt 2013)

Characteristic Parameters (mg/L)	**Crude source**	**Final effluent source**	**Settled source**
COD	700	90	400
BOD	300	20	175
Suspended solids	400	30	200
Nitrite (NO_3-N)	<1	20	<1
Ammonia (Amm.N)	40	5	40
TOC	200	30	90

2.3.2.3 Municipal wastewater

Municipal wastewater (MW) is any wastewater that has been discharged to a publicly operated wastewater treatment plant. Institutional, commercial, and industrial facilities are primary contributors of municipal wastewater, as are residential wastewaters (Jetten, Horn and van Loosdrecht 1997; Qu *et al.* 2019).

Water recovered from municipal wastewater treatment is commonly employed in agriculture and, in the majority of cases, dumped into rivers. Similarly, if the discharged water somehow doesn't meet the effluent standard, it pollutes river bodies, causing harm to the aquatic ecosystem (Jetten, Horn and van Loosdrecht 1997; Joss *et al.* 2006).

Table 2-2 summarizes the constituents of domestic wastewater (MW), sugar refinery wastewater (SRW), and municipal wastewater (MW). BOD and COD, which measure the concentration of organic waste in the wastewater, are used to determine its strength. High

BOD/COD levels in wastewater classify it as mild, medium, strong, or extremely strong. Tables 2-3 depicts the wastewater strength in terms of BOD and COD concentration.

Table 2-2**:** Summary of the characteristics of DW, MW, and SRW wastewater and the accepted discharge limit (Von Sperling 2007; Tebbutt 2013; Kushwaha 2015; Qasim 2017; Negwamba and Dinka 2019)

Wastewater Composition parameter(s)	**Raw wastewater composition concentration**	
	DW & MW	**SRW**
Biological oxygen demand (BOD) (mg/L)	110-400	350-2750
Chemical oxygen demand (COD) (mg/L)	200-700	1000-4340
pH	6.7-7.5	5.0-6.5
Total solids (TS) (mg/L)	375-1800	--
Volatile solids (VS) (mg/L)	105-300	--
Total suspended solids (TSS) (mg/L)	120-360	760-800
Volatile suspended solids (VSS) (mg/L)	--	173-2190
Total organic carbon (TOC) (mg/L)	80-290	--
Total dissolved solids (TDS) (mg/L)	250-800	400-1650
Alkalinity (mg/L)	50-200	---
Oil and grease (mg/L)	--	7-12

Table 2-3: Characterisation of wastewater strength in terms of BOD and COD (Mara 2013)

Strength of wastewater	**BOD content (mg/L)**	**COD content (mg/L)**
Very strong	>750	>1500
Strong	500	1000
Medium	350	700
Weak	<250	<400

2.3.3 Waste activated sludge (WAS)

The solid by-product of wastewater treatment that can be semi-liquid or liquid depending on the treatment technique is known as waste activated sludge (WAS). It includes roughly 0.20-12% solids and the rest is liquid. This WAS can also be called municipal sewage sludge, and it is made up of sludge from the primary, secondary, and tertiary treatment sludge (Evans 2016;

Kacprzak *et al.* 2017). Owing to the fact that it is high in organic and inorganic matter, pH, heavy metals, nutrients, alkalinity, and some biological components such as viruses, bacteria, protozoa, and so on, as well as pollutants that can be harmful to the environment, disposal of this sludge becomes a problem after municipal waste has been treated (Appels *et al.* 2008; Fytili and Zabaniotou 2008; Ghaleb *et al.* 2020a). Because of its high nutrient content, this sludge is sometimes utilized as fertilizer for crops; nonetheless, the sludge can contain chemicals that are detrimental to the environment, contaminating the environment and posing health hazards if not treated before disposal (Bachmann *et al.* 2015).

Table 2-4 illustrates the composition of the solid part of the WAS, which demonstrates that the organic matter content is quite high; as such, using WAS for anaerobic digestion for energy generation has been utilized. To prevent the disposal issue, using WAS in wastewater treatment to generate energy has been explored and the residual sludge (digestate) is used as agricultural fertilizer (Appels *et al.* 2008; Bachmann *et al.* 2015). Table 2-4 shows the percentage composition of WAS for untreated/digested primary sludge and subsequent treatment sludge as reported by McCarty, Bae and Kim (2011), Fito, Tefera and Van Hulle (2019) and (Kacprzak *et al.* 2017).

Table 2-4: Characterisation of Waste activated sludge (Kacprzak *et al.* 2017)

Parameter	**Type of sludge**		
	Untreated primary sludge	**Digested primary sludge**	**Secondary/ Activated sludge**
Total dry solids (TS) (%)	2-8	6-12	0.8-1.2
Volatile solid (%TS)	60-80	30-60	59-88
Protein (%TS)	20-30	15-20	32-41
Cellulose (%TS)	8-15	8-15	7-9.7
pH	5-8	6.5-7.5	6.5-8.0
Grease and fats (%TS)	7-35	N/A	5-12
Nitrogen (%TS)	1.5-4	1.6-6	2.4-5
Potassium (%TS)	0-1	0-3	0.5-0.7
Phosphorus (%TS)	0.8-15	1.5-4	2.8-11

2.3.4 Wastewater treatment

The process of converting contaminated water into clean and valuable products is known as wastewater treatment (Mitchell *et al.* 2014). Water treatment is divided into four stages: pre-treatment, primary, secondary, and tertiary. Physical, chemical, biological, and advanced oxidation treatment approaches have been classified under these stages (Arun 2016).

2.3.4.1 Pre-treatment

Large solid objects/materials such as sticks, stones, rags, and so on are removed during the pre-treatment stage. Bar racks are used to remove bigger things, while grit chambers are used to remove inert dense materials such as shattered glass, pebbles, sand, and so on. Pre-treatment is required to prevent solid items from interfering with the biological process and to avoid operational issues during secondary treatment (Change 2006).

2.3.4.2 Primary treatment

The sedimentation process that occurs before secondary treatment is referred to as primary treatment. Primary treatment in residential water treatment eliminates approximately 25% of the organic content and all non-organic materials with or without the use of chemicals. Primary treatment removes 60% of solids and approximately 35% of biological oxygen demand (BOD). Sedimentation, settlings, clarity, and thickening are some of the procedures employed to achieve this treatment process (Arun 2016; Liu and Lipták 2020).

2.3.4.3 Secondary treatment

This is the stage in which residual organic and suspended particles are treated. Biological mechanisms remove around 80% of BOD at this stage (Sonune and Ghate 2004; Shah and Shah 2020). Aerobic digestion, anaerobic digestion, biofiltration and biotrickling are the most often employed biological treatment methods in WWTPs (Sonune and Ghate 2004; Tetteh *et al.* 2019). Organic waste degrades and decomposes because of this process.

2.3.4.4 Tertiary treatment

The recalcitrant organic molecules that evaded secondary treatment are exposed to additional treatment employing advanced treatment methods during tertiary treatment. Any technique that produces effluent of greater quality than the primary and secondary treatments is considered advanced treatment (Sonune and Ghate 2004; Arun 2016; Isiaka and Olaniran 2021).

This study employed the use of biological treatment, which is a secondary treatment. The primary treatment method is limited and does not eliminate all types of toxins adequately. Organic-rich wastewater cannot be efficiently treated employing primary treatment methods, necessitating the development of a more efficient treatment technology. The biological treatment of organic waste, which turns it to energy and improves pollution removal efficiency, is effective (Henze *et al.* 2008; Tetteh *et al.* 2019). This study looked into the usage of biological treatment technologies for producing biogas from wastewater.

2.3.5 Biological treatment method

Biological treatment is also a secondary treatment in which microorganisms are used to decompose dissolved organic materials in wastewater. This degradation involves two biological processes: biological oxidation and biosynthesis. Some biological oxidation end-products, such as minerals, remain in the solution and are released with the effluent, whereas biosynthesis converts colloidal and dissolved organic matter into new cells, forming dense biomass that can be removed by sedimentation (Gray 2005; Samer 2015).

Biological techniques are widely used in wastewater treatment around the world to eliminate developing toxins through the biodegradation mechanism. Wastewater containing biodegradable compounds and a biological oxygen demand to chemical oxygen demand (BOD/COD) ratio of 0.5 can be treated biologically with the required analysis and environmental management (Chan *et al.* 2009; Fito, Tefera and Van Hulle 2019). In order to remediate wastewater, anaerobic and aerobic digesting methods can be used. While aerobic means that microbes use dissolved oxygen to transform organic water to biomass and carbon dioxide (CO_2). In the absence of oxygen, complex organic waste is digested into methane, CO_2, and water by anaerobic digestion (Chan *et al.* 2009; Yazdani *et al.* 2019). Aerobic digestion includes the use of activated sludge, membrane bioreactors, and sequence batch reactors. Anaerobic approaches include anaerobic sludge reactors and anaerobic film reactors. The features of the wastewater are important in the choosing of biological treatment (Ahmed *et al.* 2017). The anaerobic digesting process was the focus of this research.

2.4 Anaerobic Digestion (AD) Process

Anaerobic digestion (AD) is a biological process which involves the use of microorganisms to break down biodegradable material in the absence of oxygen. AD produces biogas and digestate. Biogas is commonly mentioned as the gas produced by an anaerobic system. Microorganisms hydrolyse the input materials to break down insoluble organic polymers such as carbohydrates, proteins, and lipids, which is the first step in the digestive process (Ahmed *et al.* 2017; Nzila 2017).

2.4.1 Stages of the AD process

Hydrolysis, Acidogenesis, Acetogenesis, and Methanogenesis are the four major biological and chemical steps of anaerobic digestion. These stages are addressed, and the AD process flow chart is presented in Figure 2-4.

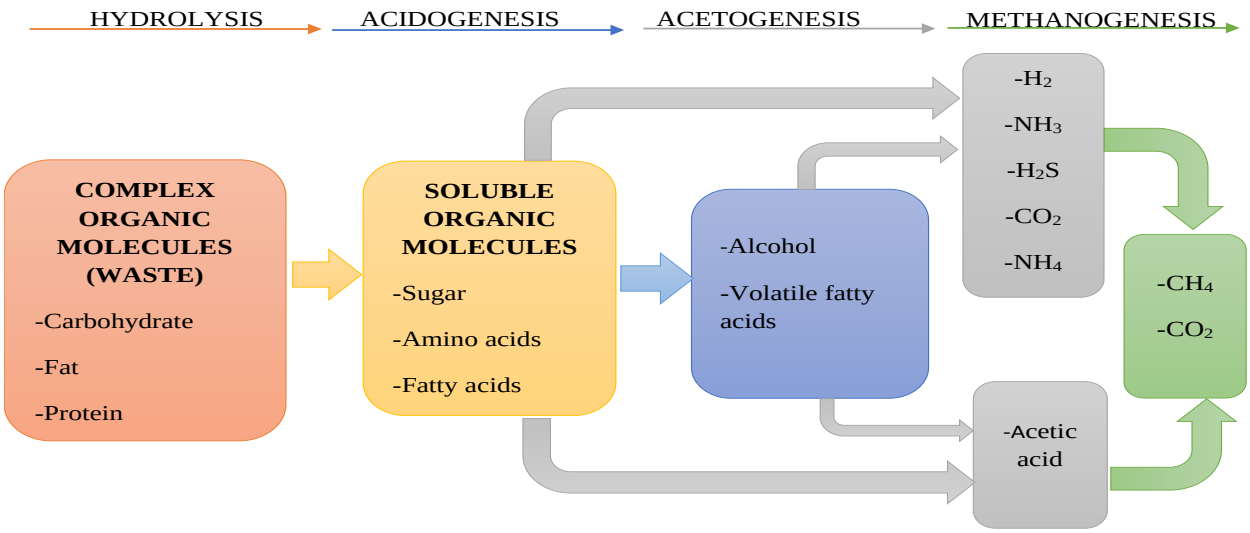

Figure 2-4: Anaerobic digestion process flow chat (Rea 2014)

2.4.1.1 Hydrolysis

Hydrolysis being the first stage of AD decomposes complex organic materials (polymers) into smaller pieces (mono- and oligomers). Biomass is primarily composed of complex polymers. These complex polymers must first be broken down into smaller units before the bacteria in an anaerobic digester can utilize the material's energy potential. Complex organic compounds such as carbohydrates, proteins, and lipids are hydrolysed into simple sugars, amino acids, and fatty acids, respectively (Ahmed *et al.* 2017; Nzila 2017).

2.4.1.2 Acidogenesis

Soluble molecules and simpler units are produced when the hydrolytic bacteria excrete hydrolytic enzymes, which break down biopolymers during hydrolysis. These soluble molecules from hydrolysis stage are converted by acidogenic (fermentative) bacteria into methanogenic substrates during acidogenesis. Amino acid, fatty acid and simple sugars are degraded (70%) into acetic acid, carbon dioxide, and hydrogen, as well as volatile fatty acids (VFA) and alcohols (30%) (Merlin Christy, Gopinath and Divya 2014).

2.4.1.3 Acetogenesis

Acidogenesis products that cannot be efficiently converted to methane by methanogenic bacteria are transformed into methanogenic substrates during acetogenesis. This is the third

stage of the AD process. Simple molecules produced during the acidogenesis phase, such as volatile fatty acids (VFA) and alcohols, are digested further by acetogens to yield primarily methanogenic substrates such as acetic acid, as well as carbon dioxide and hydrogen (Ahmed *et al.* 2017; Nzila 2017). This step's products are then processed in the last stage, methanogenesis.

2.4.1.4 Methanogenesis

The final stage of AD is known as methanogenesis. This is a biological process that generates the final products of the AD process. Microorganisms known as methanogens use intermediate products created in the preceding processes, such as acetic acid and hydrogen, to transform them into methane, carbon dioxide, and water. These are the components that make up the majority of the biogas. This is an important phase in the AD process that is greatly influenced by operational variables such as pH and temperature. The digestate is made up of the residual non-digestible material as well as any dead bacterial remnants (Chaudhary *et al.* 2013; Jain *et al.* 2015).

2.4.2 Factors affecting the AD process

Anaerobic digestion efficiency is influenced by three major factors: bioavailability and feedstock properties, reactor design, and operating conditions, which can induce inhibitions in the process, constraining the output and gas quality produced (Cioabla *et al.* 2012; Lohani and Havukainen 2018). Temperature, retention time, and pH are among the operating parameters that affect the AD process and play an essential role in its performance; hence they have been highlighted.

2.4.2.1 Temperature

Temperature is a critical component in the AD process since it influences not only enzyme activities and co-enzyme activity, but also methane yield and digestate quality. It functions in three temperature ranges: psychrophilic (10ºC – 25ºC), mesophilic (30ºC – 40ºC), and thermophilic (45ºC – 60ºC) (El-Mashad *et al.* 2004; Ward *et al.* 2008).

Digesters operating at thermophilic temperatures have a higher loading rate and a higher methane yield while also digesting the substrate and destroying microorganisms. Because the reaction is faster at high temperatures, this system accelerates the breakdown of organic matter. However, because of the high temperature requirement of this system, the required energy is similarly considerable, making it unsuitable for commercial applications (Choorit and Wisarnwan 2007; Wilson *et al.* 2008; Chen and Neibling 2014; Sun *et al.* 2016).

Digesters use a microbial population with a high tolerance for environmental variations, as well as a stable and easy-to-maintain microbial community, under mesophilic conditions. Digesters consume very little energy for heating under mesophilic conditions. However, due to the low energy input, the retention time is greater than in thermophilic digesters, and the biogas produced is occasionally insufficient. Despite these disadvantages, mesophilic digesters are favoured for commercial use since they are simple to maintain and operate at a cheap cost. Furthermore, because methanogens are temperature sensitive, they must operate in mesophilic environments with temperature fluctuations of less than 0.5°C/d (Sanchez *et al.* 2000; Choorit and Wisarnwan 2007; Stronach, Rudd and Lester 2012; Chen and Neibling 2014; Sun *et al.* 2016; Lohani and Havukainen 2018; Zamri *et al.* 2021).

2.4.2.2 Retention time

The retention time is the amount of time required for organic compounds to degrade. In an AD process, there are two types of retention time: solid retention time (SRT) and hydraulic retention time (HRT). SRT is the average time it takes for solids to be digested in an anaerobic digester, whereas HRT is the time it takes for wastewater or slurry to be digested in the digester. High SRT increases elimination capacity while decreasing digester volume. It also aids in the biological adaptation of hazardous compounds (Mao *et al.* 2015; Laiq Ur Rehman *et al.* 2019).

Because of the slow metabolic activity and growth of anaerobic bacteria, the retention period should be twice as long as the production time of slow-growing methanogens. The optimal HRT value for each process is determined by the feedstock quality and composition, process temperature and technology, and digester type. Lowering the retention time reduces the cost of running a biogas plant by reducing digester capacity, but also reduces the amount and quality of biogas generated (Schmidt, McCabe and Harris 2018; Guermazi-Toumi, Chouari and Sghir 2019; Laiq Ur Rehman *et al.* 2019; Tena, Perez and Solera 2021).

A higher HRT tends to result in a higher reduction of volatile solids and thus a higher biogas output in anaerobic digestion. An optimum HRT duration, on the other hand, is preferred for AD stability. Higher HRT improves volatile mass removal, digester volume requirements, and buffering capability for shock loadings and harmful chemicals protection in reactor effluent and sludge during AD (Valijanian *et al.* 2018; Laiq Ur Rehman *et al.* 2019; Christou *et al.* 2021).

2.4.2.3 pH

The digesting process is influenced by the operational pH. The rate of growth of the microbe is affected by changing the pH of the digester. Although studies have indicated that the best pH for operation is neutral (7.0), a pH range of 6.8 to 7.4 is commonly used (Mao *et al.* 2015). Methanogens are sensitive to acidic environments because they impede their growth, which has an impact on methane generation. In biogas generation, a pH range of 7.5 – 8 is recommended for increased yield and substrate degradation. A buffer solution such as $CaCO_3$ is frequently used to achieve pH balance by maintaining a neutral pH environment (Sanchez *et al.* 2000; Lohani and Havukainen 2018; Laiq Ur Rehman *et al.* 2019).

Studies by Zhou *et al.* (2021) showed that an increase in pH from 5 to 7 favours the production of VFAs. It increased acetate production while decreasing the production of ethanol and butyrate. Other researchers (Azizan, Yuzir and Abdullah 2021; Nabaterega *et al.* 2021) have found that acetogens and acidogens produce more volatile fatty acids (VFAs) in the pH range of 8-11, although operating an AD system in alkaline conditions is expensive. However, operating at an ideal pH range of 6.5–7.5 is more beneficial for higher methane output (Azizan, Yuzir and Abdullah 2021; Nabaterega *et al.* 2021; Zhao *et al.* 2021). Table 2-5 shows findings by various researchers as well as waste products used with the AD process parameters.

Table 2-5: Anaerobic digestion of different kinds of waste

Type of feed	Operation Conditions	Results	Reference
Food waste	Temp: 37ºC, OLR range of 6-8 gVS/L/d, pH of 5.5 and HRT of 34 days	The performance of an immersed membrane bioreactor was evaluated at OLRs ranging from 4 to 10 gVS/L/d; high OLRs were effective in terms of VFA buildup, with a maximum yield of 0.52 g VFA/gVS_{added} achieved at 6 gVS/L/d and at 8 gVS/L/d a maximum yield of hydrogen of 14.7 NmL/gVS was obtained.	(Wainaina *et al.* 2020)
Wastewater sludge	Temp: 35ºC, SRT of 15-20 days, OLR 19 Kg/m^3d and 8 kg/m^3d	AnFBR treated a primary sludge at an OLR of 19 kg/m^3d, eliminated 68% COD, had a VSS destruction efficiency of 70%, and TWAS of 20%, an ORL of 8 kg/m^3d removed 55% of COD and 56% of VSS.	(Mustafa *et al.* 2014)
Cow dung	Temp: 53ºC, pH of 6.65-7.81, HRT: 10days	With a VS of 47%, a COD reduction of 48.5%, and a biogas yield of 15 biogas/kg was achieved, it was established that cow dung might be one of the feedstocks for successful biogas generation.	(Abubakar and Ismail 2012)
Sugarcane bagasse (SCB)	Temp: 37 ± 1ºC, pH of 3 and HRT: 35 days	The combination of HPT180 + $Ca(OH)_2$ yielded a maximum of 220 mL/g-VS of methane, resulting in a 61.3% increase in methane yield over the untreated SCB.	(Mustafa *et al.* 2018)

2.4.3 Advantages and disadvantages of AD

AD has various advantages, including lower energy bills, decreased use of fossil fuels, reduced emissions of greenhouse gases, reduced methane emissions to the atmosphere from manure and slurries, and waste treatment (Mao *et al.* 2015). Nevertheless, there are some drawbacks to using this method; the high operating costs, low COD degradation, and there is an issue with heavy metals that cause inhibition, which lowers the yield and quality of biogas produced (Stuart 2006).

2.4.4 Improving the performance of the AD process

Although anaerobic digestion is the finest treatment method for energy generation and wastewater treatment, it also has drawbacks that make it a lengthy process (Stuart 2006; Ajay *et al.* 2020). In line with this, numerous studies in various fields have been conducted throughout the years to increase biogas and AD performance in terms of waste treatability. These consist of co-digestion with different substrates, adjusting operational settings, modifying the reactor, pre-treating the substrate, and using nanoparticle additions (Stuart 2006; Zaidi *et al.* 2018; Ajay *et al.* 2020). In addition to these, the introduction of nanoparticle additives appears to be the most favourable in terms of increasing the AD process performance.

2.5 Nanotechnology

Nanotechnology is important in the formation of nanoparticles with various chemical compositions, diameters, and regulated uniformity in size. The sequence of components or elements to form a whole compound is referred to as synthesis. Functionalization via conjugation to bioactive compounds is another type of synthesis (Gutierrez, Mendez and Vazquez 2017). The employment of traditional ways of synthesizing materials has been the foundation of formulation methods for nanoscale structures in previous years; yet the introduction of new technologies provides advantages that have been exploited in current years to generate nanoscale structures. To produce nanostructures, many technologies such as ultrasonic irradiation, thermal breakdown, co-precipitation, hydrothermal, zeolite encapsulation, microwave, and sol-gel have been used (Mohanraj and Chen 2006; Sakka 2013). Electronics, the food industry, medicine, catalysis, construction, cosmetics and sunscreens, renewable energy, and environmental remediation all use nanotechnology (Ealias and Saravanakumar 2017).

2.5.1 Magnetic nanoparticles

Magnetic nanoparticles (MNPs) are gaining popularity in advanced biological and medicinal applications. Magnetic nanoparticles have piqued the attention of researchers owing to their magnetic and catalytic capabilities, and several have attempted to synthesise magnetic nanoparticles with high functionality (Osaka *et al.* 2006; Zhu *et al.* 2018). Biomedicine, catalysis, and environmental purification are three areas where MNPs are discussed and widely applied. MNPs can be used in magnetic resonance imaging, image-guided medication delivery, and photothermal therapy, and they can detect or target biological entities after being modified with specific biomolecules (Yadollahpour 2015; Majidi *et al.* 2016b; Vaghari *et al.* 2016; Martinez-Boubeta and Simeonidis 2019; Maksoud *et al.* 2020; Tetteh, Amo-Duodu and Rathilal 2021).

Various preparation procedures have been investigated to manufacture MNPs with desired features and structures to understand the fundamental behaviour of superparamagnetism and identify related prospective uses of the MNPs (Shu and Wang 2009; Mahmoudi *et al.* 2011; Yadollahpour 2015; Fayazzadeh *et al.* 2020). However, preparing well-defined magnetic nanostructures which are considered the next generation of improved magnets, remains a difficulty. To establish control over the chemical composition, size, and structure of MNPs in this case, effective synthetic procedures are necessary (Willard *et al.* 2004; Okoli *et al.* 2011; Yadollahpour 2015; Elhambakhsh *et al.* 2020).

2.5.2 Synthesis of magnetic nanoparticles

Nanoparticle synthesis can be done in two ways: top-down and bottom-up. These two approaches are described below.

2.5.2.1 Top-down approach

This method involves a solid-state technique of breaking down bulk material into smaller units using physical processes such as crushing, milling, and grinding, among others. The shape and dimensions of this method are consistent. Though it has a well-uniform shape, it has a flaw on the surface of its structure that has a substantial effect on its physical properties and surface chemistry (Yadav, Yadav and Singh 2012).

2.5.2.2 Bottom-up approach

Bottom-up approaches work from the bottom up, atom by atom, molecule by molecule, to create nano-sized particles. This method results in nanomaterials that are homogenous in size, shape, and distribution (Das *et al.* 2020). This is a chemical process that is dependent on the

availability of a precursor. Sonochemistry (ultrasonic irradiation), thermal breakdown, co-precipitation, hydrothermal, zeolite encapsulation, microwave, gas-phase technique, sol-gel, and more types of this chemical process exist.

2.5.3 Types of synthesis method of magnetic nanoparticles

Magnetic nanoparticles can be created using a variety of techniques. Sonochemistry, hydrothermal, sol-gel, microwave, and co-precipitation are only a few examples. Liquid-phase chemical syntheses, for example, are a new method for creating magnetic nanostructures that allows for fine control over the nucleation and growth processes of nanoparticles with a variety of shapes and properties (Kefeni, Msagati and Mamba 2017; Zhu *et al.* 2018). However, the co-precipitation approach was utilized in this investigation because it produces more precipitates, employs widely available apparatus, and is less expensive because ordinary solvents such as water are used (Petcharoen and Sirivat 2012; Sandeep Kumar 2013; Kandpal *et al.* 2014; Majidi *et al.* 2016a)

2.5.3.1 Sonochemistry (Ultrasonic irradiation)

It is a technique that has been widely employed in biology, engineering, biochemistry, and other fields. It is a technique that has received a lot of interest recently. It is employed widely due to its short retention duration, high response selectivity, increased reaction rate, and energy savings (Bahadur *et al.* 2019). According to recent research, ultrasonic irradiation has an effect on particle size distribution due to the ultrasonic irradiation penetration into the solution, which triggers consistent activation energy of the reaction solution (Cao, Zhang and Huang 2005). The operating temperature is frequently 527°C to 14726°C or higher, with a pressure of > 100 atm, ultrasonic wavelength of 10 cm to 100 m, liquid speed of sound 1000 – 1500 ms^{-1}, and frequency ranging from 20 kHz to 12 MHz (Xia and Wang 2002; Casadonte, Li and Mingos 2007).

2.5.3.2 Hydrothermal synthesis

It is conducted in a pressured autoclave reactor filled with water or aqueous solution. In this technique, the temperature in the autoclave is frequently raised much over the boiling point of water in order to achieve saturation vapour pressure. Controlling particle size, morphology and surface chemistry, and the crystalline phase of nanoparticles is frequently useful by adjusting the temperature, pressure, composition, aging time, and solvent characteristics of the solvent (Chiu and Yeh 2007; Gan *et al.* 2020). The temperature ranges from 250ºC to 350ºC, the pressure usually ranges 10-80 MPa and sometimes up to 300 MPa, the reaction period ranges

3-10 hours, and the pH of the solution ranges 10-13 (Chiu and Yeh 2007; Hayashi and Hakuta 2010).

2.5.3.3 Microwave

Because of the electromagnetic irradiation, the molecules are excited in this process. The capability of the molecule to absorb microwave energy and transform it into heat is the important feature in this process, which is based on the efficient heating of materials by "microwave dielectric heating" (Brollo *et al.* 2017). Instead of being applied conductively through a vessel, heat is applied directly during this operation. Microwave dielectric heating is a non-quantum mechanical phenomenon that results in sample volumetric heating (Casadonte, Li and Mingos 2007; Dhinakar and Sundar 2017). Microwave synthesis operates under numerous parameters, including a temperature range of 120ºC to 260ºC, pressure of roughly 60 bar, electromagnetic vacuum wavelength of 0.1-100 cm, and frequency of 0.3 – 300 GHz (Bilecka and Niederberger 2010; Brollo *et al.* 2017).

2.5.3.4 Sol-gel

This approach comprises several stages, including hydrolysis of the metal precursor to make metal hydroxide solution, condensing the hydrolysed solution to form a three-dimensional gel, and drying to form the gel (xerogel or Aerogel) depending on the manner of drying used. The sol-gel method is classified into two pathways based on the media used for the reaction: aqueous sol-gel, which uses water as the reaction medium, and non-aqueous sol-gel, which uses an organic solvent as the reaction medium. Water, acid or base, or alcohol can be used to influence the kinetics reaction. Temperature and pH values can be employed to achieve the desired particle size and concentration of the precursor (Yang *et al.* 2006; Rao, Mukherjee and Reddy 2017). Based on these parameters, the Sol gel technique of synthesis processes; a temperature range of 120ºC to 800ºC, heating rate of 3ºC/cm (Vollath 2008).

2.6 Co-precipitation

As shown in Figure 2-5, the co-precipitation synthesis process incorporates varied salt solubility, where two or more salts that are soluble in water are used for the reaction. This entails the coexistence of growth, nucleation, coarsening or agglomeration processes (Ding *et al.* 2010; Mascolo, Pei and Ring 2013; Rane *et al.* 2018). When the solubility concentration of the solution of the product value is exceeded during this process, two or more water-insoluble salts are formed in the liquid phase, and precipitates form (Cervadoro *et al.* 2018; Rane *et al.* 2018; Wang, Li and Chen 2018). This occurs under extreme supersaturation circumstances.

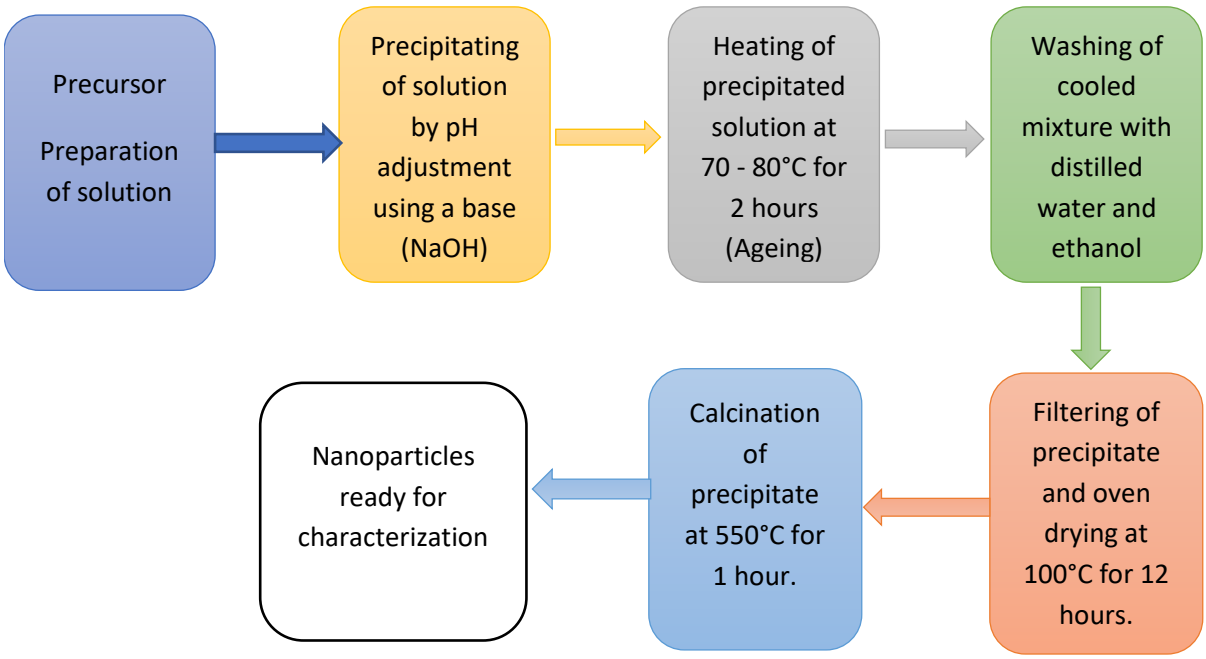

Figure 2-5: Flow diagram of the nanoparticle co-precipitation production process (El Ghandoor *et al.* 2012).

2.6.1 Advantages and disadvantages

Co-precipitation has the benefits of being a straightforward and quick process, easy to control particle size and composition, energy efficient, and employing commonly available apparatus. However, it has disadvantages such as containing residues of contaminants and being time intensive owing to being a batch-to-batch process (Maaz *et al.* 2007; Rane *et al.* 2018).

2.6.2 Application of synthesized magnetic nanoparticles on biogas production

Several researchers have investigated magnetic nanoparticles (MNPs). The application of MNPs to improve biogas generation has received a lot of attention. Several studies have confirmed the efficiency of MNPs in increasing biogas and methane output. This occurs because MNPs increase microbial activity, enhancing biogas and methane yield (Abdelsalam *et al.* 2016, 2017; Abdelwahab *et al.* 2020; Ajay *et al.* 2020). Chen, Steele and Stuckey (2018) reported that when 100 mg/L of Fe_2NiO_4 was added to the AD system on the seventh day, the cumulative output of methane was raised by 1.3 times the control. Abdelsalam *et al.* (2017) also stated that cumulative biogas and methane yields of 584 mL VS/g and 351 mL VS/g were

achieved, which were 1.66 and 1.96 times higher than the control, respectively. Different MNPs were tested in this study, and their effect on biogas and methane yield was measured.

A review by Ajay *et al.* (2020) highlighted on the physicochemical characteristics of nanoparticles, explaining why they are more advantageous in their application in biological systems. The authors reported that the solubility, catalytic nature, surface structure and area and size etc allows the nanoparticles to influence the direct interspecies electron transfer which enhances biogas production in AD. Nanoparticles have the capability to increase the rate of methane formation and also reduces the lag phase in AD (Baniamerian *et al.* 2019; Abdelwahab *et al.* 2020; Ajay *et al.* 2020).

Hassanein, Lansing and Tikekar (2019) revealed that adding NPs to poultry litter enhanced methane production using 12 mg/L Ni by 38.4%, 5.4 mg/L Co by 29.7%, 100 mg/L Fe by 29.1%, and 15 mg/L Fe_3O_4 by 27.5%. H_2S generation was significantly reduced when nanoparticles were used. The findings suggest that greater MNP mixture concentrations (in mg/L) (> 100 Fe, 12 Ni, and 5.4 Co) are more successful in reducing H_2S than increasing CH_4 production, but lower MNP concentrations enhanced CH_4 production and decreased the number of days required to reach maximum biogas production.

2.7 Biochemical methane potential with external magnetic exposure

The use of an external magnetic field in an anaerobic digestion system has been shown to be beneficial. According to Niu *et al.* (2014), exposing the AD system to a 20-40 mT magnetic field enhances microbial enrichment and improves the activity of activated sludge microorganisms at cold temperatures. A magnetic field of 7 mT improved bacterial growth and formaldehyde elimination in industrial wastewater, according to Łebkowska, Narożniak-Rutkowska and Pajor (2013). Other research has found that subjecting the AD system to a static external magnetic field increased microbial activity, resulting in improved biogas and methanation yields as well as improved wastewater AD treatability performance (Łebkowska, Narożniak-Rutkowska and Pajor 2013; Niu *et al.* 2013; Niu *et al.* 2014; Jia *et al.* 2018; Jia *et al.* 2020).

2.8 Kinetic models

The study of anaerobic digestion (AD) kinetics aids in the monitoring of digestion performance over time, including organic matter breakdown, biogas composition, biomass growth and

methane production (Fedailaine *et al.* 2015). As a result, kinetic models are utilized to evaluate and analyse the AD process. The kinetic model aids in determining inhibitor variables in the process and can be applied to simulate the AD process (Ondari 2015; Xie *et al.* 2016). The models used in the AD kinetic investigation are Monod, first-order, modified Gompertz, Chen and Hastimoto, Haldane, and dual pooled first order kinetic models (Rea 2014; Xie *et al.* 2016). In this survey, however, first-order and modified Gompertz kinetic models has been discussed.

2.8.1 First order kinetic model

The hydrolysis rate constant and potential maximum methane yield are calculated using a first-order kinetic model (Corbett 1972; Husain 1998; Pramanik *et al.* 2019). The information regarding the hydrolysis rate constant in the first-order kinetic model is based on the notion that hydrolysis drives the process (Pramanik *et al.* 2019). The cumulative methane yield determined during an experiment is the basis for this model (Dennehy *et al.* 2016). With an empirical relationship, a linear regress model is applied. The first-order kinetic model equation is given as,

$$\frac{dU}{dt} = -kU \ \ (U = U_0 \ at \ t = 0) \qquad (2.1)$$

Where:

k = first order kinetic degradation rate constant (1/d)

U = biodegradable substrate concentration (COD).

Integrating equation 2.1 over time, t (day) = 0 to t, produces equation 2.2.

$$\left[\frac{U_t}{U_0}\right] = e^{-kt} \qquad (2.2)$$

Where:

U_t = Substrate concentration at time t

This model, however, can be simply used when the gas yield is utilized instead of the substrate. The relationship between gas yield and substrate concentration is expressed as

$$\frac{U_t}{U_0} = \frac{S_m - S_t}{S_m} \quad (2.3)$$

Rearranging equation 2.3 gives equation 2.4.

$$S_t = S_m\,(1 - e^{-K_H t}) \quad (2.4)$$

Where:

S_t = Cumulative methane yield (mL)

S_m = Maximum methane yield, (mL)

K_H = rate constant for hydrolysis

t = time, day

2.8.2 Modified Gompertz

Researchers have adapted a modified Gompertz kinetic model over the years to explain the cumulative biogas production in an AD process (Yusuf, Debora and Ogheneruona 2011; Budiyono and Sumardiono 2014). The equation assumes that the specific growth rate of methanogen bacteria in a biodigester corresponds to the rate of biogas production (Seno 2010; Yusuf, Debora and Ogheneruona 2011; Budiyono and Sumardiono 2014). As seen in equation 2.5, this model helps to define the exponential development of bacteria in terms of its lag phase and growth rate (Nguyen *et al.* 2016; Deepanraj, Sivasubramanian and Jayaraj 2017).

$$S_t = S_m \times exp\left\{-exp\left[\frac{Ae}{S_m}(\lambda - t) + 1\right]\right\} \quad 2.5$$

Where

A = Maximum methane production rate (mL/g COD. day)

ʎ = Lag phase (day)

e = exp (1) = 2.7.183

t = time (day)

the constants: A, ʎ and S_m are determined by Microsoft Excel® Solver 365 tool set which uses a non-linear regression approach to determine the results.

2.9 Design of Experiment (DoE)

Design of experiment (DoE), in contrast to one-factor-at-a-time (OFAT), is a systematic approach to analyse several variables and responses in a process at the same time. It similarly produces a link between the factors that influence a process and its outcomes (Nasrabadi and Razavi 2010; N. Politis *et al.* 2017). Design expert is used in the design of experiment to examine the entire process after the experimental runs. The data from the experiment is used to create a mathematical model of the process. The experimental data obtained from the DoE can then be evaluated using response surface methodology (RSM) to optimise and predict parameters following the process (Nasrabadi and Razavi 2010; Montgomery 2017; Möller *et al.* 2019).

2.9.1 Response surface methodology (RSM)

Process optimization is an important component of engineering and process design in processes. This enables engineers to replicate the process devoid of wasting resources, lowering production costs.

Fractional factorial design, central composite design (CCD), and response surface methodology (RSM) are commonly used statistical design techniques used in optimisation to maximize the operating conditions of the process in order to achieve the best outcomes (Montgomery 2017; Politis N. *et al.* 2017).

When the influence of the reaction is subjective to various parameters, the application of RSM to optimise the process is required in the anaerobic digestion process. RSM is a combination of statistical and mathematical approaches that can be used to predict, design, optimise, and stimulate for optimal process conditions. It can also be applied to create a statistical correlation between the desired response and the input components or variables (Nasrabadi and Razavi 2010).

RSM determines the best operational conditions using the second-order and first-order polynomial models provided in equations 2.6 and 2.7. The second order design model is used in central composite design (CCD), which can modify factors over 5 levels; however, Box-Behnken design is used when factors are to be varied over 3 levels. These are two common reaction surface designs (Ferreira *et al.* 2007; Montgomery 2017).

$$Y = \beta_0 + \beta_1 B_1 + \beta_2 B_2 + \cdots + \beta_n B_n + \delta \qquad 2.6$$

$$Y = \beta_0 + \sum_{i=1}^{n} \beta_i B_i + \sum_{i=1}^{n} \beta_{ii} B_{ii}^2 + \sum_{i<j}^{n} \beta_{ij} B_i B_j + \delta \qquad 2.7$$

Where, Y is the response (dependent variable), β_0 is the constant (intercept), $\beta_{1,2,n,i}$ is the regression coefficient, B is the factor and δ is the error.

Because of its excellent findings and reasoning design, BBD is recommended for optimisation in most processes. Another advantage of the BBD is that it excludes combinations in which all elements are at their highest or lowest values at the same time. As a result, BBD designs are helpful in preventing trials conducted under harsh conditions, which may yield unsatisfactory findings (Tian *et al.* ; Ferreira *et al.* 2007; Goli and Sahu 2018; Kamyab *et al.* 2021). When the BBD and central composite design matrices were compared, the BBD matrix was shown to be somewhat more effective than the central composite design. The advantages of the BBD as a response surface tool for developing second order models were discussed in length by Bosque-Sendra *et al.* (2001). According to a survey by Ferreira *et al.* (2007), BBD is a good design for response surface methodology since it allows for the calculation of quadratic model parameters, the construction of sequential designs, the identification of lack of model fit, and the utilization of blocks.

2.9 Summary

So far, the literature review has proved that the anaerobic digestion process is the highly appropriate approach for organic waste disposal to produce energy. The energy generated by this AD process is a renewable source of energy that will compensate for the limitations of fossil fuels, namely the pollutions caused by the combustion of fossil fuels (Stuart 2006; Ajay *et al.* 2020). As a result, researchers have worked in a variety of methods to increase the performance of the AD system by increasing biogas and methane yield as well as wastewater treatability. Among the options investigated, the employment of nanotechnology has shown to be the most effective. It is with this perspective in mind that this study investigates several types of magnetic nanoparticles to improve biogas production and optimise the system to develop a more cost-effective and feasible wastewater treatment technology for generating energy.

Chapter Three

METHODOLOGY

Chapter three presents in detail the experimental work of the project. Section 3.1 describes the feasibility study that was carried out prior to the start of the research study using various metal nanoparticles. Section 3.2 describes the materials and equipment as well as chemicals and reagents used in the study.

Section 3.3 explains the experimental framework of the study. It describes the sample collections and characterisation, the synthesis method of the magnetic nanoparticles and how the characterisation of the synthesized particles were performed and also the application of the synthesized magnetic nanoparticles on the anaerobic digestion process via biochemical methane potential test (BMP) for biogas production from wastewater.

Finally, sections 3.4 and 3.5 outlines the optimisation of the BMP system, comparative study between magnetic and non-magnetic BMP systems and the kinetic studies.

3.1 Feasibility study of an anaerobic digestion system coupled with metal compounds

To ascertain whether the metal additives are effective in improving the performance of the anaerobic digestion system, a feasibility test was carried out using three metal compounds. The biochemical methane potential (BMP) test protocol used for the study was adapted from Mu, Chen and Xiao (2011). Iron (III) chloride (Fe), nickel (II) nitrate hexahydrate (Ni) and copper (II) nitrate trihydrate were the metal compounds used for the study.

The sample used for the study was obtained from a local sugar refinery industry in South Africa. The point of collection was the final effluent. This served as the feed to the bioreactors. The feasibility study was carried out to help the author understand the applicability of the nanoparticles (metals additives) in AD as well as give the author an understanding of the ranges of the additives loading rate for the AD systems.

The study was carried out by charging eight (8) bioreactors with 0.3 L waste activated sludge (WAS) and 0.5 L wastewater (WW), Table 3-1 presents the distribution of the samples and the metal additives loading. The bioreactors after charging were purged with nitrogen gas to

establish anaerobic conditions. They were then immersed in a thermostatic water bath operated at 40°C and digested for 10 days as shown in Figure 3.1. Daily monitoring of the biogas was done using the downward displacement method of gas collection. After the digestion period, the water quality and biogas compositions were evaluated.

Table 3-1: Sample and nanoparticles distribution in a BMP system

Bioreactor	Metals Loading (g)	Wastewater (L)	Activated sludge (L)
A- Fe	1	0.5	0.3
B- Fe	2	0.5	0.3
C- Cu	1	0.5	0.3
D- Cu	2	0.5	0.3
E- Ni	1	0.5	0.3
F- Ni	2	0.5	0.3
G- FeNiCu	2	0.5	0.3
H- Control	No NPs	0.5	0.3

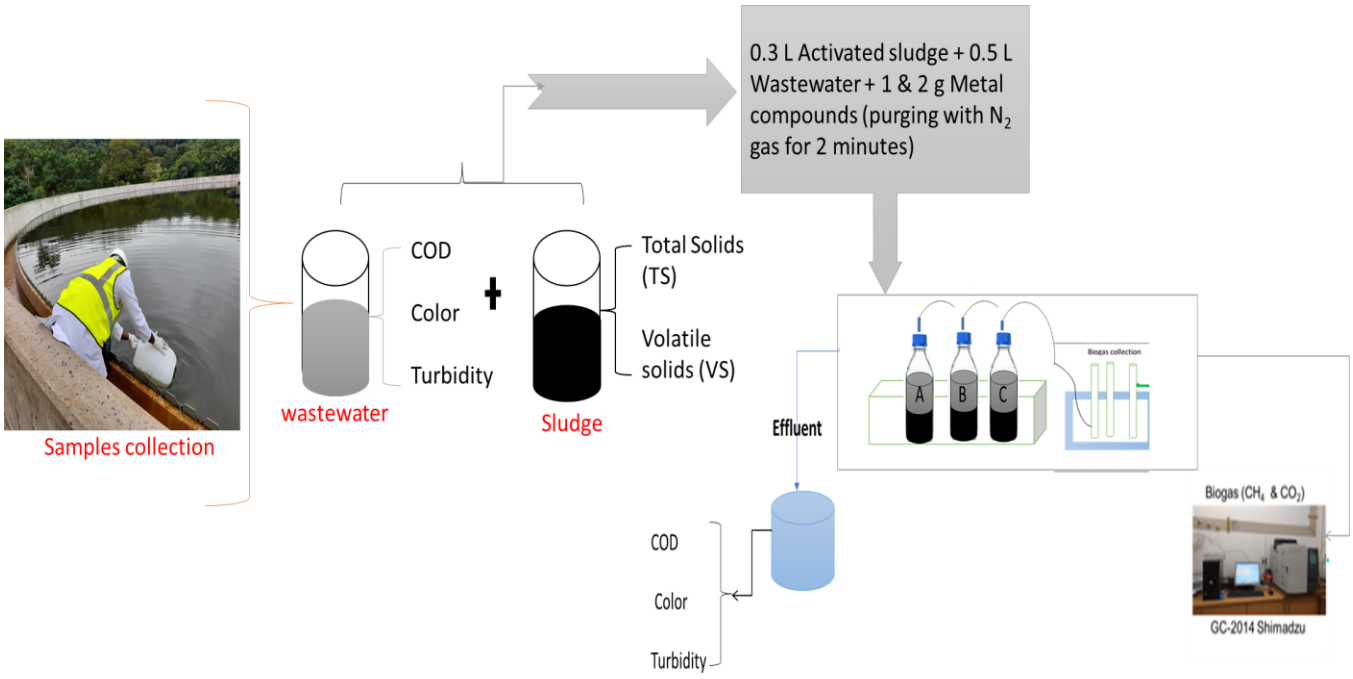

Figure 3-1: Diagrammatic representation of the biochemical methane potential assay of sugar refinery wastewater.

3.2 Materials and analytical equipment

3.2.1 Chemicals and reagents

All the chemicals and reagents utilized for the research study are listed in Table 3-2. These chemicals, which were purchased from local suppliers, were used for the synthesis of the magnetic nanoparticles. Three inorganic chemicals which include nickel (II) nitrate hexahydrate (Ni), iron (III) chloride (Fe) and copper (II) nitrate trihydrate were the metal nanoparticles used for the feasibility study. The other inorganic chemicals which include ferrous sulphate heptahydrate ($FeS0_4.7H_2O$), oleic acid (surfactant), ethanol, ferrous chloride hexahydrates ($FeCl_3.6H_2O$), nickel (II) nitrate hexahydrate, aluminium sulphate hexadecahydrate, magnesium sulphate heptahydrate, copper (II) nitrate trihydrate, and sodium hydroxide pellets (NaOH) were used for the synthesis of the magnetic nanoparticles.

Table 3-2: List of chemicals and reagents used for the study

Chemical	Purity	Supplier
Iron (III) chloride hexahydrate	ACS reagent, 97%	Sigma Aldrich, SA
Nickel (II) nitrate hexahydrate	(2N), 99.99% trace metal basis	Sigma Aldrich, SA
Copper (II) nitrate trihydrate	Analysis grade, 99%	Sigma Aldrich, SA
Sodium hydroxide pellets (NaOH)	ACS Grade-solid, 97.8% for pH adjustment.	Sigma Aldrich, SA
Ferrous sulphate heptahydrate ($FeS0_4.7H_2O$)	A.R, 98%	MINEMA, SA
Oleic acid (surfactant)	Technical grade, 90%	Sigma Aldrich, SA
Aluminum sulphate hexadecahydrate	ACS Grade, ≥ 97%	Sigma Aldrich, SA
Ethanol	anhydrous, ≥ 99.5%	Sigma Aldrich, SA
COD analysis	COD vials high range (0-1500 mg/L), HACH	Sigma Aldrich, SA

3.2.2 Analytical Equipment

The list of all the analytical tools used for the study are listed in Table 3-3 and pictures of the units has been presented in Appendix C. The equipment used for the analysis of the wastewater contaminants are presented in Table 3-3, with the procedure explained in detailed below in Section 3.3. The analysis conformed to the standard methods of water examination which also conforms to the National Water Act (AHPA 2007; SANS-SABS 2007; AHPA 2012).

Table 3-3: List of analytical equipment used in the study.

Water quality analysis	Instrument used	Method used
Turbidity (NTU)	HACH 2100N turbidimeter	Standard method
COD (mg/L)	DR3900 HACH spectrophotometer	Standard method and USEPA reactor gestion digestion method 8000
Colour (Pt. Co)	DR3900 HACH spectrophotometer	Standard method
Total solids (mg TS/L)	HCB602H analytical balance (22 ADAM)	Standard method
Volatile solids (mg VS/L)	HCB602H analytical balance (22 ADAM)	Standard method
pH	Hanna pH meter (HI2002 edge)	Standard method
CH_4 (%)	GC-2014 Schimadzu	Standard method
CO_2 (%)	GC-2014 Schimadzu	Standard method
Magnetic field (mG)	Electromagnetic field radiation tester (EMF-832)	Standard method

***** GC – Gas Chromatography**.**

3.3 Methods (Experimental framework)

3.3.1 Wastewater and Sludge samples collection

Three different kinds of wastewater were used for this research study. One was obtained from a local sugar refinery industry, while the second was from Umbilo water works with two sampling points (biofiltration and aeration system) and the final was obtained from Umgeni water, all in the KwaZulu-Natal province in South Africa. The point of collection was the effluent and the sample collected was the feed to the anaerobic digestion system. Two activated sludge samples were collected from the sugar refinery industry and the eThekwini municipal

water treatment plants. Figure 3-2 presented below, shows some images of the students at the sampling sites for the wastewater and activated sludge samples.

Figure 3-2 Images from the sampling points (Umgeni and Umbilo water works sites)

3.3.2 Characterisation of wastewater and activated sludge samples

The wastewater and activated sludge samples collected were characterised by following the standard methods for water and wastewater examinations by AHPA and were in conformity to the national water acts and SANS-SABS (SANS-SABS 2007; AHPA 2012). The general removal efficiency equation shown in eqn. 3.1 was used to determine the removal percentage of the pollutants. Sample calculations shown in Appendix A.

$$Removal\ Efficiency\ (\%) = \frac{Initial\ concentration\ (Ci) - Final\ concentration\ (Cf)}{Initial\ concentration\ (Ci)} \times 100 \quad (3.1)$$

3.3.2.1 Chemical Oxygen Demand (COD)

The level of pollution by organic matter is often accessed by determining the amount of chemical oxygen demand (COD) and biological oxygen demand (BOD). Studies have shown that COD is an important water quality parameter which is often used to ascertain the degree of pollution with organic matters (Pisarevsky, Polozova and Hockridge 2005; Li *et al.* 2018; Meng *et al.* 2020). COD in this study was determined by standard methods where 0.2 mL of

the samples were taken and dropped into the COD vials. It was digested for two hours and using the spectrophotometer, the COD content was determined (AHPA 2012; Meng *et al.* 2020). Using eqn. 3.1 the removal percentage of COD was determined.

3.3.2.2 pH

As described in section 2.4.2.3, pH is one of the AD factors which affects its performance. As such, the pH of the samples were analysed following the standard protocol using a pH meter (AHPA 2012).

3.3.2.3 Turbidity

Turbidity is a measure to assess the clarity of water. It is known to have an effect on the appearance of the water hence an important parameter to ascertain the quality of the treated water (Gumbi 2020). The turbidity of the samples in this study was determined by filtering 10 mL of the sample and using the turbidity meter to measure how turbid the water was. The removal efficiency was determined using the eqn. 3.1.

3.3.2.4 Colour

Colour is equally an important parameter in water quality analysis. The colour of the water also influences its appearance. In drinking water, high amount of colour shows poorly treated water. This study measured the colour by filtering 10 mL of the sample following the AHPA standard method (AHPA 2012) and using the spectrophotometer, the colour content was measured. Eqn. 3.1 was used to determine the removal efficiency.

3.3.2.5 Total Solids (TS)

For anaerobic digestion the amount of solids to be digested is important. The total solid is the residual left after evaporating the samples which was achieved in an oven. This was carried out by measuring 20 mL of the sample (sludge), placing it in a crucible and heating in an oven at a temperature of 100°C for 24 hours. This was done by following the standard methods (AHPA 2012).

The total solid content was determined by weighing the residue after heating along with pre-determined mass of the crucible; the total solid after digestion is determined using eqn. 3.2.

$$Total\ solids\ \left(\frac{mg}{L}\right) = \frac{B - A\ \times 1000}{Vs} \tag{3.2}$$

Where:

A is the mass of crucible (mg), ***B*** is the mass of crucible and sample after heating in an oven (mg) and ***Vs*** is the volume of sample measured (L).

3.3.2.6 Volatile Solids (VS)

According to standard methods for water and wastewater examination, volatile solids describe the weight which is lost after ignition in a furnace at a temperature of 550℃. The ignition is done for one hour. In this study, the volatile solid was determined using the activated sludge. After heating in the oven, the cooled residue was calcined in a furnace at 500℃ for 1 hour and the weight measured by following the standard method (AHPA 2007; AHPA 2012). The value of the volatile solids was calculated using eqn. 3.3.

$$Volatile\ solids\ \left(\frac{mg}{L}\right) = \frac{B - C\ \times 1000}{Vs} \tag{3.3}$$

Where:

B is the mass of crucible and sample after heating in an oven (mg), ***C*** is the mass of the crucible (mg) and residue after ignition and ***Vs*** is the volume of sample measured (L).

3.3.3 Synthesis of Magnetic nanoparticles

Magnetic nanoparticles are known to have many advantages that makes it most suitable for many industrial processes of which anaerobic digestion (AD) of wastewater to produce energy is a part of. To explore the full potential of the magnetic nanoparticles (MNPs) for AD process enhancement the co-precipitation method of synthesis was adapted. This involves the synthesis, characterisation, and application of the MNPs. The co-precipitation method used is described below.

3.3.3.1 Preparation of stock solution

The first step in the synthesis of magnetic nanoparticles via the co-precipitation method is the stock solution preparation of the chemicals to be used. With the known molecular weight of chemicals, concentration, and volume of solution to be prepared, the Sigma Aldrich mass molarity calculator was used to determine the mass to be measured. Table 3-4 presents the list of chemicals with their molecular weights and masses used for the stock solution preparation. The procedure is described as follows

- To prepare 1 L of 0.4 M Fe^{3+}, using the Sigma Aldrich mass molarity calculator, the mass was determined. Measuring the mass obtained that is 108.12 g of $FeCl_3.6H_2O$ salt was poured into a 1 L beaker and the salt was dissolved by adding 1 L distilled water.

The same procedure was repeated for all the salt stock solutions prepared by dissolving the mass presented in Table 3-5 of each salt in 1 L distilled water.

- The NaOH solution was also prepared using the same procedure, with the known molecular mass and concentration (3 M), 199.99 g of NaOH was then dissolved in a 1 L distilled water.
- The stock solutions were then transferred into a 1 L bottles, covered, and labelled for safety purposes.

Table 3-4: List of chemicals and their molecular weights and masses used for the 1 L stock solutions

Chemical	Molecular weight (g/mol)	Mass (g)
Ferrous chloride hexahydrates (Fe^{3+})	270.29	108.12
Ferrous sulphate heptahydrate (Fe^{2+})	287.55	55.61
Sodium hydroxide (NaOH)	39.997	199.99
Copper (II) nitrate trihydrate (Cu^{2+})	241.6	48.32
Nickel (II) nitrate hexahydrate (Ni^{2+})	290.79	58.16
Magnesium sulphate heptahydrate (Mg^{2+})	120.37	24.07
Aluminium sulphate hexadecahydrate (Al^{2+})	630.38	126.08

3.3.3.2 Co-precipitation synthesis method

Co-precipitation synthesis method is one of the mostly used synthesis method for nanoparticles synthesis due to their flexibility and simple procedure. In this study adapting and modifying the protocol used by Maaz *et al.* (2009) and El Ghandoor *et al.* (2012), the magnetic nanoparticles (MNPs) were synthesized. Figure 3-3 shows the graphical representation of the co-precipitation method. Synthesizing magnetite (Fe_3O_4) nanoparticle, a volume ratio of 1:1 (0.5 L/ 0.5 L) for 0.4 M Fe^{3+} and 0.2 M Fe^{2+} was measured. The precursor solutions were poured into a 2 L beaker on a magnetic hotplate. Using a mixing rate of 50 rpm the solution was stirred for homogeneity and the pH was found to be 2. Dropwise, 2 mL of oleic acid (surfactant) was then added to the mixture while stirring continuously. 250 mL of 3M NaOH

solution was then added dropwise while stirring (pH adjustment) until a thick black precipitate was formed, and the pH was found to be within 11-12. The mixture was stirred for 20 minutes before it was heated at 70°C for 2 hours while stirring continuously at 30 rpm (ageing). The mixture was allowed to cool at room temperature and filtered. The residue was washed thrice with distilled water and ethanol. It was then dried in an oven at 80°C for 12 hours and the dried precipitate was calcined at 550°C for 1 hour to get the magnetic nanoparticle (magnetite).

Hybrid nanoparticles that is the Al, Cu, Ni and Mg ferrites were synthesized using the same procedure, however, using the volume ration of 3:2:1 as presented in Table 3-5. The stock solutions prepared were measured for the ferrite nanoparticles. The resultant magnetic nanoparticles (MNPs) were bagged, and the samples characterised.

Table 3-5: Nanoparticle preparation volume distribution for co-precipitation

Nanocomposite	**Volume of solution measure (mL)**	**Symbols**
Fe_3O_4	Fe^{3+} = 500 Fe^{2+} = 500	mFe
$AlFe_2O_4$	Fe^{3+} = 500 Fe^{2+} = 333 Al = 167	AmFe
$MgFe_2O_4$	Fe^{3+} = 500 Fe^{2+} = 333 Mg = 167	MmFe
$NiFe_2O_4$	Fe^{3+} = 500 Fe^{2+} = 333 Ni = 167	NmFe
$CuFe_2O_4$	Fe^{3+} = 500 Fe^{2+} = 333 Cu = 167	CmFe

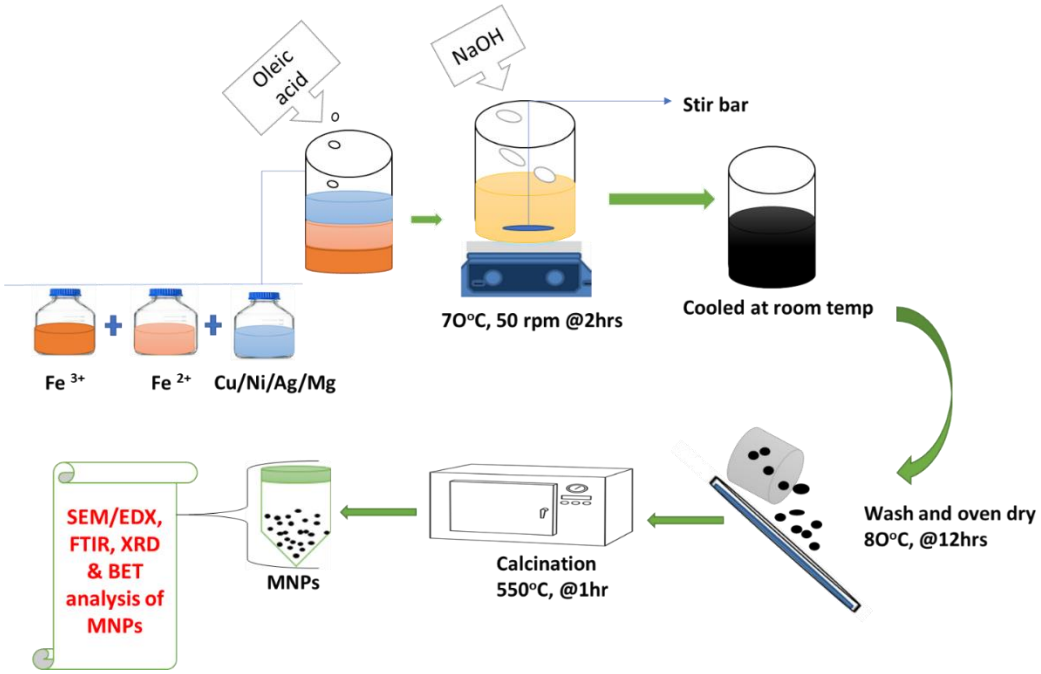

Figure 3-3 Schematic flow diagram of the co-precipitation synthesis of magnetic nanoparticles (El Ghandoor *et al.* 2012; Amo-Duodu *et al.* 2022).

3.3.6 Characterisation of MNPs

Characterisation of the synthesized MNPs was done to affirm the success of the synthesis by analysing the surface morphology, elemental composition, crystallinity and surface area and pore size using the scanning electron microscopy/energy dispersive X-ray, Fourier-transforms infrared spectroscopy, X-ray powder diffraction and Brunauer-Emmett-Teller analysis. The details of the analysis are described as follows:

3.3.6.1 Fourier-transform infrared spectroscopy (FTIR)

The organic, polymeric, and inorganic molecular structures and functional groups of the NPs were recorded using a Fourier Transform Infrared (FTIR) spectrometer in the 400 to 4000 cm^{1} range (Shimadzu FTIR 8400) as reported in the previous study by Amo-Duodu *et al.* (2022).

3.3.6.2 X-ray powder diffraction (XRD)

The crystal structures of the produced MNPs were studied using X-ray diffractometer equipment (Bruker AXS, D8 Advance) and PANalytical software at a target current of 40 mA and a voltage of 40 kV (Empyrean, PRO MPD, Netherlands). The particles were packed tightly into a rectangular glass cell and scanned using a J-J scan in conjunction with the copper anode (Cu-K radiation: =1.5406 Å) and Bragg-Brentano design.

The MNPs to be analysed were finely powdered, homogenized, and the average bulk composition was determined before the sample was placed in the centre of the sample holder on a glass slide and levelled to the appropriate height. The measurements cover a range of 5 to 85 (2θ) with an average step size speed of 0.0340 min^{-1}.

Lyn-Eye, a position sensitive detector, is used to record diffraction data at a typical speed of 0.5 sec/step, which is similar to the effective duration of a dazzling counter, which is 92 sec/step. The Debye-Scherrer equation (1), which establishes a relationship between particle size and peak enlargement, was used to compute the diameters of the NPs from the XRD data as described in the previous study by Amo-Duodu *et al.* (2022).

$$(d = \frac{k\delta}{\beta Cos\ \theta}) \quad (3.4)$$

Where β is the line broadening in radians obtained from the full width at half maximum height (FWHM) of the peak (determined using Origin software), d is the particle size of the crystal, k is the Sherrer constant (0.98), δ is the wavelength of X-ray radiation (CuKα = 0.15406 nm) and θ is the Bragg diffracting angle of the XRD diffraction patterns.

3.3.6.3 Scanning electron microscopy/energy dispersive X-Ray spectroscopy (SEM/EDS)

Scanning electron microscopy and energy dispersive X-ray (SEM/EDX) were used to determine the morphology and elemental analyses of the resultant materials (MNPs) at the University of Cape Town in South Africa (Nova Nano SEM coupled with EDT and TLD detectors. This was done at a magnification of 10–50 k and a 5 kV acceleration voltage (Amo-Duodu *et al.* 2022).

3.3.6.4 Brunauer-Emmett-Teller (BET)

The specific surface areas, pore volumes, and pore diameters of synthesized magnetic nanoparticles (MNPs) were measured using a BET Micrometric analyser (micromeritics TriStar II PLUS). 2 g of the samples were weighed and placed into the sample holder, which was then degassed for 24 hours at 400°C. It was allowed to cool before being placed under nitrogen gas at a pressure of 5 mmHg for the night (24 hours). The gasses used in the experiment were helium and nitrogen (Amo-Duodu *et al.* 2021b).

3.3.7 Application of synthesized MNPs on different wastewaters and sludge

The aim of the study was to evaluate the performance of synthesized magnetic nanoparticles on biogas production using anaerobic digestion. The synthesized MNPs were applied on three wastewater samples; industrial wastewater (sugar refinery plant) and municipal wastewater

(Umbilo water works and Umgeni water) which was obtained from local South African wastewater treatment plants (WWTPs). These wastewater was found to be suitable for anaerobic digestion since the organic contaminants were highly degradable. In this vein, biochemical methane potential (BMP) assay was carried out to evaluate the effects of the MNPs on the water quality, biogas, and methane yield.

3.3.7.1 Biochemical methane potential (BMP) test

The biochemical methane potential test was done according to the protocol adapted from Mu, Chen and Xiao (2011), Patil *et al.* (2014) and Hülsemann *et al.* (2020) which comprises of bioreactors with two outlets with connecting tubes, measuring cylinder immersed in a water trough, and thermostatic water bath. Figure 3-4 shows the experimental set-up for the BMP test. This was carried out by charging the bioreactors with wastewater and activated sludge in a volume ratio of 1:0.6 (0.5 L/ 0.3 L), leaving a head space of 20%. The bioreactors were dosed with 1.5 g of MNPs with one of the bioreactors set as the control for the experiment (no MNPs dosage). The mixture in each bioreactor was thoroughly mixed and purged with nitrogen gas to create anaerobic condition. The bioreactors were immersed in the water bath, operated at mesophilic temperature of 35°C and 40°C and hydraulic retention time (HRT) of 21 and 30 days. Tables 3-6 and 3-7 present the distribution of each bioreactor for each wastewater and activated sludge used. The bioreactors were left to stand for 48 hours before connecting the tube to the gas collections cylinders. Using the downward displacement method, the daily gas produced was monitored and recorded.

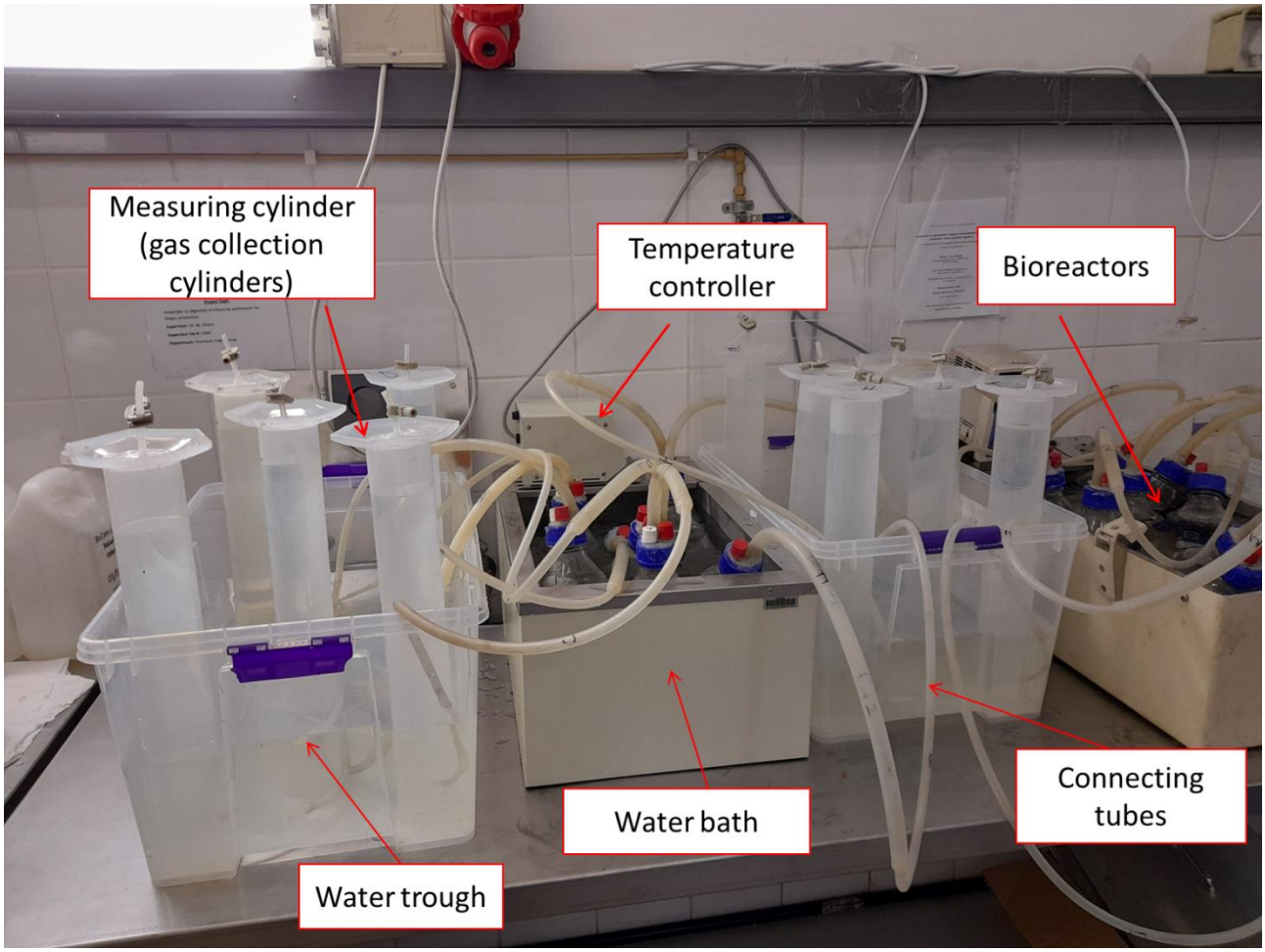

Figure 3-4 Schematic diagram of the experimental set-up of the BMP test

Table 3-6: Distribution of WW and AS for BMP test of sugar refinery WW operated at 35°C for 21 days

Bioreactor set-up	**Type of MNPs loaded**	**MNPs dosage (g)**	**Wastewater (L)**	**Activated sludge (L)**
A_{sw}	Fe_3O_4	1.5	0.5	0.3
B_{sw}	$AlFe_2O_4$	1.5	0.5	0.3
C_{sw}	$MgFe_2O_4$	1.5	0.5	0.3
D_{sw}	$NiFe_2O_4$	1.5	0.5	0.3
E_{sw}	$CuFe_2O_4$	1.5	0.5	0.3
F_{sw}	No MNPs	N/A	0.5	0.3

* SW is sugar refinery wastewater*

After the first experimental runs using all five synthesized magnetic nanoparticles, the best three performing MNPs were used for the next wastewater treatment. The BMP procedure as

described above was repeated and the distribution of the wastewater to sludge volume ratio (1:0.6 v/v) was as presented in Table 3-7.

Table 3-7: Distribution of WW and AS for BMP test of Umbilo WW operated at 40°C for 30 days (Biofiltration and Aeration system WW)

Bioreactor set-up	Type of MNPs loaded	MNPs dosage (g)	Wastewater (L)	Activated sludge (L)
Biofiltration system wastewater				
C_{bs}	Fe_3O_4	1.5	0.5	0.3
D_{bs}	$NiFe_2O_4$	1.5	0.5	0.3
E_{bs}	$CuFe_2O_4$	1.5	0.5	0.3
F_{bs}	Control	No MNPs	0.5	0.3
Aeration system wastewater				
C_{as}	Fe_3O_4	1.5	0.5	0.3
D_{as}	$NiFe_2O_4$	1.5	0.5	0.3
E_{as}	$CuFe_2O_4$	1.5	0.5	0.3
F_{as}	Control	No MNPs	0.5	0.3

The supernatant liquid of each bioreactor after the digestion period was decanted and then samples from the decant were taken for further analysis to check the water quality after treatment as described in section 3.3.2. Using eqn. (3.1), the removal efficiencies for each water quality parameter were calculated.

3.3.7.2 Gas collection and composition analysis

Using the downward displacement method for gas collection as used in the studies of Allured *et al.* (2014) and Patil *et al.* (2014), the biogas produced daily was monitored and the yield recorded.

The gas chromatography (GC-2014 Solution, Schimadzu, Japan) was used to characterise the composition of the biogas produced to determine methane and carbon dioxide yield. The Schimadzu GC-2014 solution, which had already been calibrated with pure CH_4 and CO_2 to measure the retention time, was used to determine the composition of the gas generated, according to established protocols.

The gas was collected using a 100 µl syringe and injected into the GC's gas port, which is integrated with a thermal conductivity detector and Poropak column. The system used N_2 gas

as the carrier gas hence in this study nitrogen gas was also used as the carrier gas for the analysis. The left and right column flow rates were 20 mL/min, with a column temperature of 40°C and pressures of 78–106 and 0.5–1.6 kPa for the right and left sides, respectively. The injection port had a temperature of 120°C, whereas the detector had a temperature of 250°C.

3.3.7.3 Kinetic study of BMP system

In anaerobic digestion processes, the kinetics and dynamics of the AD process are studied to understand the process mechanism and its performance over a digestion period. This study employs two kinetic models that is first order and the modified Gompertz models used by Budiyono and Sumardiono (2014) and Husain (1998) for the kinetic study of the BMP system. The cumulative biogas yield data obtained from the BMP experimental analysis were fitted on equations (3.6) and (3.7) to analyse the kinetic of each system.

$$S_t = S_m\,(1 - e^{-kt}) \tag{3.6}$$

Where,

S_t = Cumulative methane yield (mL/day)

S_m = Maximum methane yield, (mL/day)

k = rate constant for hydrolysis, (1/day)

t = time, (day)

$$S_t = S_m \times exp\left\{-exp\left[\frac{Ae}{S_m}(\lambda - t) + 1\right]\right\} \tag{3.7}$$

Where,

A = Maximum methane production rate (mL/day)

ʎ = Lag phase (day)

e = exp (1) = 2.7.183

t = time (day)

k = (A.e/Sm) is the maximum specific substrate uptake rate per the maximum biogas production, (1/day)

3.4 Optimisation of BMP system using Response surface method (RSM) analysis

In process engineering, the use of RSM is a useful tool that has been employed to optimise and understand the mechanism of processes. This study also uses this method to model and design the process to obtain optimum conditions for the BMP process. The use of Design expert was employed.

3.4.1 Design of experiment (DoE)

Utilizing the BBD from the Design-Expert software (version: 11.1.2.0) and four process variables (independent factors) were selected according to Table 3-8. Based on the process performance, pollutant removal efficiency in terms of percentage removal (%) of COD, turbidity and colour as well as biogas yield were considered as the response variables (dependent values).

Table 3-8: Box-Behnken design

Variable	**Factor code**	**Range and level of factors**		
		-1	**0**	**1**
Temperature (°C)	A	25	35	45
MNPs Loading (g)	B	0.5	1.0	1.5
Retention time (days)	C	15	30	45
Inoculum loading (mL)	D	300	400	500

These response variables were subjected to statistical analysis with RSM to ascertain the effect of interactions that the process factors had on the BMP process. The experimental data obtained based the BBD runs were fitted on a generic model equation (3.5) to generate regression models for the process as used by Ghaleb *et al.* (2020b).

$$Y = \beta_0 + \beta_1 A + \beta_2 B + \alpha_3 C + \beta_4 D + \beta_{11} A^2 + \beta_{22} B^2 + \beta_{33} C^2 + \beta_{44} D^2 s + \beta_{12} AB + \varepsilon \quad (3.5)$$

Y is the predicted response (% removal efficiency or biogas yield (mL/day)), ($\beta_0, \beta_1, \beta_2, \beta_3, \beta_4, \beta_{11}, \beta_{12}, \beta_{22}, \beta_{33}, \beta_{44}$); are the constant regression coefficient and *A, B,C* and *D* are the input variables (Process independent factors) and ε is the error

From BBD 27 experimental runs were designed with the conditions of each run generated as presented in Table 3-9.

Table 3-9: BBD design matrix for the 27 experimental runs for the BMP process.

	Factors				Responses			
Run	**A: Temperature ºC**	**B: Nanoparticle loading g/L**	**C: Retention time Days**	**D: Inoculum loading mL**	**Biogas Yield (Y_1) mL/day**	**COD (Y_2) %**	**Turbidity (Y_3) %**	**Colour (Y_4) %**
1	35	1	15	300				
2	35	1	45	500				
3	25	1	15	400				
4	25	1	30	300				
5	35	1,5	45	400				
6	35	1	45	300				
7	35	1	15	500				
8	45	1	30	300				
9	25	1	30	500				
10	45	1	15	400				
11	35	1,5	30	500				
12	35	1	30	400				
13	35	1	30	400				
14	35	0,5	15	400				
15	35	1,5	15	400				
16	35	0,5	30	300				
17	45	0,5	30	400				
18	45	1	45	400				
19	35	1,5	30	300				
20	45	1,5	30	400				
21	45	1	30	500				
22	35	1	30	400				
23	35	0,5	45	400				
24	25	1	45	400				
25	35	0,5	30	500				
26	25	0,5	30	400				
27	25	1,5	30	400				

3.4.2 Box-Behnken design (BBD) for optimisation

Numerical optimisation of the BMP process was carried out on the BBD of the Design-expert by fitting the variables obtained for the dependent responses by maximizing the response values while keeping the independent factors in range except temperature which was set at a target value of 35°C using the constraint as shown in Table 3-10. The four responses were maximized, and the optimum solutions were generated. The solutions generated from the optimisation was done at a confidence level of 95%.

Table 3-8: Constraint for BBD numerical optimisation for BMP system

Name	Goal	Lower	Upper
A: Temperature (ºC)	is target = 35	25	45
B: Nanoparticle loading (g)	is in range	0.5	1.5
C: Retention time (Days)	is in range	15	45
D: Inoculum loading (mL)	is in range	300	500
Biogas Yield (mL/day)	maximize	316	512
COD (%)	maximize	68	72
Turbidity (%)	maximize	68	72
Colour (%)	maximize	68	72

3.4.3 Validation analysis of the RSM study

Based on the numerical optimisation of the BBD matrix, optimum conditions and predicted responses were generated at a confidence level of 95%. The response models were verified by making a comparison between the predicted responses to the experimentally generated response. The predicted models were then verified using the optimum conditions to affirm the repeatability and applicability of the models at 95% confidence. A BMP test was carried out as described in section 3.5.1.1 and the distribution of the set-ups is displayed in Table 3-12. After the digestion period, each set-up was analysed based on APHA standard methods to determine the methane yield, COD reduction, turbidity and colour removal efficiencies. The results were then compared to the RSM predicted results and the deviation was determined.

The BMP test for the validation was done based on the conditions presented in Table 3-11. The set-ups were triplicated to check for repeatability.

Table 3-9: BBD- RSM optimum conditions for the validation assay.

Parameter	MNPs dosage (g)	Retention time (days)	Inoculum loading (mL)	Temperature (°C)
All maximized	0.5	45	500	35

Table 3-10: BMP set-up distribution for the validation assay.

Set-up	MNPs load (g)	Wastewater (mL)	Inoculum load (mL)
A_1	0.5	300	500
A_2	0.5	300	500
A_3	0.5	300	500
B_1	No MNP (control)	300	500
B_2	No MNP (control)	300	500
B_3	No MNP (control)	300	500

3.5 Magnetic biochemical methane potential versus non-magnetic biochemical methane potential test (m-BMP vs. nm-BMP)

From the RSM study, the optimum operational conditions for the BMP process obtained were used in this comparative study between a magnetised BMP and non-magnetised BMP system. Table 3-13 presents the optimum conditions generated from the RSM study for this BMP assay. In this comparative study, the control of the process was non-magnetised BMP, which had no external magnetic field exposure. Table 3-14 presents the BMP bioreactor distribution for each set-up used in this comparative study.

Table 3-11: Optimum operational conditions for the BMP process using BBD for RSM study.

Process	MNPs dosage (g)	Retention time (days)	Inoculum loading (mL)	Temperature (°C)
BMP	0.5	45	500	35

Table 3-12: BMP bioreactors (nm & m) distributions description using Fe_3O_4 MNP

Process	MNPs dosage (g)	Wastewater (mL)	Inoculum loading (mL)	Magnetic field Exposure (mT)
nm	0.5	300	500	No exposure
m	0.5	300	500	20

nm: non-magnetised BMP bioreactor and m: magnetised BMP bioreactor

3.5.1 Configuration of magnetic and non-magnetic BMP set-ups

A comparison analysis was conducted in this study, in which two AD systems were examined and conclusions were drawn. As shown in Figure 3-5, one of the systems was subjected to a 20 mT magnetic field while the other was not. Two magnetic stirrer/hotplates, stir bars, and two magnets (GMX 800) that serve as an external magnetic field make up the magnetic and non-magnetic BMP setups. Set-up m was exposed to an external magnetic field as illustrated in Figure 3-5, whereas set-up nm was not exposed to one.

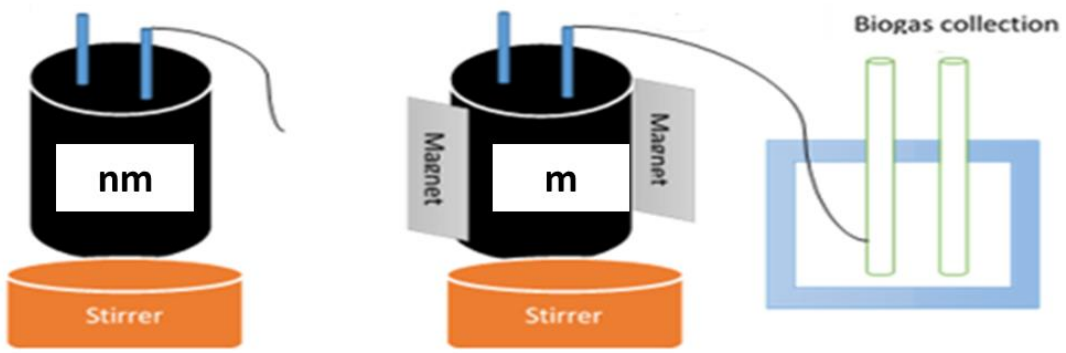

Figure 3- 5 Schematic diagram for magnetic (m) and non-magnetic (nm) BMP setups for biogas enhancement using MNPs (Kweinor Tetteh and Rathilal 2020).

3.5.2 Operation of magnetic (m) and non-magnetic (nm) BMP

Following the protocol outlined in section 3.3.7 the BMP assay was carried out. Throughout the digesting period, the set-up (m) was exposed to an external magnetic field of 20 mT for 3 hours while stirring and heating to keep the temperature at 35°C. The second set-up (nm) did not have an external magnetic field, but it was stirred and heated continually to keep the temperature at 35°C. As shown in Table 3-14, both setups were charged with wastewater feed

(300 mL) and inoculum (500 mL) leaving a headspace of 20% as described in section 3.3.7. Both setups were dosed with 0.5 g MNPs and digested for 45 days at a mesophilic temperature of 35 °C. The hotplates were used to control the temperature of the systems during the digestion period, as previously stated. Nitrogen gas was utilized to purge each system after charging and the set-ups were allowed to stand for 2 days to generate anaerobic conditions, and the biogas produced was monitored daily using the downward displacement method.

3.5.3 Analysis of samples after the magnetic (m) and non-magnetic (nm) BMP process

The samples from the nm-BMP and m-BMP systems were collected and analysed per standard methods as described in section 3.3.2 to determine the performance of the two systems. The efficiency of the systems in terms of pollutant removal were the COD degradation, turbidity and colour percentage removal and were calculated using equation 3.1 and the biogas compositions were analysed with the GC-2014 solution.

3.5.4 Kinetic study of magnetic and non-magnetic BMP system

The cumulative biogas yield data obtained from the BMP experimental analysis were fitted on equations (3.6) and (3.7) to analyse the kinetics of each system and deductions were made from the observations as described in section 3.3.7.3.

Chapter Four

RESULTS AND DISCUSSION

This chapter discusses the results obtained from the research study. The results include the feasibility study which was conducted prior to the study and is presented in section 4.1. Section 4.2 presents the characteristics of the wastewater samples used and synthesized magnetic nanoparticles while section 4.3 presents the biochemical potential test coupled with magnetic nanoparticles of the two wastewater samples used for the study, sugar refinery and municipal wastewater. Also, section 4.3 presents the optimisation study conducted for the BMP system. Finally, section 4.4 discusses the comparative study between the magnetic and non-magnetic BMP systems and the kinetic studies

4.1 Feasibility study of a BMP system coupled with metal compounds

This section discusses in detail all the results obtained from the feasibility study using the BMP assay for sugar refinery wastewater. The biogas yield and compositions are presented as well as the treatability performance of the BMP systems are discussed. The sugar refinery wastewater and active sludge characteristics which were analysed using standard methods (AHPA 2007; APHA 2012) before the BMP analysis are presented in Table 4-1. Also, the description of each BMP set-ups (A-H) in terms of the type of metal additives dosed with is presented in Table 4-2. The results presented show that the wastewater is above the limit for discharge as required by the Department of Water Affairs (DWA, 2020) and standards by Environmental Protection Agency (EPA) and Southern African National Standards (SANS-SABS 2007; Affairs 2014; University Of Pretoria 2013).

Table 4-1: Characteristics of wastewater and activated sludge sample

Water Parameter	Sugar refinery wastewater
COD (mg/L)	666 ± 28.90
Colour (Pt. Co)	3330 ± 232.67
Turbidity (NTU)	990 ± 40.23
pH	6.75 ± 0.26
Activated sludge	
TS (mg TS/L)	91.5 ± 10.78
VS (mg VS/L)	52.5 ± 8.98

Table 4-2: BMP bioreactor set-ups description

Bioreactor (s)	Metal additives
A	1 g – Fe
B	2 g – Fe
C	1 g – Cu
D	2 g – Cu
E	1 g – Ni
F	2 g – Ni
G	2 g – FeNiCu
H	No NPs (control)

4.1.1 Effect of metals of biogas and methane yield via BMP test

The anaerobic digestion process is characterised by two main products which includes the biogas (methane, carbon dioxide and traces of other gases) and the digestate. The biogas produced which is of major interest in this study is mainly made up of 55-65% methane and 45-35% carbon dioxide (Bachmann *et al.* 2015). In this study the aim was to enhance the yield of biogas as well as the methane produced by reducing the amount of carbon dioxide. It is in this vein that the metal compounds were added to serve as micronutrients and to stimulate the microbial activities which will increase the methane and biogas yield. The metal additives as studied by Abdelsalam *et al.* (2017), Baniamerian *et al.* (2019) and Abdelwahab *et al.* (2020) produces hydrogen which serves as a reducing agent to reduce the CO_2 to methane.

From Figures 4-1 and 4-2, the cumulative biogas yield and biogas composition respectively, have been displayed. The bioreactor dosed with 1 g of iron (Fe) metal NP, was found to have the highest biogas yield (13 mL/day). The yield was in order as follows: A (13 mL/day) > G (10 mL/day) > C (< 9 mL/day) > D (8 mL/day) > E (< 6 mL/day) > F (< 6 mL/day) > B (< 5 mL/day) > H (< 3 mL/day). it was observed that in the control set-up H, the yield recorded; < 3 mL/day which was less than that of the least yield amongst the bioreactors dosed with NPs, which is B (2 g of Fe) which recorded < 6 mL/day as presented in Figure 4-1 (Amo-Duodu *et al.* 2021a).

It was observed from Fig. 4-2 that upon the addition of the NPs to bioreactors A-G, there was more than 20% increase in methane as compared to the control which had 60-65% methane yield as already reported in the literature (Bachmann *et al.* 2015). The results from this study as presented in Amo-Duodu *et al.* (2021a) was consistent with studies by other researchers (Abdelsalam *et al.* 2017; Amen *et al.* 2018; Abdelwahab *et al.* 2020; Ajay *et al.* 2020).

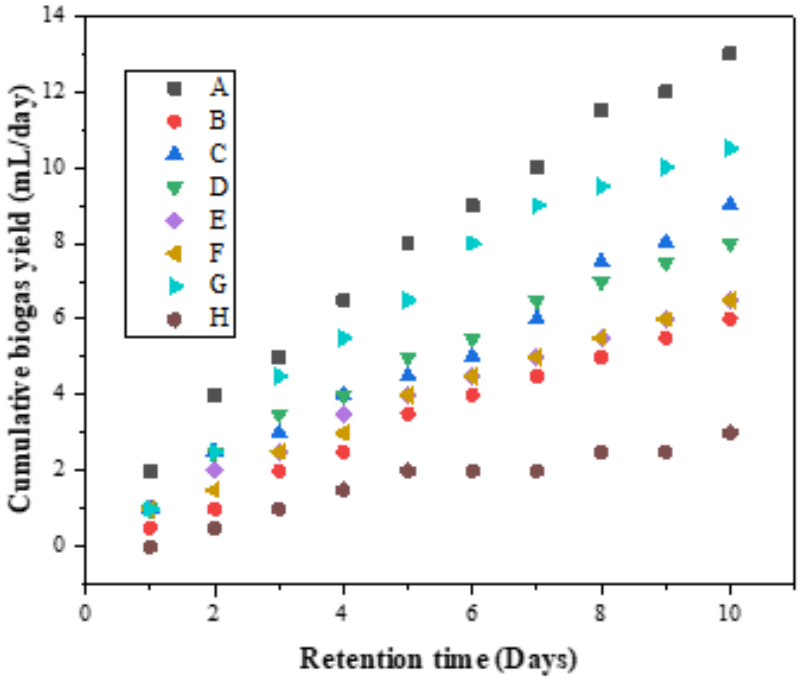

Figure 4-1 Cumulative biogas yield for BMP bioreactors A-H with metals loading of 1-2 g, temperature of 40ºC and HRT of 10-days.

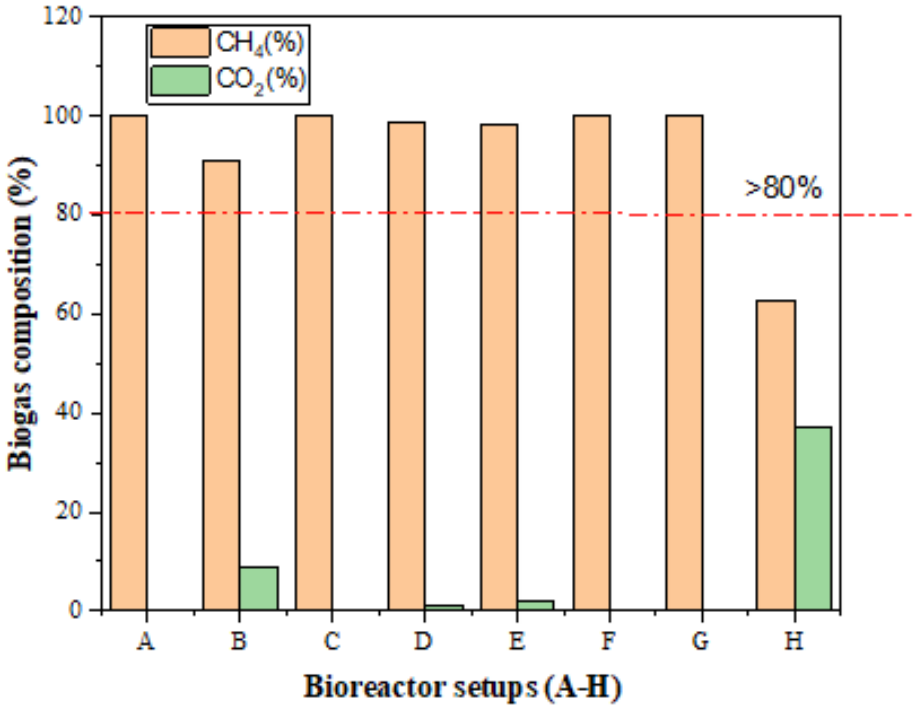

Figure 4-2 Biogas composition for BMP bioreactors A-H with NPs loading of 1-2 g, temperature of 40ºC and HRT of 10-days.

Table 4-3 presents the total solids and volatile solids of the activated sludge used for the digestion process. It is observed from the results displayed that after 10-days digestion the TS and VS were reduced in all the reactors with reactor A (24.5 mg TS/L and 17/7 mg VS/L remaining) recording the highest degradation of the solids (consistent with the highest biogas yield). Comparing the remaining TS and VS of the bioreactors dosed with other NPs (A-G) to the control bioreactor (H), it could be observed that the systems with NP additives showed high degradation of the solids as compared to the control (79 mg TS/L and 36 mg VS/L) with a VS/TS ratio of 0.4557.

Table 4-3: Characteristic of digestate (activated sludge after 10-days digestion) for bioreactors A-H.

Set-up	TS (mg TS/L)	VS (mg VS/L)	VS/TS
A	24.5	17.5	0.7143
B	53	31	0.5849
C	41.5	20	0.4819
D	48	24.5	0.5104
E	51	28	0.5490
F	50.5	27.5	0.5446
G	40	18.5	0.4625
H	79	36	0.4557
Feed	91.5 ± 10.78	52.5 ± 8.98	0.5738

4.1.2 Treatability performance of BMP test couple with nanoparticles on sugar refinery wastewater treatment

Figure 4-3 presents the results obtained from the treated wastewater after the 10-days digestion via BMP assay. These results show the percentage of COD, colour, and turbidity removal efficiency for the eight bioreactors (A-H). The results showed good degradation of organic content in terms of turbidity and COD for all the bioreactors dosed with NPs (A-G), of which bioreactors A, C, D, and G showed above 80% COD degradation with A dosed with 1 g of Fe being the highest for COD removal. It is also observed that only bioreactor G, dosed with 2 g of the mixture of three metals (FeNiCu) had over 80% degradation of COD, colour, and turbidity which was the best performing set-up among all the BMP systems and this was in consistent with other stuides (Nassar 2013; Peeters *et al.* 2016; Singh *et al.* 2019).

Comparing the performance of the BMP bioreactors (A-G) dosed with NPs to the control system H (no NPs), it is observed that they had much better reduction of COD and turbidity removal as compared to the control system (Singh *et al.* 2019). Again, it is observed that,

besides G which had above 80% colour removal efficiency, none of the systems was able to achieve 50% colour removal efficiency as reported by Amo-Duodu *et al.* (2021a).

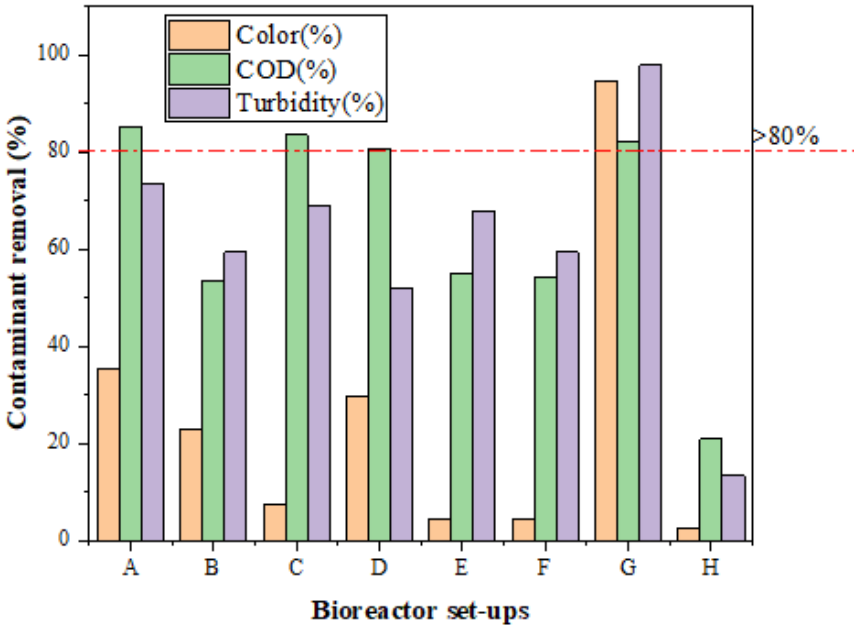

Figure 4-3 Contaminant removal of BMP bioreactors A-H with NPs loading of 1-2 g, temperature of 40ºC and HRT of 10-days.

4.1.3 Kinetic study of the BMP system coupled with nanoparticles.

The kinetics of the anaerobic digestion process is studied over the digestion period. This is done to understand the stability, biogas yield, reaction rate, and characteristics of the AD process (Chen and Hashimoto 1978; Husain 1998; Abu-Reesh 2014; Budiyono and Sumardiono 2014). The BMP process kinetics of each bioreactor was modelled using their cumulative biogas yield to fit on first order and modified Gompertz models as presented in Eqns. 3.6 and 3.7. Table 4-4 presents the summary of the kinetics study which showed a good correlation between the predicted biogas yield and actual biogas yield. It is observed that a good correlation between the predicted and actual biogas yield for all models existed, however, the correlation coefficient (R^2) values for modified Gompertz (>0.98) were higher as compared to the first-order kinetic model. Again, it is worth noting that the rate constant (k) values for both models showed were high indicating that a lower retention time is required to achieve a higher biogas yield and this was affirmed by the lag phase (ʎ) results obtained from the modified Gompertz as described by Amo-Duodu *et al.* (2021a). The cumulative yield of

bioreactor A with the highest R^2 value (0.9975) was fitted on the models which is shown in Figure 4-4. This also gives a pictorial explanation of how best modified Gompertz explains the dynamics, stability, and kinetics of the BMP set-ups as reported by (Budiyono and Sumardiono 2014); Amo-Duodu *et al.* (2021a).

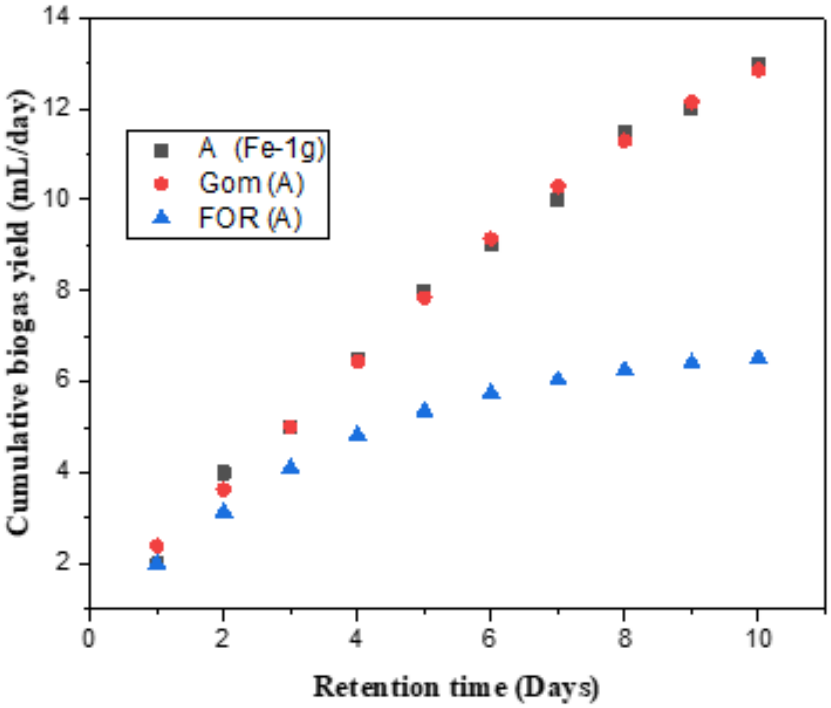

Figure 4-4 Fitting of cumulative biogas yield of set-up A (Fe - 1 g) on modified Gompertz (Gom) and First-order (FOR) kinetic models.

Table 4-4: Summary of the kinetic study results for the BMP Set-ups A-H

	First-Order kinetic model (FOR)						Modified Gompertz kinetic model (Gom)						
Set-up	St (mL/g COD)	Sm (mL/g COD)	Sp (mL/g COD)	k (1/day)	R^2	SSR	St (mL/g COD)	Sm (mL/g COD)	Sp (mL/g COD)	k (1/day)	R^2	SSR	ʎ
A	13	9.3374	11.5213	1.2061	0.9885	138.4375	13	15.6728	12.8500	1.7061	0.9975	0.5148	3.53
B	6	25.8469	5.3871	0.6212	0.988	0.2777	6	6.8438	5.8500	0.8712	0.9964	0.1509	3.94
C	9	44.1854	8.8134	0.8455	0.9874	0.9680	9	17.0378	8.9404	0.7413	0.9883	0.9084	2.99
D	8	12.5501	6.9925	0.7485	0.9787	0.2240	8	9.2115	7.8902	1.1652	0.9947	0.4673	3.25
E	6.5	9.9858	5.8370	0.5909	0.9857	0.0996	6.5	7.5988	6.4404	0.8612	0.9966	0.1978	3.34
F	6.5	12.7311	5.9560	0.6218	0.9880	0.1199	6.5	7.4234	6.3352	0.8617	0.9964	20.9998	4.88
G	10.5	18.0186	10.8268	1.0606	0.9607	1.1386	10.5	11.2381	10.4004	1.9564	0.9969	0.4957	3.08
H	3	4.1915	2.0731	0.2758	0.8930	0.5276	3	2.4950	2.4556	0.6508	0.9804	0.4460	6.88

*Sm: Maximum biogas yield, St: Measured biogas yield, Sp: predicted biogas yield by models, k: rate constant, R^2: correlation coefficient, SSR: Sum of square error, ʎ: Lag phases

4.1.4 Summary

This investigation was conducted before the main research study to confirm the feasibility of using nanoparticles as additives in anaerobic digestion for biogas production. The results of this feasibility study revealed that adding nanoparticles to the AD system has a significant impact on its performance. It is also worth noting that after adding nanoparticles to the BMP system, the methane yield increased by over 20% in all bioreactors dosed with the NPs.

It was also found to improve the degradability of the BMP system, with an increase in COD and turbidity reduction of over 20% when compared to the control system, which had no NPs. The kinetic analysis confirms the AD system's stability as a result of the NPs' biostimulation and explains that while the NPs had a considerable impact on the AD system, it was within acceptable limits. This was because the performance of the AD system was found to be lowered as the dose was increased from 1 g to 2 g. Though the use of NPs improves the AD system, it was also noticed that the NPs could not be recovered from the digestate after the digestion period. Hence, when disposed of may be dangerous to the environment, necessitating the need to recover and reuse or appropriately dispose of these NPs to minimize any future threats. Magnetic nanoparticles were proposed for this investigation in this vein for their ease of recovery, in addition to other advantages.

4.2 Characterisation of wastewater samples and synthesized magnetic nanoparticles (MNPs).

This section presents the results obtained from the characterisation of wastewater, activated sludge samples, and the synthesized magnetic nanoparticles used for the study.

4.2.1 Characterisation of wastewater and activated sludge samples

The characteristics of the wastewater obtained from the different sampling points (industrial and municipal) as presented in Table 4-5 show that they do not meet discharge standard limits as required by the Department of Water Affairs (DWA, 2020) (SANS-SABS 2007; Affairs 2014; University Of Pretoria 2013). The chemical oxygen demand of above 1000 mg/L shows high organic content and high degradability of the wastewater hence, rich for the anaerobic digestion as described by Enitan *et al.* (2015).

Table 4-5: Characteristics of wastewater (WW) and activated sludge (WAS) samples

Water parameter	Sugar refinery WW	Umbilo water works WW		Umgeni water works WW
		Biofiltration system (BS)	Aeration system (AS)	
COD (mg/L)	3570 ± 248.90	2380 ± 236.78	1340 ± 121.91	2300 ± 216.02
Colour (Pt. Co)	1340 ± 132.67	570 ± 13.73	170 ± 10.09	234.33 ± 5.31
Turbidity (NTU)	200 ± 10.23	73.2 ± 5.72	37.3 ± 5.03	37.3 ± 1.25
pH	4.27 ± 0.26	5.42 ± 0.67	6.59 ± 0.26	6.67 ± 0.47
ACTIVATED SLUDGE CHARACTERISTICS				
TS (mg TS/L)	584 ± 10.78	305 ± 7.89		41.33 ± 5.04
VS (mg VS/L)	419 ± 8.98	230 ± 5.90		32.33 ± 2.49

4.2.2 Characterisation of synthesized magnetic nanoparticles (MNPs)

The synthesized magnetic nanoparticles via the co-precipitation method with their volume compositions was presented in Table 3-6 and characterisation methods described in section 3.4**.** The results obtained are presented in this section. Table 4-6 describes the synthesized MNPs used in this study while Figure 4-6 shows the images of the synthesized MNPs.

Table 4-6: Synthesized magnetic nanoparticles (MNPs)

MNPs	Assigned Alphabet	Abbreviation used
Fe_3O_4	A	mFe
$CuFe_2O_4$	B	CmFe
$NiFe_2O_4$	C	NmFe
$AlFe_2O_4$	D	AmFe
$MgFe_2O_4$	E	MmFe

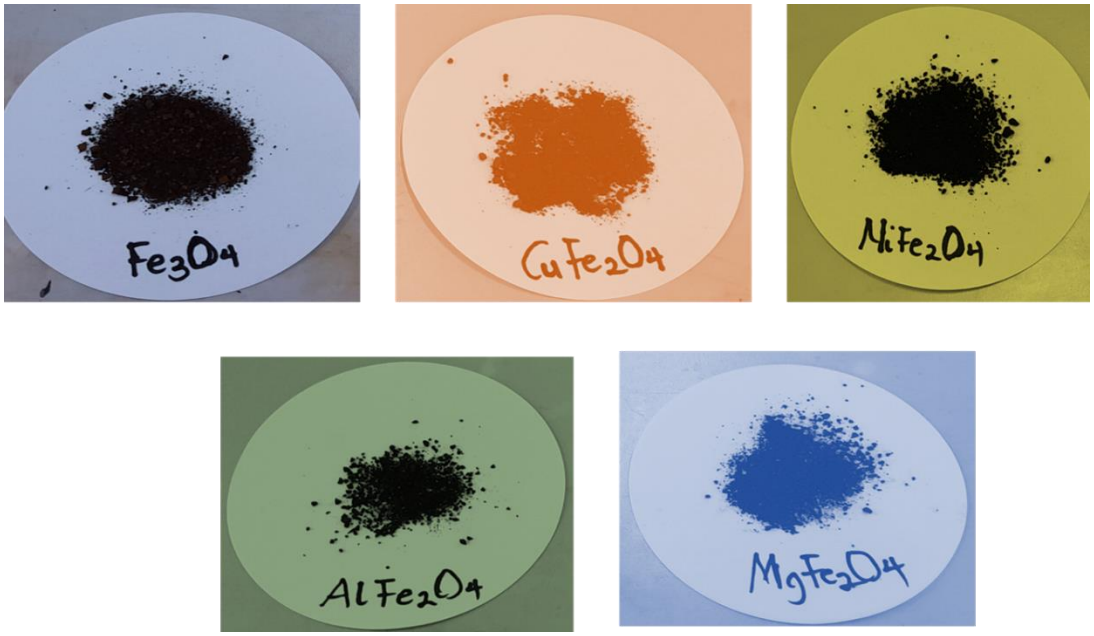

Figure 4-5 Images of the synthesized magnetic nanoparticles via co-precipitation.

4.2.2.1 Surface morphology and elemental composition of synthesized MNPs

The elemental compositions were obtained after the morphological study of a single MNP (magnetite) and its hybridized NPs. The SEM and EDX images of the synthesized MNPs are shown in Figures 4-6 and 4-7, with their compositions listed in Table 3-6. Figure 4-6 depicts a face-centred structure with agglomerated particles, which were detected at a microscale of 10 µm, with a magnification of 5000 kx and a landing energy capacity of 20 keV within a width distance (WD) of 5 - 6.5 mm.

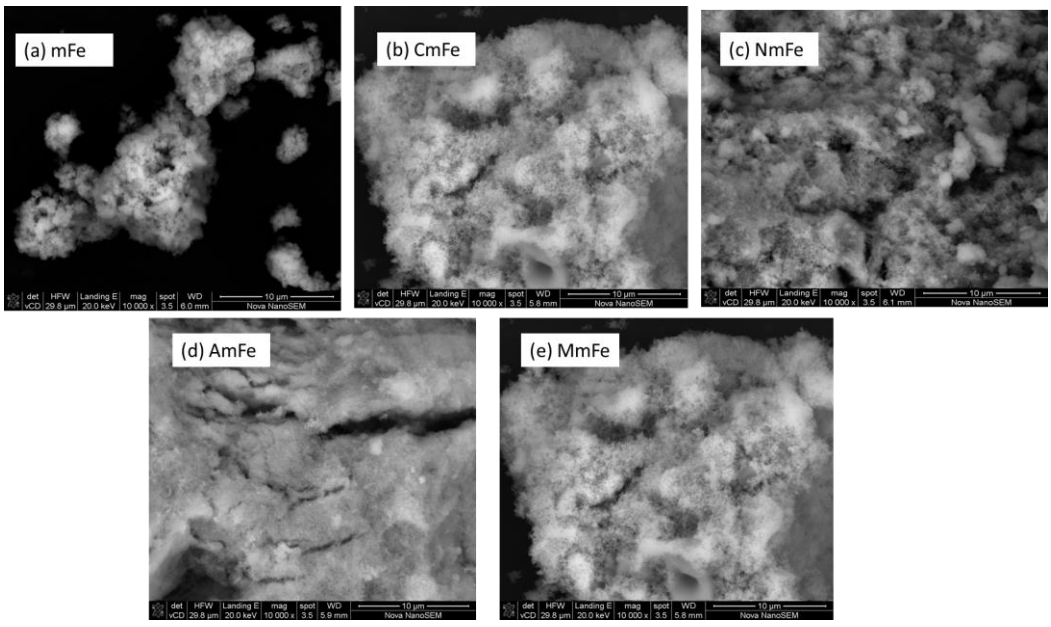

Figure 4-6 SEM images of synthesized MNPs as described in Table 3-6

Figure 4-7 shows the elemental compositions derived from the EDX spectra, which confirms the success of the nanoparticle magnetisation synthesis. The binding energies of Fe were discovered to be the peaks detected in the spectra from EDX images at 0.8, 6.3, and 6.8 keV, and they were shown to be common in all the images of the MNPs. The weight composition of magnetite (Fe_3O_4) was found to be 28.23% Fe and 27.59% O. These components are known to be the fundamental elements of magnetite, and they were found in all of the MNPs' spectra, confirming the synthesis success and the presence of magnetite in all of them (Shu and Wang 2009; Petcharoen and Sirivat 2012; Kandpal *et al.* 2014; Amo-Duodu *et al.* 2022).

The element weights for each MNP, as shown in Figure 4-7 and Table 4-7, revealed a homogeneous distribution of elements and no hysteresis in the magnetisation of the MNPs, which was also confirmed by Daou *et al.* (2006). They reported that MNPs are superparamagnetic and this was also reported in the previous study by Amo-Duodu *et al.* (2022).

Table 4-7: Elemental compositions of the MNPs obtained from the EDX analysis

Elements	**Weight (%)**				
	mFe	**CmFe**	**NmFe**	**AmFe**	**MmFe**
Fe	28.23	40.47	36.63	39.59	50.98
O	44.17	33.21	37.23	41.21	33.63
C	27.59	20.18	19.97	14.21	14.0
Ni	-	-	6,17	-	-
Al	-	-	-	3.18	-
Na	-	-	-	1.89	-
Cu	-	6.14	-	-	-
Mg	-	-	-	-	1.39

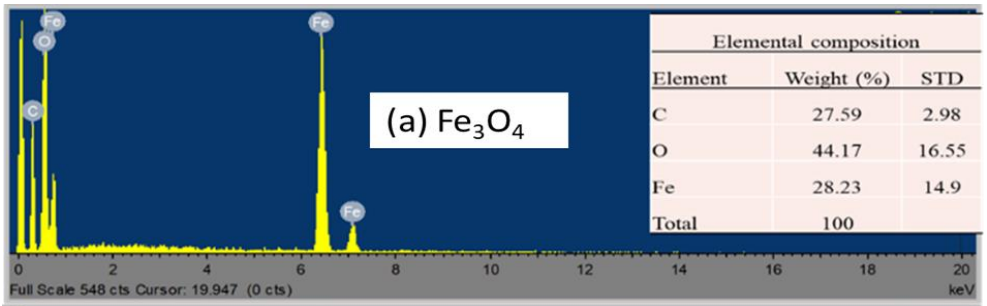

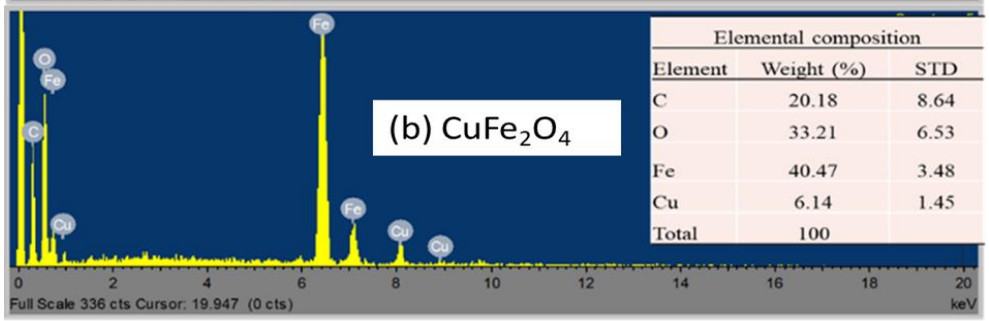

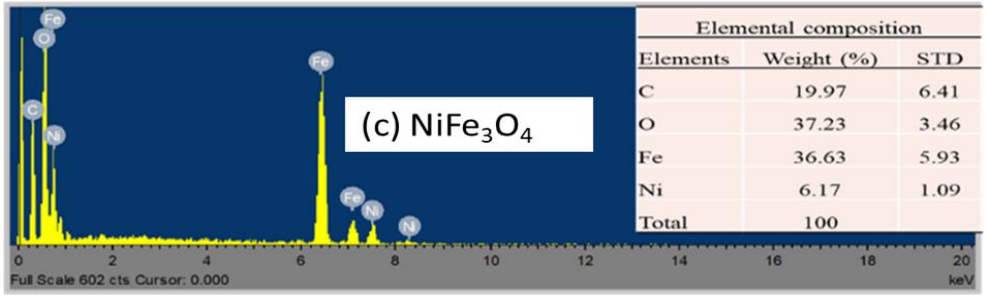

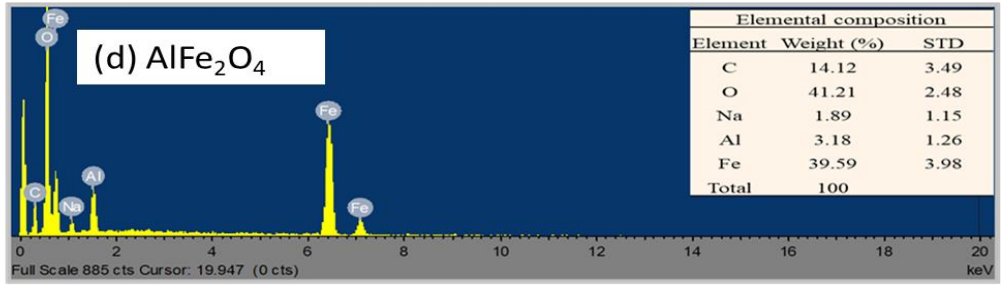

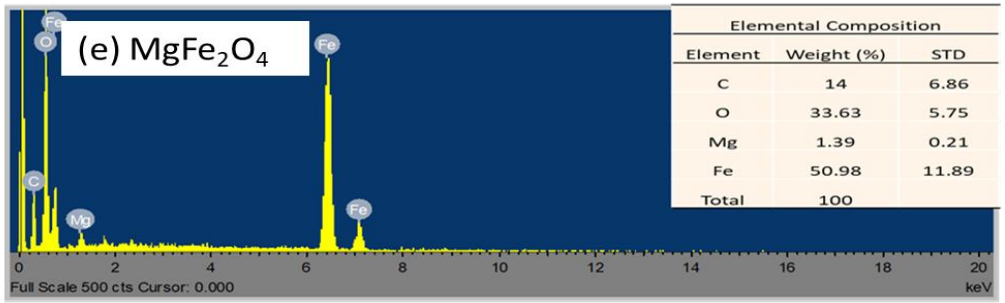

Figure 4-7 EDX images of synthesized MNPs as described in Table 3-6

4.2.2.2 Crystal structure analysis of synthesized MNPs

The XRD patterns for the MNPs are shown in Figure 4-8, along with their crystal diffractograms, which correspond to their original indexing in JCPDS data (Table 4-8). The diffractogram at 21.398° (2θ), for example, corresponds to the reflection (14) of ferrimagnetite with an interplanar distance of 3.893 Å indexed in JCPDS 00-070-2091, while the magnetite dominant at 35.423° (2θ) links to the image (227) index JCPDS 00-019-0629 with an interplanar distance of 5.197 Å indexed in JCPDS 00-019-0629. Thus, the MNPs' high crystalline nature (227) is consistent with the EDX images (Figure 4-7), which revealed magnetite (mFe) in all of the modified NPs. Furthermore, the strong peaks indicate that the MNPs have an excellent crystallised structure with tiny particle size and a well-indexed cubic spine Fe_3O_4 structure (Shu and Wang 2009; Petcharoen and Sirivat 2012; Kandpal *et al.* 2014; Amo-Duodu *et al.* 2022).

Table 4-8: Physical and chemical properties of the MNPs obtained from the XRD

2θ (degree)	**Miller indices (hkl) Plane**	**dhkl (nm)**	**Crystal structure**	**Nanostructure**	**JCPDS pattern**
21.398	(14)	3.202	Monoclinic	Ferrimagnetite	00-070-2091
35.423	(227)	5.197	Face-centred cubic	Magnetite	00-019-0629
65.976	(227)	5.420	Face-centred cubic	Copper Iron Oxide	01-077-0010

Other crystal structures of transition metal oxides, silicates, and carbonates were disclosed by combining their XRD pattern with their JCPDS data in Appendix A (Table A-7), which can be linked to the hydrolysis and condensation reactions of their metal ions (Petcharoen and Sirivat 2012; Kefeni, Msagati and Mamba 2017). In addition, the presence of carbon in the mFe (Figure 4-7) impacted majority of the MNPs surface strain, causing their magnetite peaks to shift (Figure 4-8). Other iron oxides, such as ferrimagnetite, ferromagnetite, maghemite, mikasite, magnesioferrite, thermonatrite, and sylvite, were discovered (Table A-7). Magnetite and maghemite, for example, are reported by (Daou *et al.* 2006); Petcharoen and Sirivat (2012);

(Amo-Duodu *et al.* 2022) to have high biocompatibility and superparamagnetic characteristics

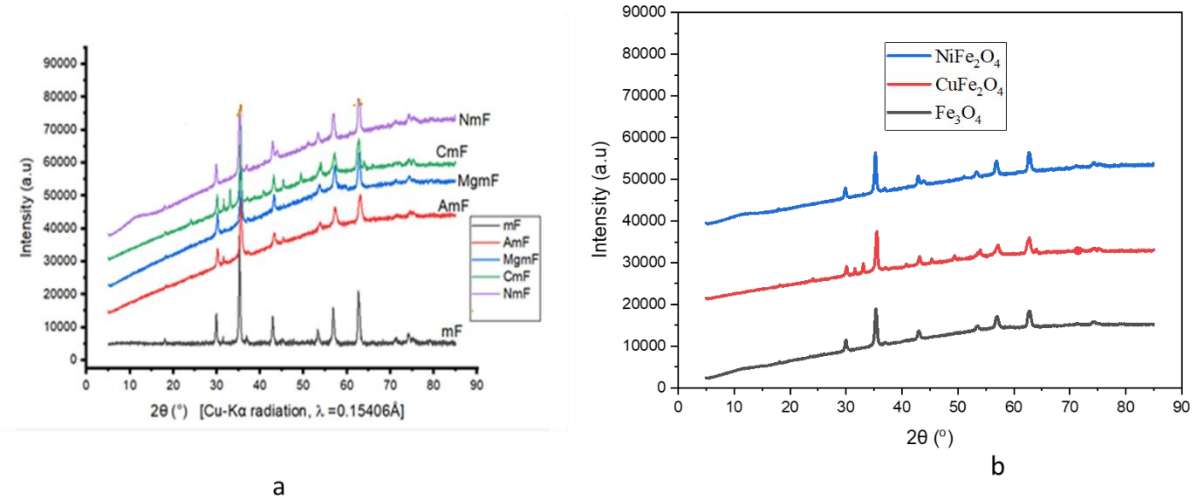

Figure 4-8 XRD spectra of (a) all five and (b) best performing synthesized MNPs as described in Table 3-6.

4.2.2.3 Functional group characteristics of synthesized MNPs.

The FTIR spectra of the MNPs are shown in Figure 4-9, revealing their functionality in terms of stability, oxidation, and reactivity. Surprisingly, the fingerprint region of wavenumber 2000 – 400 cm^{-1} contains the majority of the chemical and functional groups. In addition, the O-H vibrations of water have been linked to the spectrum range 4000 – 1500 cm^{-1}, which includes bands that emerge at 3600 cm^{-1}, 3000 cm^{-1}, and 1620 cm^{-1} (Petcharoen and Sirivat 2012; Kefeni, Msagati and Mamba 2017).

Table 4-9 presents the common peaks observed in all the FTIR spectra for the MNPs. The fact that these peaks have shifted significantly indicates that the hydrocarbon chains encircling the MNP monolayers were tightly packed in their crystalline phases (Petcharoen and Sirivat 2012; Kefeni, Msagati and Mamba 2017). The area of vibrations in the 1500-900 cm^{-1} ranges correlates to the emergence of surfactant and NP molecules (Amo-Duodu *et al.* 2022).

Furthermore, the bands were seen at 584 cm^{-1} and 629 cm^{-1} between 850 and 500 cm^{-1} can be attributed to magnetite and maghemite in their oxidized forms (Petcharoen and Sirivat 2012). The absorption peaks at 530 cm^{-1} is due to Fe-O vibrations and are related to the magnetite phase, as reported by Shen *et al.* (2014).

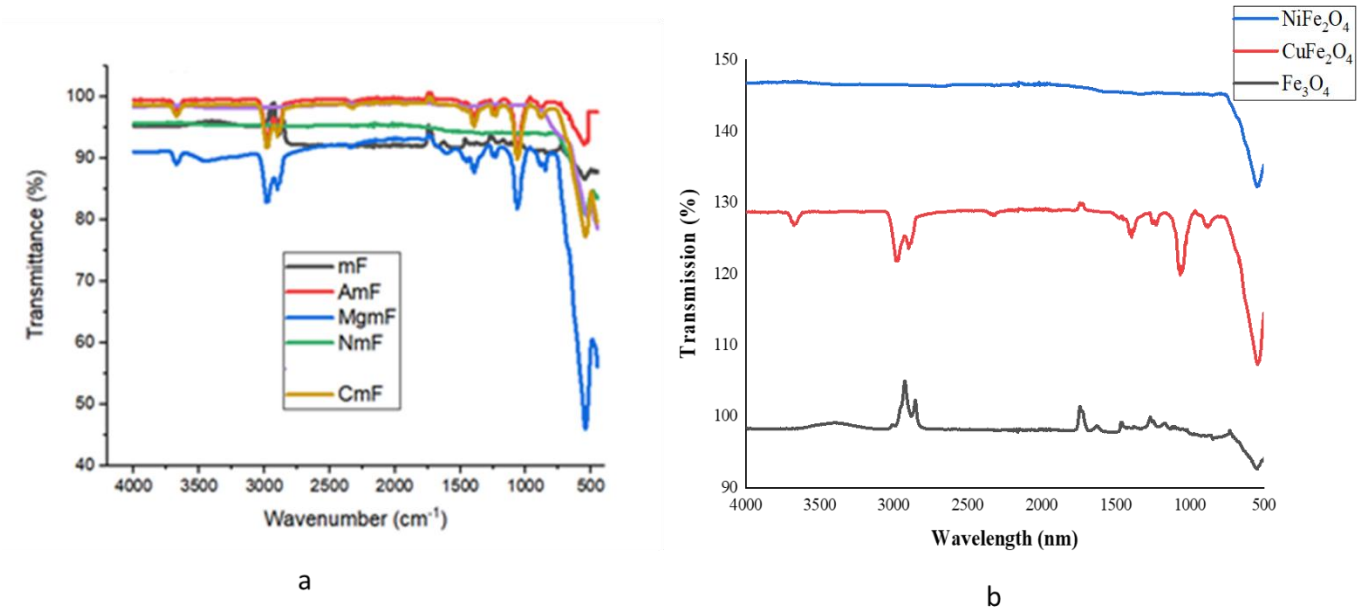

Figure 4-9 FTIR spectra of (a) all five and (b) best performing synthesized MNPs as described in Table 3-6.

Table 4-9: Functional groups identified from the FTIR analysis of synthesized MNPs

Wavelength (cm^{-1})	**Functional group**
3600, 3000, 1620	O-H stretching
2924, 2854	CH_2 stretching
1394, 1120	C-Vibration
1250-1000	Carboxyl
584, 629	Magnetite, maghemite
530	Fe-O vibration

4.2.2.4 Pore size, volume, and surface area of synthesized MNPs.

The BET analysis of the synthesized MNPs with their compositions presented in Table 3-6 reveals the pore size and volume as well as the surface area of the MNPs. In the application of MNPs, the surface area and particle size have an impact on its performance (Lee *et al.* 2005; Petcharoen and Sirivat 2012; Houshiar *et al.* 2014; Danso-Boateng *et al.* 2021). The pore volume, size, and surface area obtained for the MNPs are presented in Table 4-10. It was observed that the order of highest surface area follows mFe > CmFe > NmFe > MmFe > AmFe.

The high calcination temperature (550°C), which improved the liquid-solid adsorption capacity, may be linked to the development of a broad pore size range, spanning from narrow microspores to vast mesopores as reported in the previous study by Amo-Duodu *et al.* (2021b).

Table 4-10: BET analysis results of synthesized MNPs

MNPs	BET surface area (m^2/g)	Pore volume (cm^3/g)	BJH Pore size (nm)
mFe	27.597	0.008	1.484
CmFe	19.289	0.005	1.404
NmFe	10.085	0.003	0.995
AmFe	9.733	0.017	1.537
MmFe	10.017	0.009	1.444

4.2.3 Summary

The surface morphology, crystallinity, functional groups, surface area, pore size, and volume, as well as the elemental composition of each of the synthesized magnetic nanoparticles (MNPs) were all examined during the characterisation process. The results reveal that the co-precipitation synthesis procedure was successful; the elemental compositions showed that magnetite (Fe and O) is present in each of the MNPs, with particle sizes ranging from 3.2 to 5.42 nm. The surface area of magnetite (27.59 m^2/g) was found to be larger than that of hybridized NPs (less than 20 m^2/g but greater than 9 m^2/g). The goal of the synthesis was realized when the co-precipitation approach was employed to magnetise all the NPs successfully.

4.3 Biochemical methane potential (BMP) test.

The results obtained from all the BMP tests carried out for the two types of wastewaters and activated sludge samples are presented in this section. Table 4-11 presents the distribution of MNPs as per the BMP set-ups used for the study for the various wastewater samples.

Table 4-11: BMP set-ups (bioreactors) assigned to each MNPs

MNPs	Assigned Set-up (Sugar refinery wastewater treatment)	Assigned Set-up (BS & AS wastewater treatment)
$AlFe_2O_4$	A_{SW}	-
$MgFe_2O_4$	B_{SW}	-
Fe_3O_4	C_{SW}	C_{AS} & C_{BS}
$CuFe_2O_4$	D_{SW}	D_{AS} & D_{BS}
$NiFe_2O_4$	E_{SW}	E_{AS} & E_{BS}
Control (no MNPs)	F_{SW}	F_{AS} & F_{BS}

*SW- sugar refinery wastewater, AS- Aeration system wastewater and BS- Biofiltration system wastewater.

4.3.1 BMP assay on sugar refinery wastewater and activated sludge samples

The results that were obtained from this BMP study using the sugar refinery wastewater are presented in this section. As mentioned in the methodology, the sugar refinery wastewater was found to have a high chemical oxygen demand (COD) content which confirms the studies by Enitan *et al.* (2015). They reported that high COD content shows that the wastewater is highly degradable and can be used as a feed for the anaerobic digestion process. The results presented reflect the 21-days digestion period.

4.3.1.1 Effect of magnetic nanoparticles on water quality

The use of anaerobic digestion for wastewater treatment has been widely used over the past decade where the organic matter is degraded, and the removal efficiency evaluated (Chollom *et al.* 2020). The AD process, however, falls shorts in degrading all organic matter, hence the need to improve its efficiency (Chollom *et al.* 2020; Amo-Duodu *et al.* 2021b). In this study, the effect of synthesized magnetic nanoparticles with their composition presented in Table 3-6 was evaluated on the water quality after treatment of which COD, colour, and turbidity were the water parameters observed.

Figure 4-10 presents the efficiency for each BMP bioreactor over the 21-day digestion. The bioreactors dosed with MNPs had above 70% removal efficiency for COD and turbidity.

However, only bioreactor Csw dosed with mFe showed over 70% colour removal efficiency with the rest having around 60% except the control set-up (Fsw) which had below 50% removal efficiency.

The results affirm that the addition of MNPs to the BMP system had a significant impact on its performance in comparison to the control (Fsw) which had around 60% removal efficiency for COD (56.27%), colour (49.91%), and turbidity (53.20%) (Brar *et al.* 2010; Abdelsalam *et al.* 2017; Ajay *et al.* 2020; Amo-Duodu *et al.* 2021a; Amo-Duodu *et al.* 2021b). Among the BMP bioreactors dosed with MNPs, it was found that bioreactors Csw, Dsw, and Esw had over 60% removal efficiency in terms of COD, colour, and turbidity. Turbidity reflects the clarity of the water and does not always indicate a health risk; however, it is critical to remove the turbid particles before discharge to meet the discharge limit as specified by the standards (Gumbi 2020). The obtained results indicated that the majority of the turbidity was removed with approximately 70% efficiency. Colour removal was less than effective, showing less than 70% removal efficiency obtained.

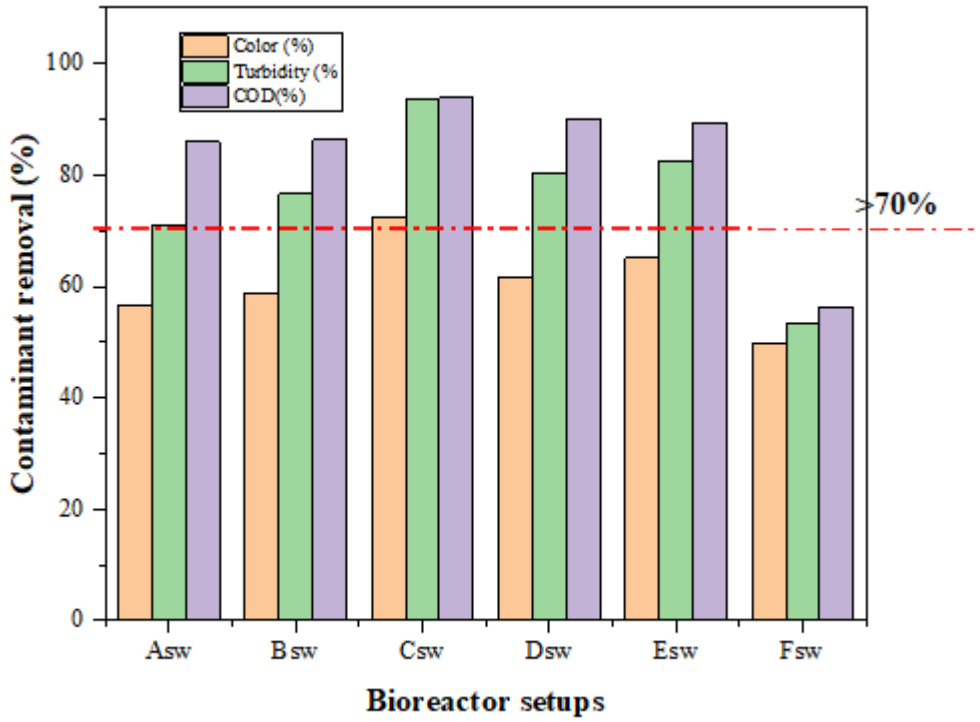

Figure 4-10 Reactor removal efficiency for BMP bioreactor A_{sw} – F_{sw} with MNP loading of 1.5 g at 35ºC and HRT of 21 days.

4.3.1.2 Biostimulation effect of magnetic nanoparticles of BMP for biogas production

Anaerobic digestion as a well-known biological process mostly used for waste treatment to generate energy depends mostly on the temperature, pH, organic loading rate and retention for good performance (Deublein and Steinhauser 2011; Chen and Neibling 2014; Dobre, Nicolae and Matei 2014; Bachmann *et al.* 2015). The biostimulation effect of MNPs for biogas production was analysed in this study.

The BMP bioreactors biogas yield was recorded daily using the downward displacement method of gas collection and the cumulative yield was obtained as presented in Figure 4-11. The results showed a high yield for the bioreactors (Asw -Esw) which were dosed with MNPs as compared to the control system (Fsw). Bioreactor Csw was found to have the highest biogas yield (280 mL/day) with 85.94% COD degradation. The biogas yield for the bioreactors reported was found to follow the order Csw (280 mL/day) > Dsw (175 mL/day) > Esw (145 mL/day) > Bsw (135 mL/day) > Asw (80 mL/day) > Fsw (45 mL/day). The MNPs added were found to stimulate the microbial activities which in turn helps in the degradation of the organic matters to energy. The performance of the microorganisms was improved which also increased the yield of methane (Abdelsalam *et al.* 2016, 2017; Ajay *et al.* 2020; Kweinor Tetteh and Rathilal 2020; Amo-Duodu *et al.* 2021a).

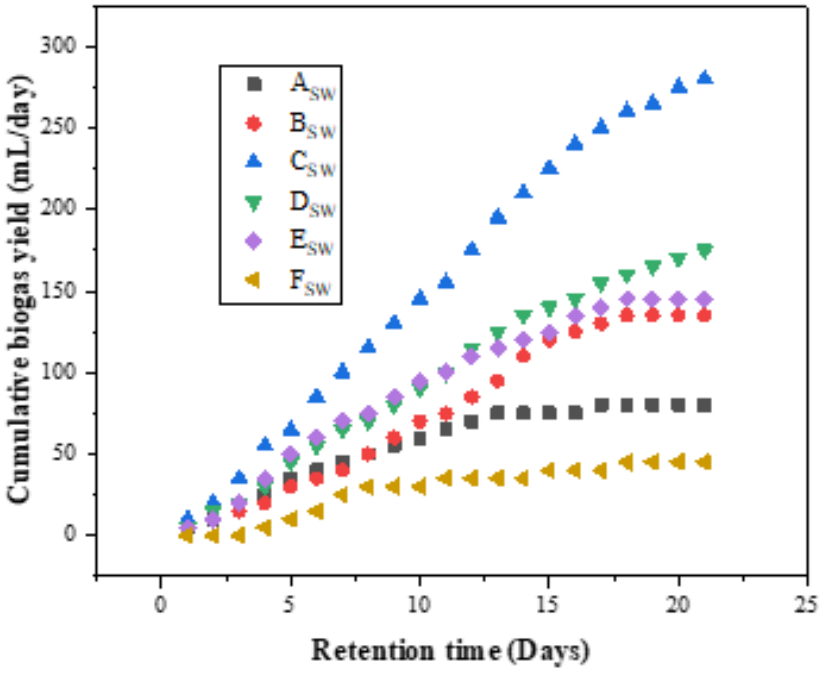

Figure 4-11 Cumulative biogas yield for BMP bioreactors A_{sw} – F_{sw} with MNP loading of 1.5 g at 35ºC and HRT of 21 days.

Figure 4-12 and Table 4-12 shows the results of an analysis of the total and volatile solids in each bioreactor to determine the percentage degradation of the digestate. The results show that all of the bioreactors dosed with MNPs had significantly higher digestate degradation than the control bioreactor Fsw (688 mg TS/L & 475 mg VS/L). It was observed that among the MNP-augmented bioreactors, bioreactors Csw (319 mg TS/L & 121 mg VS/L), Dsw (347.5 mg TS/L & 269.5 mg VS/L), and Esw (427.5 mg TS/L & 217.5 mg VS/L) had the lowest digestate, and the highest biogas, as shown in Table 4-12. This demonstrates that the microbial activities in these bioreactors were increased, resulting in a low digestate with a high biogas yield (Zhang and Lu 2016; Zaidi *et al.* 2018; Tetteh, Amo-Duodu and Rathilal 2021).

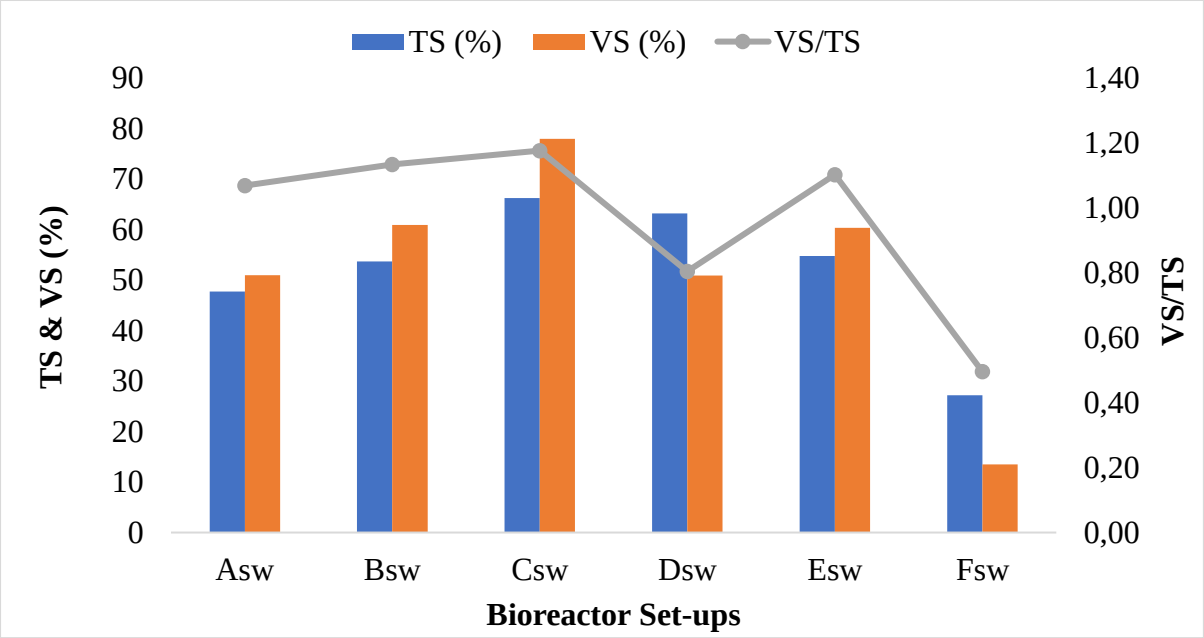

Figure 4-12 Effect of MNPs on sludge digestion for bioreactors Asw – Fsw with MNP loading of 1.5 g at 35ºC and HRT of 21 days.

Table 4-12: TS, VS, COD and pH of the BMP bioreactors (Asw – Fsw) after 21-days digestion.

SET-UP	pH	TS (mg TS/L)	VS (mg VS/L)	Biogas yield (mL/day)	COD (mg COD/L)
Asw	8.0	494	269	80	502
Bsw	8.1	437.5	214.5	135	489
Csw	8.2	319	121	280	217
Dsw	8.1	347.5	269.5	175	355
Esw	8.2	427.5	217.5	145	376
Fsw	5.6	688	475	45	1561
Feed	5.3	945	549	-	3570

4.3.1.3 Biostimulation effect of MNPs on methane yield

The methane yield of biogas has been reported to be around 55-65% of the biogas produced. To enhance the yield, the addition of MNPs was explored and the results after the 21-digestion period is displayed in Figure 4-13.

From Figure 4-13, it is observed that the bioreactors with MNPs dosage of 1.5 g had above 80% methane yield with bioreactors Csw (98.34%), Dsw (96.3), and Esw (94.6) again showing yield above 90%. The control set-up (Fsw) had a methane yield of 65.7%. The increase in methane yield for the bioreactors dosed with MNPs was due to the presence of metals (Fe, Cu, and Ni, Al, Mg) which serves as micronutrients to the microorganisms boosting their activities (Zaidi *et al.* 2018; Hassanein, Lansing and Tikekar 2019; Ajay *et al.* 2020).

It is also reported that Fe serves as a direct inter species transfer that stimulates the methanogen activities which increases the yield of methane (Abdelsalam *et al.* 2016; Zaidi *et al.* 2018; Tetteh, Amo-Duodu and Rathilal 2021). The MNPs also generate reducing agents which in turn reduce the CO_2 to methane (Abdelsalam *et al.* 2017; Abdelsalam and Samer 2019; Baniamerian *et al.* 2019).

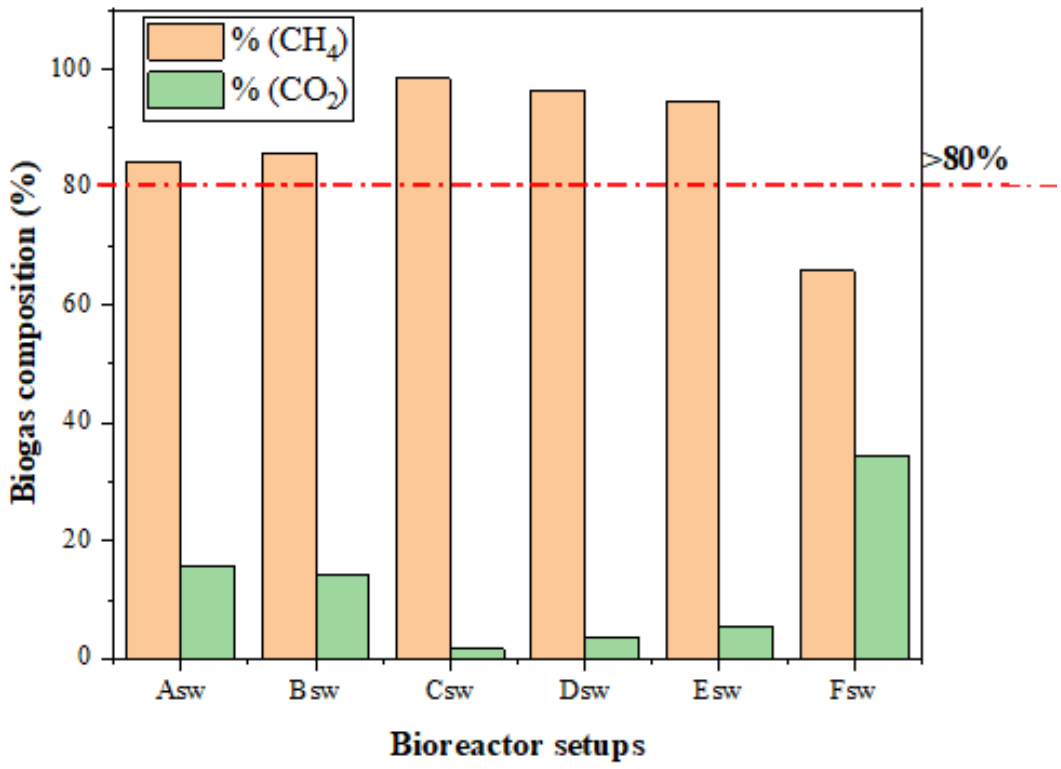

Figure 4-13 Biogas compositions of BMP bioreactors (Asw – Fsw) with MNP loading of 1.5 g at 35ºC and HRT of 21 days.

4.3.1.4 Kinetic study for the BMP bioreactors

It is critical to understand the system dynamics during the digestion period to improve the efficiency of the anaerobic digestion process. The cumulative yield of the BMP bioreactors was fitted using both first order and modified Gompertz kinetic models in the study as shown in Figure 4-14. The results obtained are presented in Tables 4-13 and 4-14.

Based on the summary provided, the correlation coefficient (R^2) was found to be greater than 0.99 and less than 0.89 for modified Gompertz and first order, respectively. The R^2 values show that modified Gompertz provided a more accurate description of the kinetics of the systems with an error of less than 2%.

In terms of biogas yield, modified Gompertz predicted better, with a difference between predicted and measured values ranging from -2.43 to 7.71 mL/day. The first-order model, on the other hand, predicted the highest yield. However, for a complete understanding of the AD systems, it is necessary to understand the lag phase, rate constant, the sum of square errors, and correlation coefficient. Of the two models used, modified Gompertz was more favourable and fitted best when compared to the first-order model.

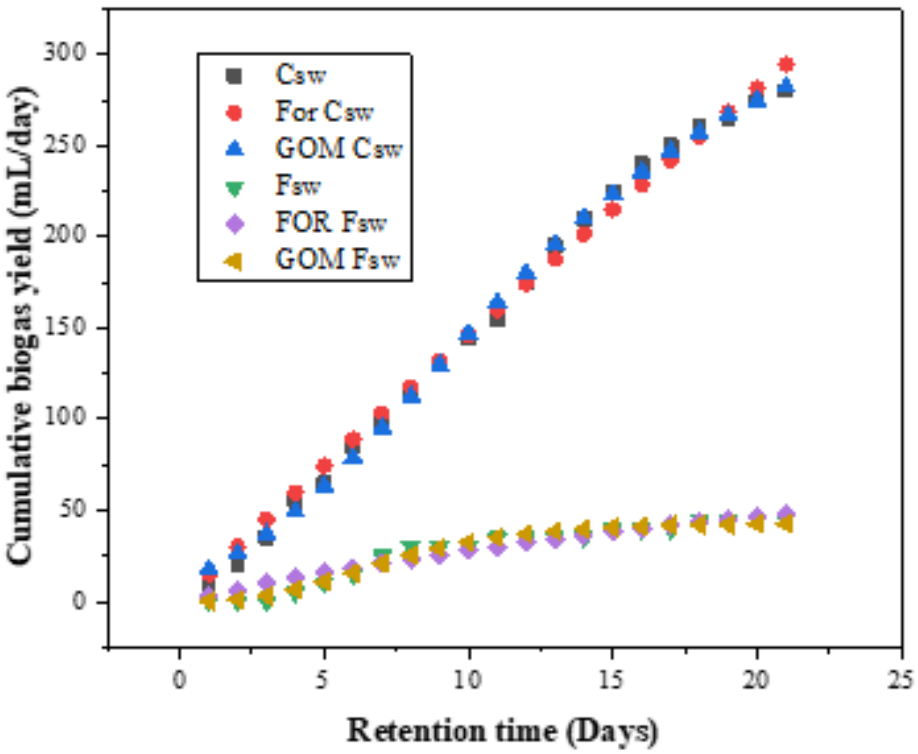

Figure 4-14 Fitting of Cumulative biogas yield on First order (FOR) and modified Gompertz (GOM) kinetic models.

The lag phase obtained for the BMP bioreactors dosed with MNPs was less than 6 days, whereas the control Fsw had an 8-day lag phase. The modified Gompertz rate constant was high, indicating that a shorter retention time is required to achieve a high biogas yield (Husain 1998; Kweinor Tetteh and Rathilal 2020; Amo-Duodu *et al.* 2021a).

Table 4-13: First order and Gompertz prediction of biogas yield for BMP bioreactors (Asw – Fsw) after 21-days digestion.

	First-order			**Modified Gompertz**		
SET-UP	**Predicted values, Sp (mL/day)**	**Measured values, St (mL/day)**	**Difference (Sp-St)**	**Predicted values, St (mL/day)**	**Measured values, Sp (mL/day)**	**Difference (Sp -St)**
A_{SW}	100.86	80	20.86	80.84	80	0.84
B_{SW}	149.27	135	14.27	142.71	135	7.71
C_{SW}	294.45	280	14.45	282.27	280	2.27
D_{SW}	182.51	175	7.51	174.14	175	-0.86

E_{SW}	154.82	145	9.82	146.73	145	1.73
F_{SW}	48.04	45	3.04	42.57	45	-2.43

* PV- Predicted biogas yield, MV- Measured biogas yield.*

Table 4-14: Summary of the kinetic study for BMP bioreactors (Asw – Fsw) over 21-days digestion

	FIRST ORDER MODEL						MODIFIED GOMPERTZ MODEL						
SET-UP	R^2	St (mL/day)	Sp (mL/day)	SSR	k (1/d)	Sm (mL/day)	ʎ (days)	St (mL/g COD)	Sp (mL/day)	k (1/d)	R^2	Sm (mL/day)	SSR
A_{SW}	0.8959	208957.25	100.86	2219.2245	0.00002	80	6.01	82.4362	80.84	0.24421	0.9955	80	57.7453
B_{SW}	0.9779	9306.72	149.27	1207.6938	0.00077	135	5.89	165.1514	142.71	0.15906	0.9929	135	323.1230
C_{SW}	0.9944	1998.22	294.45	1111.9214	0.00759	280	4.88	336.6096	282.27	0.14065	0.9978	280	366.6734
D_{SW}	0.9933	881.61	182.51	518.9477	0.01105	175	5.35	202.4531	174.14	0.14860	0.9973	175	169.4653
E_{SW}	0.9900	253.47	154.82	604.0081	0.04494	145	5.12	155.8498	146.73	0.19066	0.9937	145	286.1121
F_{SW}	0.9418	81.25	48.04	381.9431	0.04260	45	8.67	42.9181	42.57	0.32155	0.9746	45	134.3393

* Sp- Predicted biogas yield, Sm- Measured biogas yield, St- Maximum biogas yield, SSR- Sum of square errors, k- rate constant, R^2 – Correlation coefficient and ʎ - Lag phase.

4.3.2 BMP assay on municipal wastewater and activated sludge samples (Aeration wastewater and biofiltration wastewater samples from Umbilo water works)

The best performing MNPs (mFe, CmFe and Nmfe) from the previous study were tested on municipal wastewater collected from Umbilo water works in Pinetown, South Africa. Two different sampling points were identified (Aeration (AS) and Biofiltration system (BS) wastewater) and samples taken and were used for the study.

The characteristics of both the wastewaters (AS & BS) and sludge used has been presented in Table 4-5, where the COD of 2380 ± 236.78 mg COD/L and 1340 ± 121.91 mg COD/L were obtained for BS and AS, respectively. This makes the wastewater more suitable to be treated using anaerobic digestion as it is highly degradable. The results obtained from the AD process after 31-days of digestion have been presented below.

4.3.2.1 Effect of magnetic nanoparticles on water quality

The water quality after the digestion period was analysed for both wastewater samples (BS and AS) as described in section 3.5.1.1 and the results obtained are presented in Figure 4-15. The removal efficiency of each BMP bioreactor (Cas - Fbs) shows high reactor efficiency (>70%) for bioreactors Cas and Cbs which were loaded with 1.5 g Fe_3O_4.

Though bioreactors Das, Eas, Dbs, and Ebs had COD and turbidity removal efficiencies above 70%, their colour removal efficiencies were less than 70% when compared to bioreactors Cas and Cbs (>70%). However, when comparing the overall performance of all the bioreactors, it was observed that bioreactors with MNP additives had higher reactor efficiency than the control bioreactors (Fas and Fbs). The reactor efficiency of the control bioreactors was less than 60%.

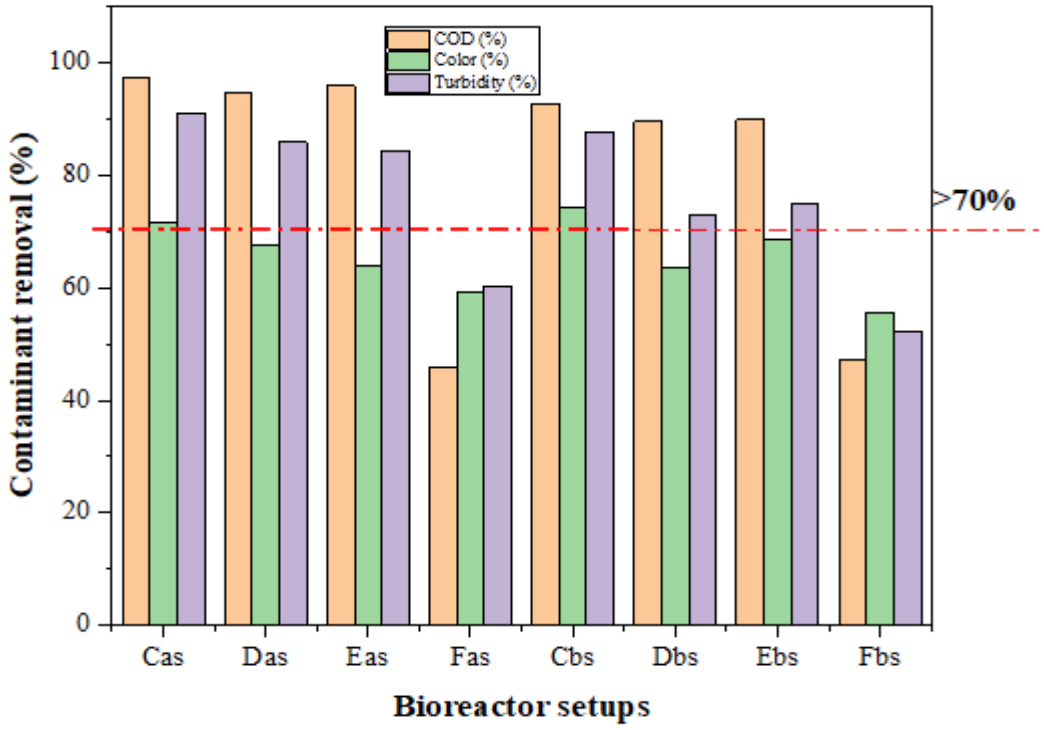

Figure 4-15 Reactor removal efficiency for BMP bioreactors (Cas – Fbs) with MNP loading of 1.5 g at 40ºC and HRT of 31 days.

Among the three MNPs (mFe, NmFe, and CmFe) used for this BMP test, bioreactors Cas and Cbs with mFe MNP additives were found to have good performance. Bioreactor Cas had 97.51% COD, 71.46% colour, and 91.11% turbidity removal efficiency while Cbs showed 92.84% COD, 74.31% colour and 87.71% turbidity removal efficiency. The trivalent nature of Fe ion gives it high adsorption properties with the capability to adsorb a wide range of organic contaminants (Brar *et al.* 2010; Li *et al.* 2011; Esfandiari *et al.* 2020).

4.3.2.2 Biostimulation effect of magnetic nanoparticles of BMP for biogas production

The biostimulation effect of MNPs on a BMP process was evaluated in terms of biogas yield for both aeration system (AS) and biofiltration system (BS) wastewater samples, as described in section 3.7. The results obtained are shown in Table 4-15 and Figure 4-16, and they showed about a 100% increase in biogas yield for the BMP bioreactors with MNPs additives when compared to the control bioreactors (Fas and Fbs).

Table 4-15: Sludge characteristics of BMP bioreactors (Cas - Fbs) with MNP loading of 1.5 g at 40ºC and HRT of 31 days

Set-up	pH	Biogas yield (mL COD/day)	TS (mg TS/L)	VS (mg VS/L)	COD (mg COD/L)
C_{AS}	7.57	1172	32	18.5	59.33
D_{AS}	7.18	1028	46	23.5	72.33
E_{AS}	7.30	1004	52	42.5	96.33
F_{AS}	7.43	525	84	42.5	1288.00
C_{BS}	7.10	1214	42	18.5	96.00
D_{BS}	7.31	940	50	23.5	140.67
E_{BS}	7.08	1023	45.5	21.5	136.30
F_{BS}	6.85	509	92	43	706.33
Feed (AS)			204.5	93.5	

The BMP reactor efficiency improved, as microbial activities were greatly stimulated and improved, resulting in a higher yield of biogas in the BMP bioreactors with MNP additives when compared to the control systems (Abdelsalam *et al.* 2016, 2017; Abdelsalam and Samer 2019). When the bioreactors with MPNs were compared, the bioreactors Cas and Cbs dosed with mFe had the highest biogas yields of 1172 mL/day and 1214 mL/day, respectively. The result is consistent with studies by Zaidi *et al.* (2018) and Abdelsalam *et al.* (2017).

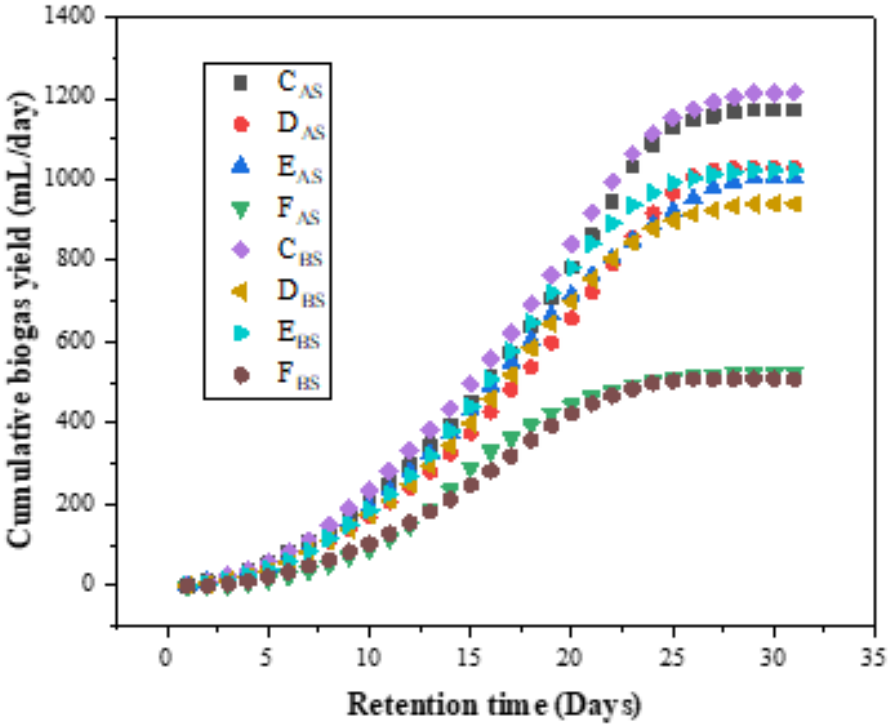

Figure 4-16 Cumulative biogas yield for BMP bioreactors Cas - Fbs with MNP loading of 1.5 g at 40ºC and HRT of 31 days.

Figure 4-17 depicts the percentage degradation of solids in sludge after 31 days of digestion in BMP bioreactors Cas -Fbs. The results confirm that MNP additives had a significant impact on sludge digestion, with over 70% TS and VS digestion obtained for all BMP bioreactors with MNP additives, except for bioreactor Eas, which had about 50% VS degradation. This demonstrates that the addition of MNPs improved microbial activities, and the results also demonstrated why bioreactors with MNPs had higher yields of biogas with low digestate, as shown in Table 4-15 (Tetteh, Amo-Duodu and Rathilal 2021).

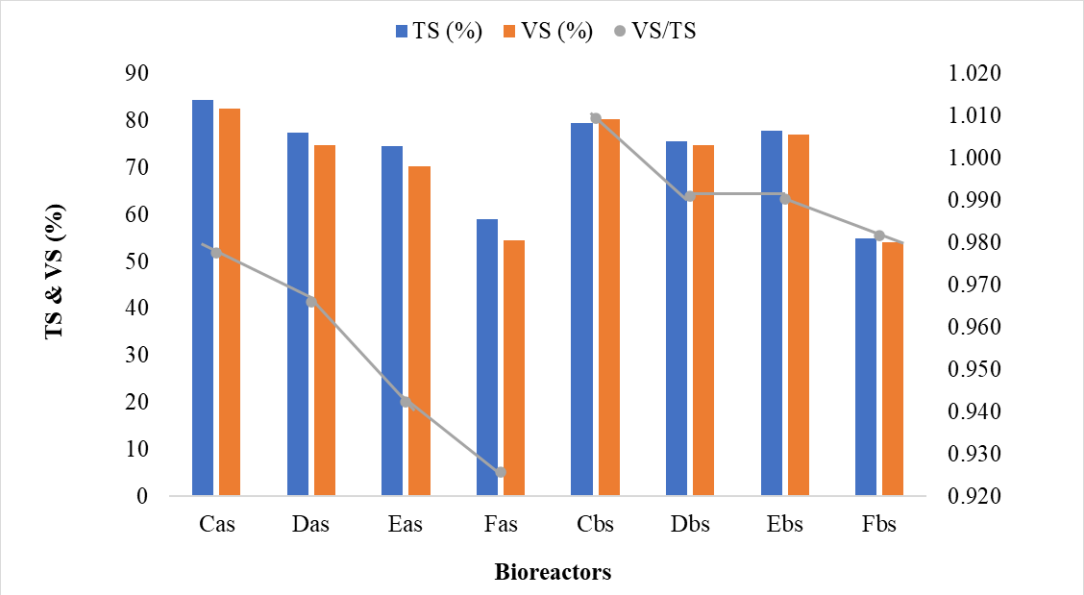

Figure 4-17 Effect of MNPs on Sludge digestion for bioreactors Cas- Fbs with MNP loading of 1.5 g at 40ºC and HRT of 31 days

4.3.2.3 Biostimulation effect of magnetic nanoparticles (MNPs) on methane yield

The biostimulation after the effect of magnetic NPs on the methane yield for each BMP bioreactor (Cas – Fbs) was determined after the 31-days digestion period. The results are presented in Figure 4-18 below. It is observed from the figure that all bioreactors with MNP additives had over 80% methane yield as compared to the control set-ups (Fas and Fbs) which had about 60-65% methane and around 35-40% CO_2.

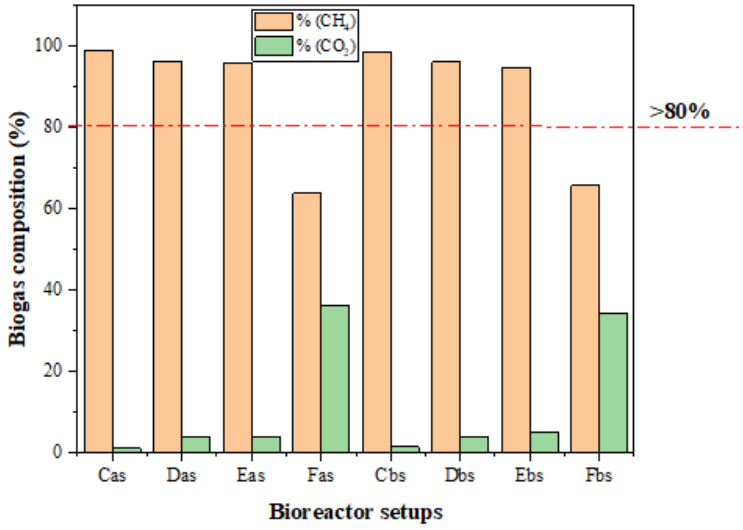

Figure 4-18 Biogas compositions of BMP bioreactors (Cas - Fbs) with MNP loading of 1.5 g at 40ºC and HRT of 31 days.

The results show that bioreactors Cas and Cbs dosed with mFe MNPs recorded the highest methane yield of 98.89% and 98.56%, respectively. The rest of the bioreactors recorded as follows; Das (96.3%) > Eas (96%) > Fas (63.8%) for AS wastewater and Dbs (96.2%)> Ebs (94.8%) > Fbs (65.7%) for BS wastewater.

As already explained in section 4.3.1.3, these MNPs stimulate the methanogens which increase its activities and results in high methane yield (Abdelsalam *et al.* 2017; Chen, Steele and Stuckey 2018; Abdelsalam and Samer 2019; Amo-Duodu *et al.* 2021b; Tetteh, Amo-Duodu and Rathilal 2021).

4.3.2.4 Kinetic study for the BMP bioreactors

To understand the dynamics and performance of the BMP systems, the cumulative yield of each bioreactor was fitted on both first order and modified Gompertz kinetic models. The cumulative yield of the bioreactor with the highest R^2 (Eas and Dbs) and that of the control (Fas and Fbs) were fitted on first order and modified Gompertz kinetic models for both wastewater samples (AS and BS). Figures 4-19 and 4-20 depict the graphical presentation of the results obtained when the cumulative yield was fitted on the two models.

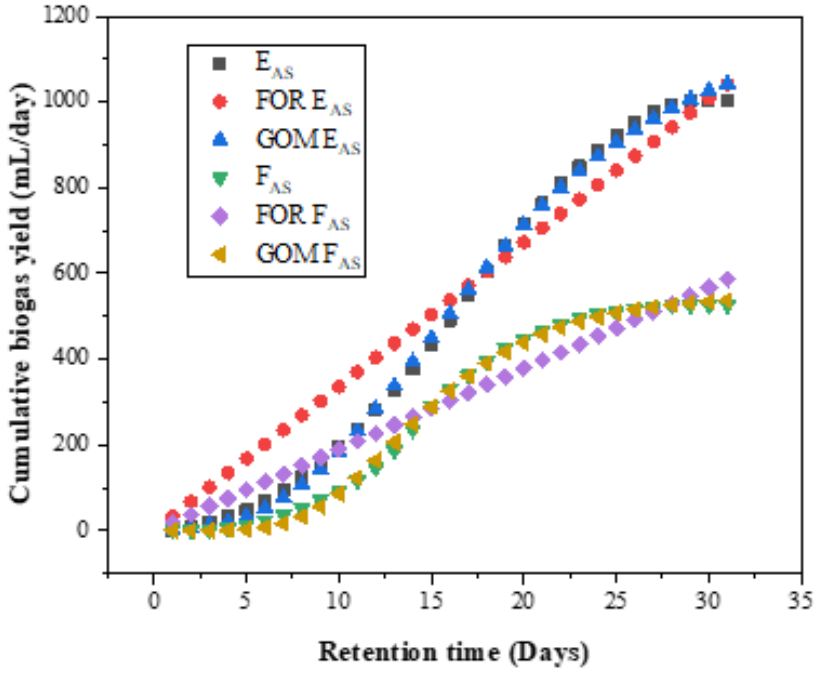

Figure 4-19 Fitting of Cumulative biogas yield on First order (FOR) and modified Gompertz (GOM) kinetic models for AS wastewater.

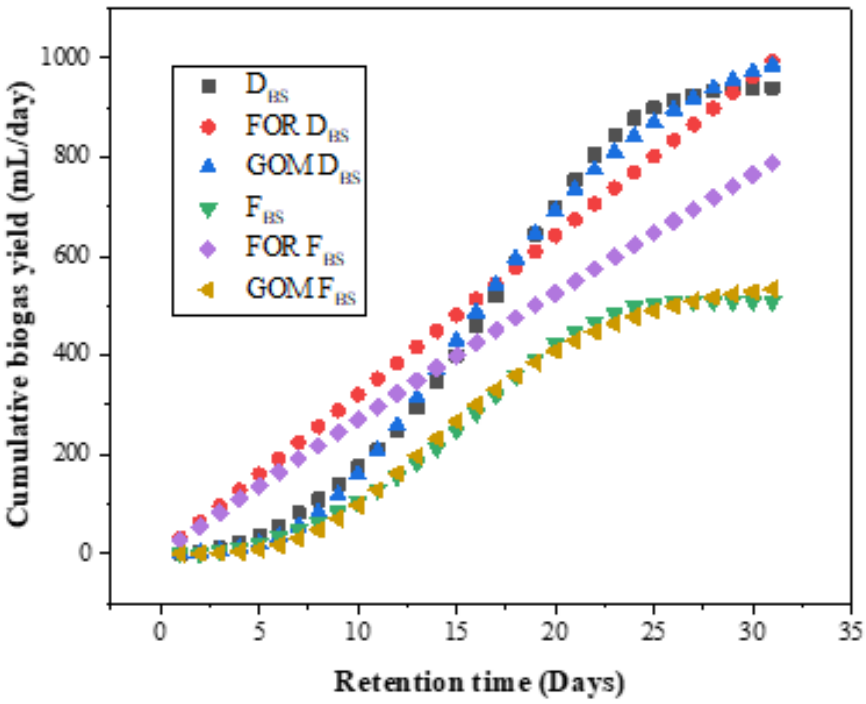

Figure 4-20 Fitting of Cumulative biogas yield on First order (FOR) and modified Gompertz (GOM) kinetic models for BS wastewater.

It is observed that the cumulative yield of the bioreactors Eas, Dbs, Fas, and Fbs were well fitted on the modified Gompertz with slight deviation as compared to the first order. This explains why the modified Gompertz had higher R^2 values than that of the first-order models. In terms of the rate constants (k), the modified Gompertz was found to record high k values (Kweinor Tetteh and Rathilal 2020; Amo-Duodu *et al.* 2021b).

Tables 4-16 and 4-17 display the summary from the kinetic study, where the modified Gompertz was again found to have a better explanation of the kinetics and dynamics of the BMP systems. The R^2 values obtained for the modified Gompertz model were above 99% with an error margin of less than 2%. In terms of predicting the biogas yield, it was found that the modified Gompertz model had the highest biogas yield (Table 4-17), however, the difference between the predicted yield and the measured yield were low for the first-order model (Table 4-16).

Table 4-16: First order and Gompertz prediction of biogas yield for BMP bioreactors (Cas - Fbs) after 31-days digestion.

		Modified Gompertz model			First-order model		
SET-UP	**Measured yield, St (mL/day)**	**Predicted yield, Sp (mL/day)**	**R^2**	**Sp - St (mL/day)**	**Predicted yield, Sp (mL/day)**	**R^2**	**Sp-St (mL/day)**
C_{AS}	1172	1250.50	0.9931	78.50	1201.16	0.9688	29.16
D_{AS}	1028	1098.46	0.9943	70.46	1033.18	0.9689	5.18
E_{AS}	1004	1042.93	0.9986	38.93	1041.84	0.9786	37.84
F_{AS}	525	536.84	0.9981	11.84	585.76	0.9433	60.76
C_{BS}	1172	1282.84	0.9954	110.84	1258.38	0.9740	86.38
D_{BS}	1028	985.84	0.9963	42.16	994.69	0.9680	33.31
E_{BS}	1004	1073.68	0.9957	69.68	1093.25	0.9636	89.25
F_{BS}	509	534.04	0.9951	25.04	788.32	0.9276	263.32

Table 4-17: Summary of the kinetic study for BMP bioreactors (Cas – Fbs) over 31-days digestion

	MODIFIED GOMPERTZ MODEL							FIRST ORDER MODEL					
SET-UP	R^2	k (1/day)	SSR	St (mL/day)	Sm (mL/day)	ʎ(days)	Sp (mL/day)	R^2	St (mL/day)	Sm (mL/day)	Sp (mL/day)	k (1/day)	SSR
C_{AS}	0.9931	0.12262	4191.8079	1172	1459.992	4.23	1250.497	0.968765	1172	7872.064	1201.163	0.00050	4615.505
D_{AS}	0.9943	0.11814	2689.3064	1028	1315.737	6.51	1098.462	0.968944	1028	1956.277	1033.176	0.00002	3834.919
E_{AS}	0.9986	0.13091	6536.8118	1004	1173.579	5.79	1042.925	0.978574	1004	1372.003	1041.842	0.00002	2431.223
F_{AS}	0.9981	0.21162	2884.4143	525	548.6227	8.69	536.8396	0.943295	525	787.604	585.7563	0.00032	1204.888
C_{BS}	0.9954	0.12465	2899.6102	1214	1475.519	3.24	1282.844	0.974026	1214	1440.118	1258.379	0.00003	4164.027
D_{BS}	0.9963	0.14644	1541.093	940	1076.653	4.41	985.84	0.967965	940	1306.758	994.6875	0.00002	2856.215
E_{BS}	0.9957	0.15501	2159.9293	1023	1156.28	4.21	1073.679	0.963575	1023	3645.682	1093.25	0.00001	3643.456
F_{BS}	0.9951	0.17145	6290.53429	509	560.0724	9.12	534.0393	0.92758	509	657.77	788.3151	0.00628	1957.762

* Sp- Predicted biogas yield, Sm- Measured biogas yield, St- Maximum biogas yield, SSR- Sum of square errors, k- rate constant, R^2 – Correlation coefficient, and ʎ - Lag phase. *

4.3.3 Summary

Due to the COD level for the municipal wastewater being high (2000-2300 mg/L), the BMP survey on the two wastewater samples (industrial and municipal wastewater) revealed that both were good feeds for the AD process. The AD method was shown to be more efficient when magnetic nanoparticles were used on these two samples. The results suggest that the BMP systems with MNP additions have good COD and turbidity degradation.

With the addition of MNPs, the biogas and methane yields increased by approximately 100% and 20%, respectively, for BMP systems. It was also discovered that adding MNPs to the AD process enhanced not only the biogas and methane yield but also the treatability of the AD systems. When compared to the control bioreactors (with no MNPs), the efficiency of the BMP bioreactors with MNPs was shown to be considerably improved by approximately 20-30%.

The use of magnetic nanoparticles, particularly Fe_3O_4 (mFe), in the AD process is promising in terms of biogas and methane yields, as well as wastewater treatment.

4.4 Response surface methodology optimisation of the BMP system

Biogas production is mostly dependent on the growth of methanogenesis bacteria and microorganisms found in organic matter, thus, boosting the growth of these microorganisms will have an impact on biogas yield. Temperature, organic loading rate (OLR), hydraulic retention time (HRT), pH, and the bioreactor design, which needs to be adjusted, are all elements that affect growth.

However, in this study, the use of magnetic nanoparticles (MNPs) to promote growth and microorganism activities was investigated, and the findings were favourable, therefore optimising the MNP loading rate as well as operational factors such as temperature, HRT, and OLR were considered.

A design matrix based on Box-Behnken design was created using the response surface methodology (RSM) from Design expert (version: 11.1.2.0) to design 27 experimental runs, as detailed in section 3.6.1. Biogas yield (mL/day), COD reduction (%), turbidity, and colour removal efficiencies (%) were all evaluated as response factors. In this section, the findings of the RSM investigation are reported.

4.4.1 Evaluation of the RSM analysis of variance (ANOVA) statistics and regression model

In process optimisation, the main aim is to achieve optimum conditions (operational factors) applied to the process and maximize the response factors. In this study, the key process factors were obtained from the previous BMP assays (section 4.3) and were used here.

As explained in section 3.4, the experimental design was done based on four operational factors, three levels (-1, 0, +1) and five centre points (replicate runs) as presented in Table 3-9 using BBD from RSM.

From Figure 4-21, the fit summary for all the response variables is shown and the linear was suggested for all the responses and cubic model was found to be aliased. However, reduced 2FI and reduced quadratic models were chosen after the analysis of variance (ANOVA). The normal probability vs residual plots, residual vs predicted as well as the diagnostic reports for all the responses have been presented in Appendix B.

Fit Summary

Response 1: Biogas Yield

Source	Sequential p-value	Lack of Fit p-value	Adjusted R^2	Predicted R^2	
Linear	**< 0.0001**	**0,3568**	**0,9595**	**0,9473**	**Suggested**
2FI	0,4153	0,3546	0,9603	0,9246	
Quadratic	0,4080	0,3498	0,9611	0,9018	
Cubic	0,4009	0,3102	0,9690	0,5224	Aliased

Fit Summary

Response 2: COD

Source	Sequential p-value	Lack of Fit p-value	Adjusted R^2	Predicted R^2	
Linear	**< 0.0001**	**1,0000**	**0,9515**	**0,9532**	**Suggested**
2FI	0,9973	0,9995	0,9353	0,9483	
Quadratic	0,3621	1,0000	0,9383	0,9288	
Cubic	0,9999	0,9847	0,8257	0,8817	Aliased

Fit Summary

Response 3: Turbidity

Source	Sequential p-value	Lack of Fit p-value	Adjusted R^2	Predicted R^2	
Linear	**< 0.0001**	**0,9970**	**0,8823**	**0,8717**	**Suggested**
2FI	0,8744	0,9927	0,8589	0,8398	
Quadratic	0,4424	0,9963	0,8590	0,7792	
Cubic	0,9817	0,9119	0,6874	0,2909	Aliased

Fit Summary

Response 4: Color

Source	Sequential p-value	Lack of Fit p-value	Adjusted R^2	Predicted R^2	
Linear	**< 0.0001**	**1,0000**	**0,8478**	**0,8571**	**Suggested**
2FI	0,9999	0,9996	0,7925	0,8468	
Quadratic	0,2967	1,0000	0,8107	0,7969	
Cubic	1,0000	0,9957	0,4419	0,7541	Aliased

Figure 4-21 The fit summary for all the process responses

Tables 4-18 and 4-19 show the ANOVA statistic summary and regression model summary for all the responses, presenting their coefficient of determination (R^2), predicted R^2, adjusted R^2, the models lack of fit (P-value) and F-values with the model equations chosen for each response. In model analysis, the adequacy, precision, model significant and reputability was determined using the analysis of variance statistics. In this study, the P-values and F-values for each response model is shown in Table 4-19. P-values less than 0.0001 were obtained for all

the models which showed the significance of the design models for the BMP system. The R^2 values obtained for each response model affirm the adequacy and variability of the models. It was found that the models can explain the approximately 90% variability of the system and only less than 10% could not be explain using the models at a confidence level of 95%. The model equations determined from the analysis was reduced quadratic and 2FI.

From Table 4-18, R^2 values of 0.9756, 0.9632, 0.9131 and 0.9115 were obtained for the process response biogas yield, COD reduction, turbidity and colour removal, respectively. The difference between the adjusted R^2 and predicted R^2 for all the models (reduced quadratic and 2FI) were less than 0.02 which showed that the adjusted R^2 and predicted R^2 are in reasonable agreement with a high adequate precision greater than 4 (Design Expert 2011). The adequate precision measures the signal to noise ratio of the models and ratios for the responses were 49.2 for biogas yield, 31.64 for COD reduction, 23.29 for turbidity removal and 17.85 for colour removal which were acceptable as they were greater than 4.

Table 4-18: ANOVA statistic summary for all the response variables

	Biogas yield (mL/day)	**COD reduction (%)**	**Turbidity removal (%)**	**Colour removal (%)**
Standard deviation	8.0891	0.2297	0.2959	0.3839
Mean	412.4888	70.0131	69.9022	69.9020
Coefficient of variance (% CV)	1.9610	0.3281	0.4233	0.5492
Coefficient of determination (R^2)	0.9756	0.9632	0.9131	0.9115
Adjusted R^2	0.9698	0.9496	0.8925	0.8722
Predicted R^2	0.9335	0.9473	0.8612	0.8010
Adequate precision	49.2003	31.6362	23.2868	17.8489

Table 4-19: the ANOVA summary for the regression models

	Biogas yield (mL/day)	COD reduction (%)	Turbidity reduction (%)	Colour reduction (%)
Coefficient of determination (R^2)	0.9756	0.9632	0.9131	0.9115
Sum of squares	54888.9784	26.2427	19.3258	27.3378
Mean squares	10977.7957	3.7490	3.8652	3.4172
F-values	167.7706	71.0277	44.1558	23.1846
P-values	<0.0001	< 0.0001	<0.0001	< 0.0001
model equation	Reduced 2FI	Reduced quadratic	Reduced 2FI	Reduced quadratic

4.4.2 Evaluation of the RSM factors on biogas yield

In anaerobic digestion, the operational conditions sometimes do interfere in the performance of the system. Over the years, in order to overcome the limitations, the operational factors pose on the system many modifications had been made. In this study in order to optimise the AD system, the Box-Behnken from RSM design was utilized to find the optimum conditions based on four operating factors. The factors were evaluated using ANOVA to assess their interactive effect on biogas yield. From Table 4-20 the regression design model which was found to be reduced 2FI presents the P-value and F-value of the model as well as the that of the model terms. The model was found to be significant with P-value less than 0.0001 and F-value of 167.7706. Beside retention time and nanoparticle loading with P-values less than 0.0001, temperature and inoculum load had P-value greater than 0.05, hence only retention time and nanoparticle loading was found to be significant which shows that they have an interactive effect on biogas yield. The P-value for lack of fit was greater than 0.05 (0.44798), hence not significant. The model equation obtained for the biogas yield is presented in equation 4.1a and 4.1b representing the coded and actual equations, respectively.

$$Y_1 = 412.29 - 39.40\,B + 50.40C + 3.93D + 11.79\,CD \qquad (4.1a)$$

$$Y_1 = 461.076 + 7.709\,Temp - 78.805\,MNP\ laod + 0.483\,HRT - 0.1965\,Inoculum + 0.00786\,HRT \times Inoculum\ load \qquad (4.1b)$$

Where Temp is temperature (°C), HRT is retention time (days) and MNP is nanoparticle loading (g).

Table 4-20: ANOVA regression model (reduced 2FI) for biogas yield (mL/day)

Source	Sum of squares	df	Mean	F-value	P-value	
Model	54888.98	5	10977.8	167.7706	<0.00001	Significant
A-Temperature	0	1	0	0	1	
B-Nanoparticle loading	18630.53	1	18630.53	284.7252	<0.00001	
C-Retention time	35517.27	1	35517.27	542.8006	<0.00001	
D-Inoculum loading	185.2957	1	185.2957	2.831823	0.107224	
CD	555.8871	1	555.8871	8.495469	0.008284	
Residual	1374.101	21	65.43337			
Lack of Fit	1290.79	19	67.93632	1.630917	0.447983	not significant
Pure Error	83.3106	2	41.6553			
Cor Total	56263.08	26				

4.4.3 Effect of the RSM factors on COD reduction

For the COD reduction design model, the interacting effects of the process parameters were also studied. The response was modelled using a reduced quadratic model, and the model's significance was demonstrated using the F-value and P-value, as shown in Table 4-21 and the P-value was less than 0.05, with an F-value of 71.02, as shown in the table. The significance of the model term was also checked, with retention time, temperature, and nanoparticles loading, all being significant, indicating that these were the components that had interactive effects on COD prediction, while the quadratic terms did not. The lack of fit was examined, and the P-value for lack of fit was 0.9998, which is greater than 0.05 but not significant when compared to pure error. The COD reduction model equation is represented by equations 4.2a and 4.2b, which represent the coded and actual equations, respectively.

$$Y_2 = 70.09 - 07298A - 0.2936B + 1.25C + 0.0268D + 0.0914BD - 0.1056A^2 - 0.0599B^2 \quad (4.2a)$$

$$Y_2 = 69.820 + 0.00958\,Temp - 0.8372\,MNP\ load + 0.0832HRT - 0.00156\,Inoculum + 0.00183\,MNP\ load \times Inoculum\ load - 0.001056\,Temp^2 - 0.2396\,MNP^2 \quad (4.2b)$$

Table 4-21: ANOVA regression model (reduced quadratic) for COD reduction (%)

Source	Sum of squares	df	Mean	F-value	P-value	
Model	26.24267	7	3.748953	71.02772	<0.0001	Significant
A-Temperature	6.390804	1	6.390804	121.0803	<0.0001	
B-Nanoparticle loading	1.027223	1	1.027223	19.46179	0.0003	
C-Retention time	18.70119	1	18.70119	354.3131	<0.0001	
D-Inoculum loading	0.00859	1	0.00859	0.162755	0.691137	
BD	0.033431	1	0.033431	0.633386	0.435947	
A^2	0.071399	1	0.071399	1.35272	0.259203	
B^2	0.022972	1	0.022972	0.435233	0.51735	
Residual	1.002849	19	0.052782			
Lack of Fit	0.283288	17	0.016664	0.046317	0.999978	not significant
Pure Error	0.719561	2	0.359781			
Cor Total	27.24552	26				

4.4.4 Effect of RSM responses on colour and turbidity removal efficiency

The design models obtained for colour and turbidity removal were reduced quadratic and 2FI, respectively. The models were found to be significant with p-values less than 0.0001 for both responses and F-values of 23.1846 and 44.1558 for colour and turbidity removal, respectively as shown in Tables 4-22 and 4-23. The models have lack of fit P-value of 1 and 0.9987 for colour and turbidity, respectively which was greater than 0.05 hence not significant to pure error. The model terms for colour removal were found to have interactive effects on the efficiency except the inoculum loading term whose P-value was 0.8119 (>0.05) making it insignificant to colour removal. Additionally, the P-values quadratic terms for temperature and

retention loading were greater than 0.05. However, reduced quadratic was the design model which explains the about 91% of the variability of the system with adequate precision of 17.8489.

Table 4-22: ANOVA regression model (reduced quadratic) for colour removal efficiency (%).

Source	Sum of squares	df	Mean	F-value	P-value	
Model	27.33778	8	3.417222	23.18459	<0.0001	significant
A-Temperature	6.390804	1	6.390804	43.35924	<0.0001	
B-Nanoparticle loading	1.027223	1	1.027223	6.96933	0.016638	
C-Retention time	18.70119	1	18.70119	126.8807	<0.0001	
D-Inoculum loading	0.00859	1	0.00859	0.058283	0.811959	
A^2	0.517874	1	0.517874	3.513582	0.077191	
B^2	0.680952	1	0.680952	4.620008	0.045449	
C^2	0.517874	1	0.517874	3.513582	0.077191	
D^2	0.680952	1	0.680952	4.620008	0.045449	
Residual	2.653056	18	0.147392			
Lack of Fit	0.08915	16	0.005572	0.004346	1	not significant
Pure Error	2.563906	2	1.281953			
Cor Total	29.99083	26				

For the turbidity removal efficiency, a 2FI design model was obtained with R^2 of approximately 91% and adequate precision of 23.2868. The model equation obtained for the colour removal efficiency is presented in equations 4.3a and 4.3b representing the coded and actual equations, respectively.

$$Y_3 = 70.09 - 07298A - 0.2936B + 1.25C + 0.0268D + 0.0914BD - 0.1056A^2 - 0.0599B^2 \quad (4.3a)$$

$$Y_3 = 69.820 + 0.00958\,Temp - 0.8372\,MNP\ load + 0.0832HRT - 0.00156\,Inoculum + 0.00183\,MNP\ load \times Inoculum\ load - 0.001056\,Temp^2 - 0.2396\,MNP^2 \quad (4.3b)$$

Table 4-23: ANOVA regression model (reduced 2FI) for turbidity removal efficiency (%).

Source	Sum of squares	df	Mean	F-value	P-value	
Model	19.32577	5	3.865153	44.15581	<0.0001	significant
A-Temperature	4.966102	1	4.966102	56.73313	<0.0001	
B-Nanoparticle loading	2.530869	1	2.530869	28.91285	<0.0001	
C-Retention time	11.53909	1	11.53909	131.8234	<0.0001	
D-Inoculum loading	0.020555	1	0.020555	0.234821	0.632988	
AD	0.269152	1	0.269152	3.074818	0.094099	
Residual	1.838223	21	0.087534			
Lack of Fit	0.91	19	0.047895	0.103197	0.998744	not significant
Pure Error	0.928223	2	0.464112			
Cor Total	21.16399	26				

The model equation obtained for the turbidity removal efficiency is presented in equation 4.4a and 4.4b representing the coded and actual equations, respectively.

$$Y_4 = 70.09 - 07298A - 0.2936B + 1.25C + 0.0268D + 0.0914BD - 0.1056A^2 - 0.0599B^2 \quad (4.4a)$$

$$Y_4 = 69.820 + 0.00958\,Temp - 0.8372\,MNP\ load + 0.0832HRT - 0.00156\,Inoculum + 0.00183\,MNP\ load \times Inoculum\ load - 0.001056\,Temp^2 - 0.2396\,MNP^2 \quad (4.4b)$$

In the model equations, the coefficients of the first order show the main effect of the factors on the responses while that of the second and third shows the interactive effects of the predictor factors on the response.

4.4.5 Effect of magnetic nanoparticle on biogas yield and water treatment.

The goal of the optimisation study was to find the best nanoparticle loading rate for achieving maximum biogas yield and good treatability efficiency. Following the BBD-RSM numerical optimisation with the constraint shown in Table 3.11. The 3D and contour plots showed the influence of sensitive factors on response patterns. MNP loading was one of the four factors studied and was found to be sensitive and had an impact on all of the responses. As the load was increased alongside other parameters, the efficiency was shown to decrease. In terms of biogas yield, it was discovered that raising temperature with the minimal MNP load increased its yield. However, at a target temperature of 35 °C and a minimal MNP load of roughly 0.7 g, a minimum biogas yield of 440 ml/day was obtained in both the 3D and contour plots, as shown in Figures 4-22 and 4-23. The RSM predicted value and the experimented yield had a strong correlation as shown in the predicted vs actual plots, and they were found to be closer on the diagonal line, indicating that the data was within the design space.

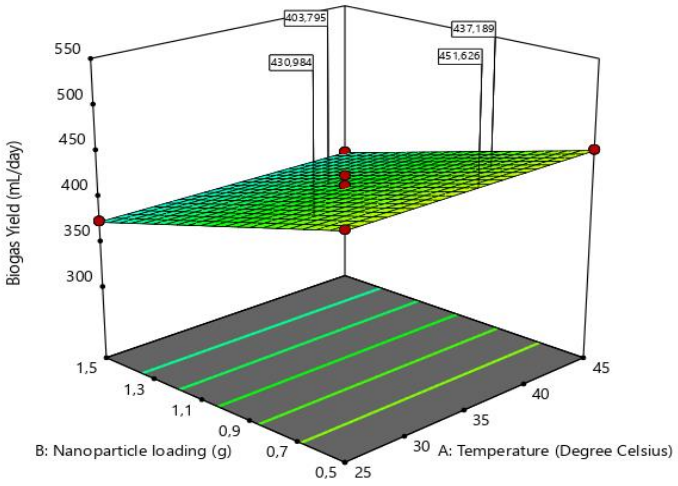

Figure 4-22 The 3D plots for biogas yield (mL/day).

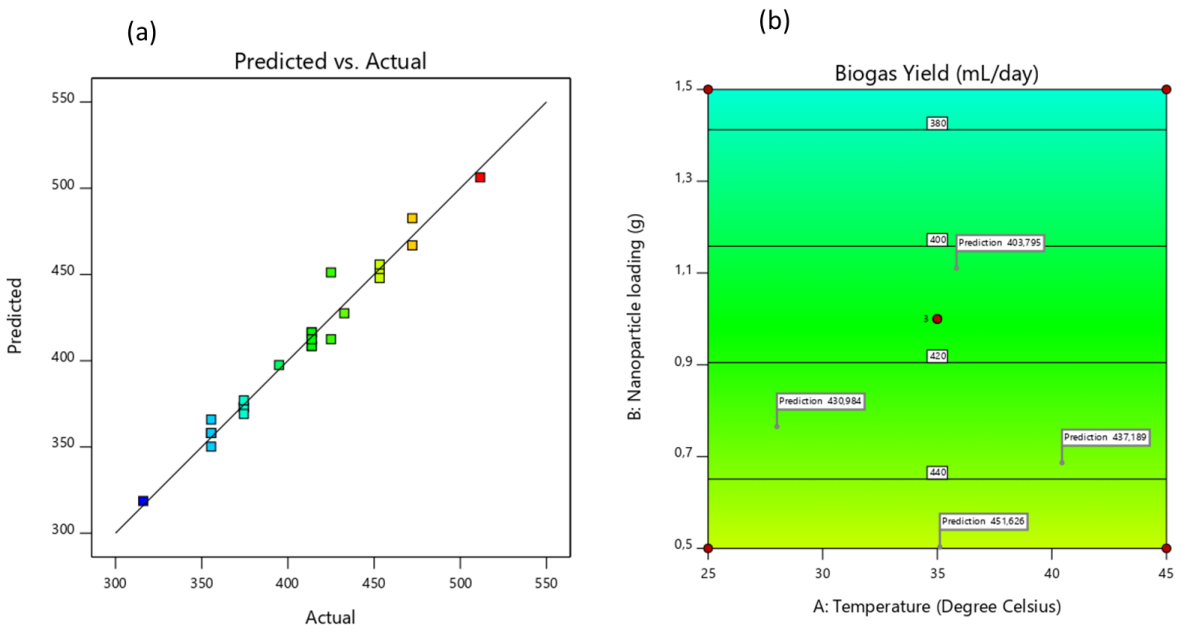

Figure 4-23 The (a) predicted vs actual and (b) contour plots for biogas yield (mL/day).

COD reduction was observed in a similar way as mentioned above, as illustrated in Figure 4-24 and Figure 4-25. The predicted vs. actual plots revealed that all of the data were on the diagonal line with one or two outliners, indicating a high agreement between the design model prediction and the experimented values. The contour plot also revealed that temperature and MNP load were both sensitive factors that influenced the response's regression model.

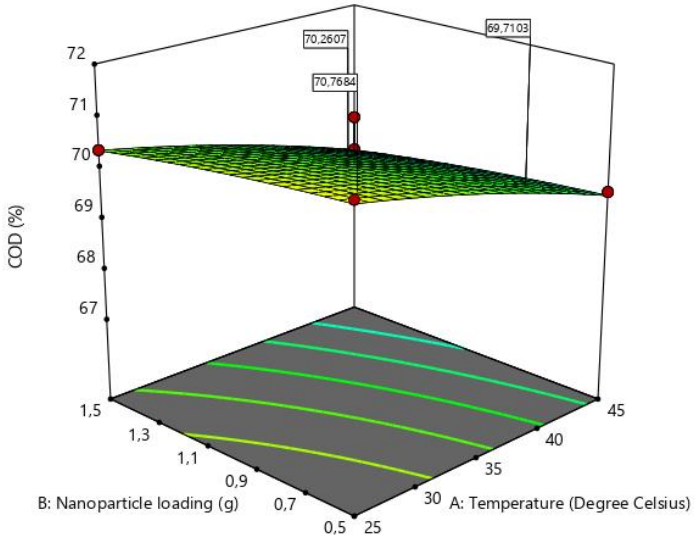

Figure 4-24: The 3D plots for COD reduction (%).

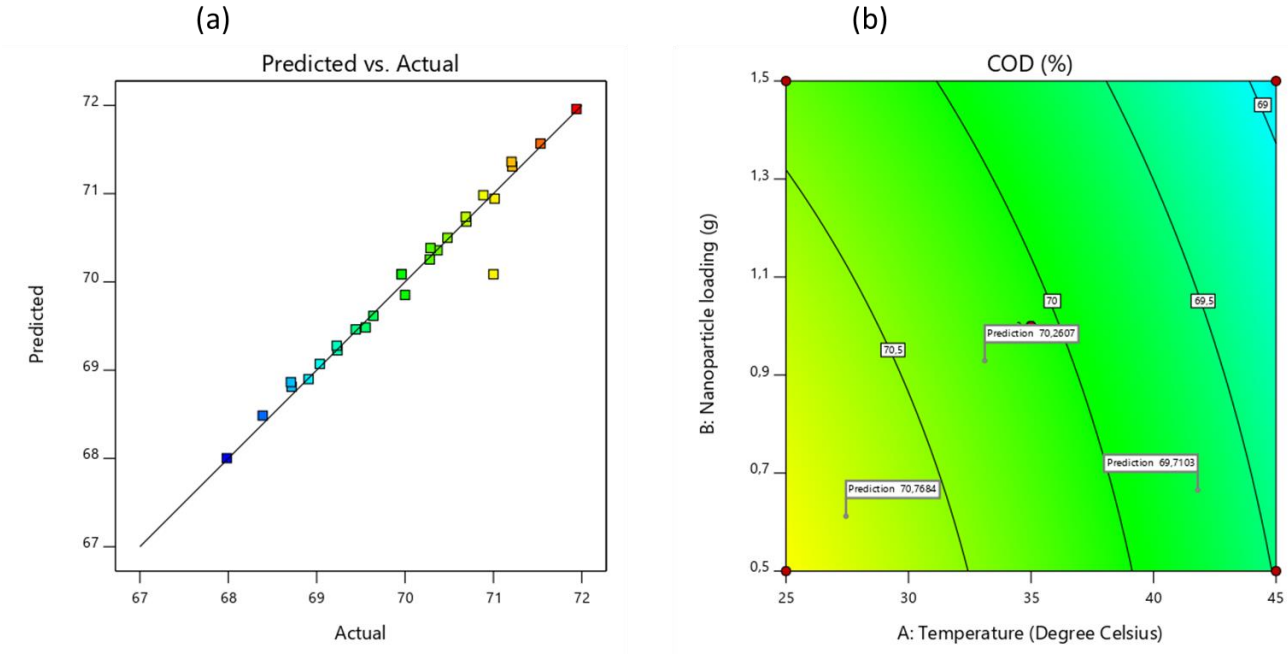

Figure 4-25 The (a) predicted vs actual and (b) contour plots for COD reduction (%)

The sensitive parameters that impacted the regression model of responses were temperature and MNP loading, as indicated in the contour and 3D plots from Figures 4-22 to 4-27. As a result, it was discovered that modifying the MNP load within a certain limit improved the efficiency and yield, however increasing the load decreased efficiency and yield. This conclusion was consistent with a prior study (Amo-Duodu *et al.* 2021a) that revealed that as the load of MNP was increased, the performance of the BMP decreased.

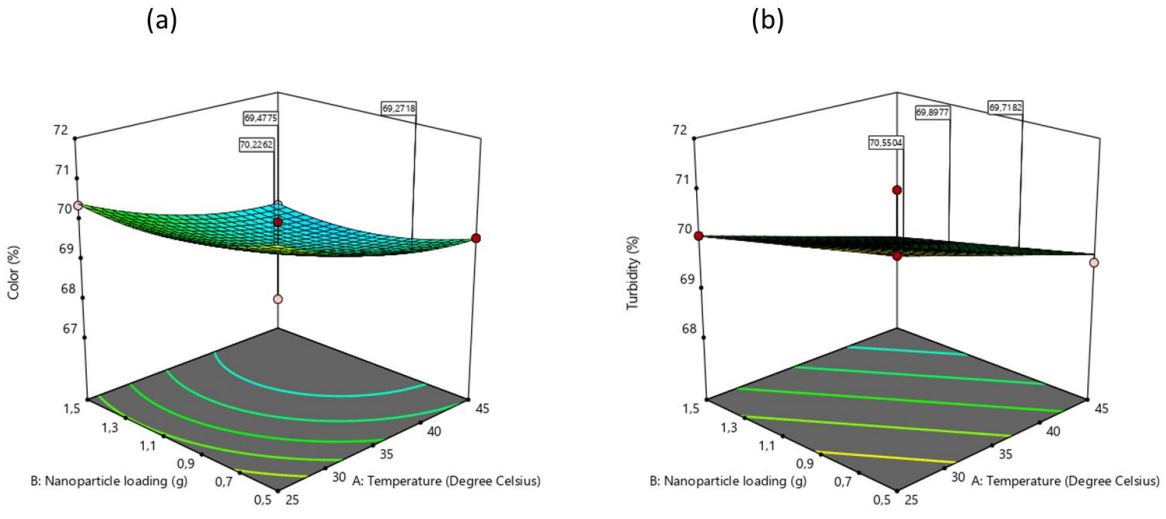

Figure 4-26 The 3D plots for (a) Colour and (b) turbidity removal.

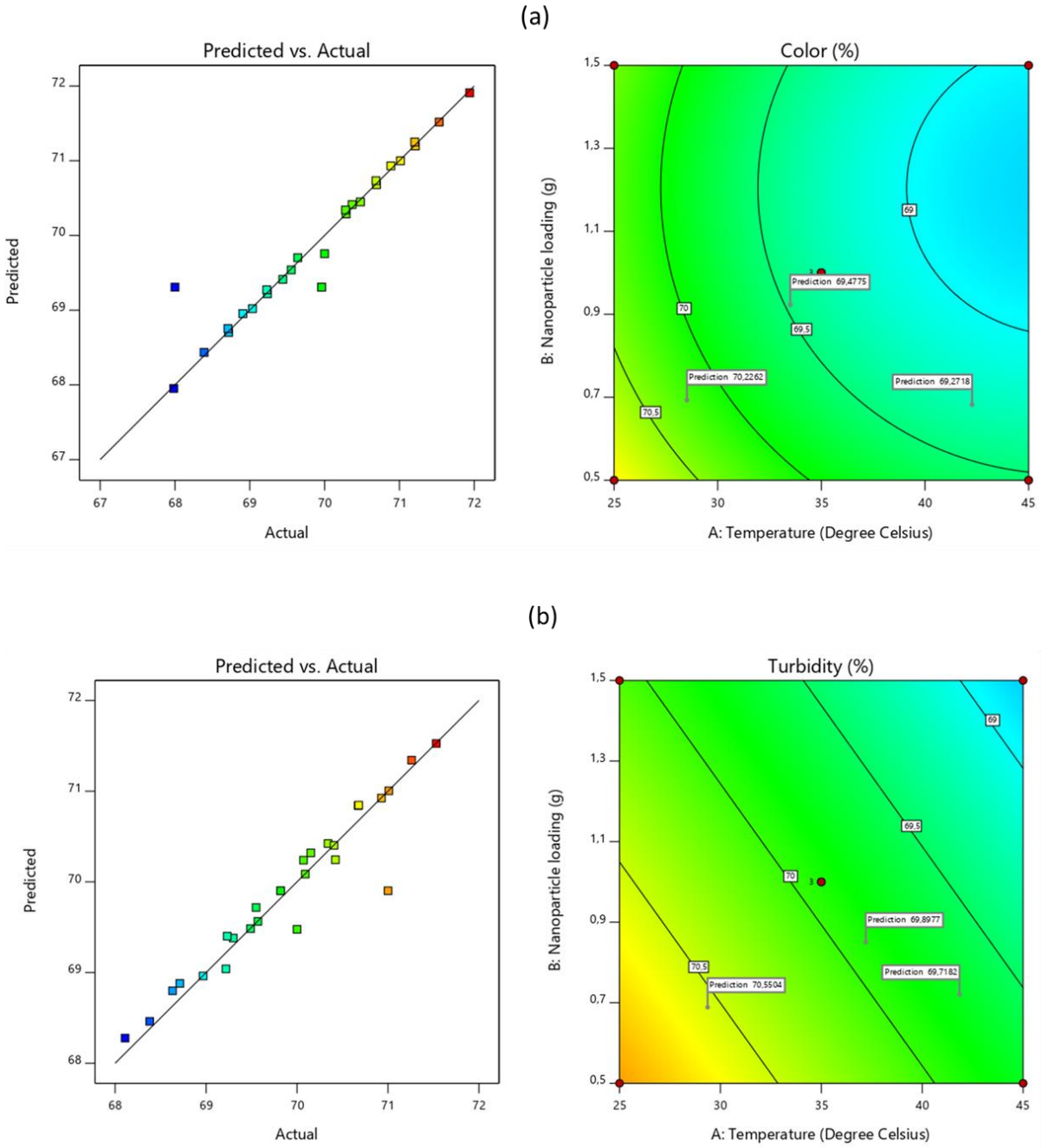

Figure 4-27 The predicted vs actual and contour plots for (a) colour and (b) turbidity removal

Table 4-24: BBD matrix and their respective experimental and predicted response

Runs	A-Temperature (C)	B-retention time (day)	C- Inoculum loading (ml)	D-MNPs Loading (g)	Y_1-Biogas yield (mL/day)		Y_2-COD reduction (%)		Y_3-Colour removal (%)		Y_4-Turbidity removal (%)	
					Expt	Pred	Expt	Pred	Expt	Pred	Expt	Pred
1	35	15	300	1	355.49	365.94	68.72	68.81	68.72	68.88	68.71	68.70
2	35	45	500	1	472.15	482.61	71.21	71.36	71.21	70.92	70.93	71.25
3	25	15	400	1	355.49	358.08	69.44	69.46	69.44	69.56	69.57	69.41
4	25	30	300	1	413.82	408.56	70.69	70.68	70.69	70.24	70.42	70.68
5	35	45	400	1.5	432.75	427.49	70.89	70.98	70.89	70.42	70.34	70.93
6	35	45	300	1	425.00	451.17	71.21	71.31	71.21	70.84	70.67	71.20
7	35	15	500	1	355.49	350.23	68.71	68.87	68.71	68.96	68.97	68.75
8	45	30	300	1	413.82	408.56	69.24	69.22	69.24	69.48	70.00	69.22
9	25	30	500	1	413.82	416.42	70.69	70.74	70.69	70.85	70.68	70.73
10	45	15	400	1	355.49	358.08	67.98	68.00	67.98	68.28	68.11	67.95
11	35	30	500	1.5	374.42	377.02	70.00	69.85	70.00	69.48	69.49	69.76
12	35	30	400	1	413.82	412.49	71.00	70.09	68.00	69.90	71.00	69.31
13	35	30	400	1	425.00	412.49	69.96	70.09	69.96	69.90	69.82	69.31
14	35	15	400	0.5	394.89	397.49	69.04	69.07	69.04	69.38	69.30	69.02
15	35	15	400	1.5	316.09	318.68	68.39	68.49	68.39	68.46	68.38	68.44
16	35	30	300	0.5	453.22	447.96	70.29	70.38	70.29	70.32	70.15	70.29
17	45	30	400	0.5	453.22	451.89	69.55	69.48	69.55	69.72	69.55	69.54
18	45	45	400	1	472.15	466.89	70.48	70.50	70.48	70.24	70.07	70.45
19	35	30	300	1.5	374.42	369.16	69.64	69.62	69.64	69.40	69.23	69.70
20	45	30	400	1.5	374.42	373.09	68.91	68.90	68.91	68.80	68.63	68.95
21	45	30	500	1	413.82	416.42	69.23	69.28	69.23	69.04	69.22	69.27
22	35	30	400	1	413.82	412.49	69.96	70.09	69.96	69.90	69.82	69.31
23	35	45	400	0.5	511.56	506.29	71.53	71.57	71.53	71.34	71.26	71.52
24	25	45	400	1	472.15	466.89	71.94	71.96	71.94	71.53	71.53	71.91
25	35	30	500	0.5	453.22	455.82	70.28	70.25	70.28	70.40	70.41	70.34
26	25	30	400	0.5	453.22	451.89	71.01	70.94	71.01	71.00	71.01	71.00
27	25	30	400	1.5	374.42	373.09	70.37	70.36	70.37	70.09	70.09	70.41

4.4.6 Optimisation of the BMP system using BBD

The conditions of variables that had an effect on maximizing the responses were determined using the design expert's numerical and graphical optimisation. The optimum conditions and their corresponding responses were derived from the constraints indicated in Table 2-11, and 10 out of 100 solutions were reported in Table 4-25, with the selected solution shown in the ramp plot below (Figure 4-28). According to the optimisation, an MNP load of 0.50 g, temperature of 35ºC, retention time of 45 days, and inoculum load of 500 ml will yield 522 ml of biogas, 71.50% COD reduction, 71.38% and 71.90% turbidity and colour removal, respectively, at a 95% confidence level and desirability of 96.6%. Based on the proposed solutions presented in Table 4-21, the first option was selected for verification to show the repeatability and applicability of the design models at 95% confidence level.

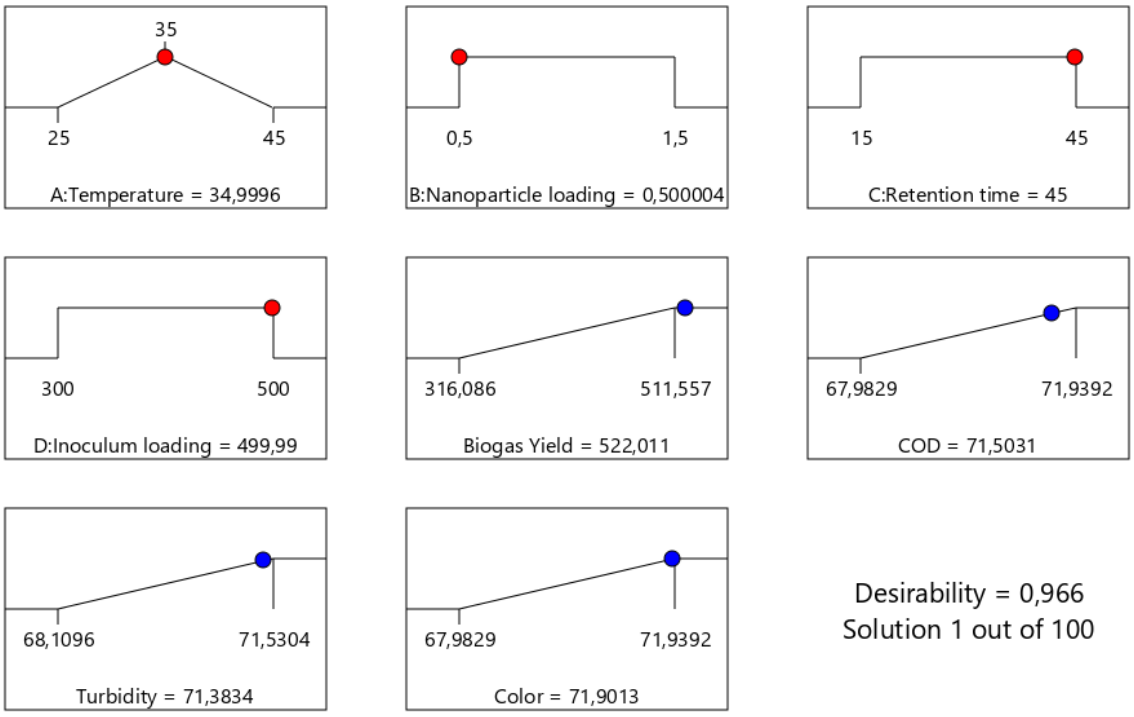

Figure 4-28 Ramp plots of optimisation study of the BMP system.

Table 4-25: BBD optimisation solutions

N^{o}	Temperature (°C)	Nanoparticle loading (g)	Retention time (day)	Inoculum loading (ml)	Biogas Yield (ml/day)	COD (%)	Turbidity (%)	Colour (%)	Desirability	
1	35	0.50	45	500	522	71.50	71.38	71.90	0.9665	Selected
2	35	0.50	45	499	522	71.50	71.38	71.90	0.9660	
3	35	0.50	45	497	522	71.50	71.38	71.90	0.9654	
4	35	0.51	45	500	522	71.50	71.37	71.90	0.9648	
5	35	0.50	45	500	522	71.40	71.37	71.90	0.9645	
6	35	0.50	45	494	522	71.50	71.38	71.90	0.9643	
7	35	0.50	45	500	522	71.52	71.41	71.90	0.9639	
8	35	0.50	45	493	522	71.50	71.38	71.90	0.9639	
9	35	0.52	45	500	522	71.50	71.37	71.90	0.9635	
10	35	0.50	45	491	522	71.50	71.38	71.90	0.9634	

4.4.7 Validation of the RSM optimisation results.

The optimum characteristics from the BDD-RSM optimisation analysis were validated to see if the experimental response results would match the expected responses. Figure 4-29 shows the findings achieved for biogas yield and Figure 4-30 presents that efficiency of the BMP for COD reduction, colour and turbidity removal after the experiment was completed. The results revealed a strong correlation between the predicted and experimental response results, with a little deviation of less than 2%. The removal efficiency of colour and turbidity was found to be similar. As a result, the design models were well fitted and explains the variability of the system with a 95% confidence level and 96.6% desirability.

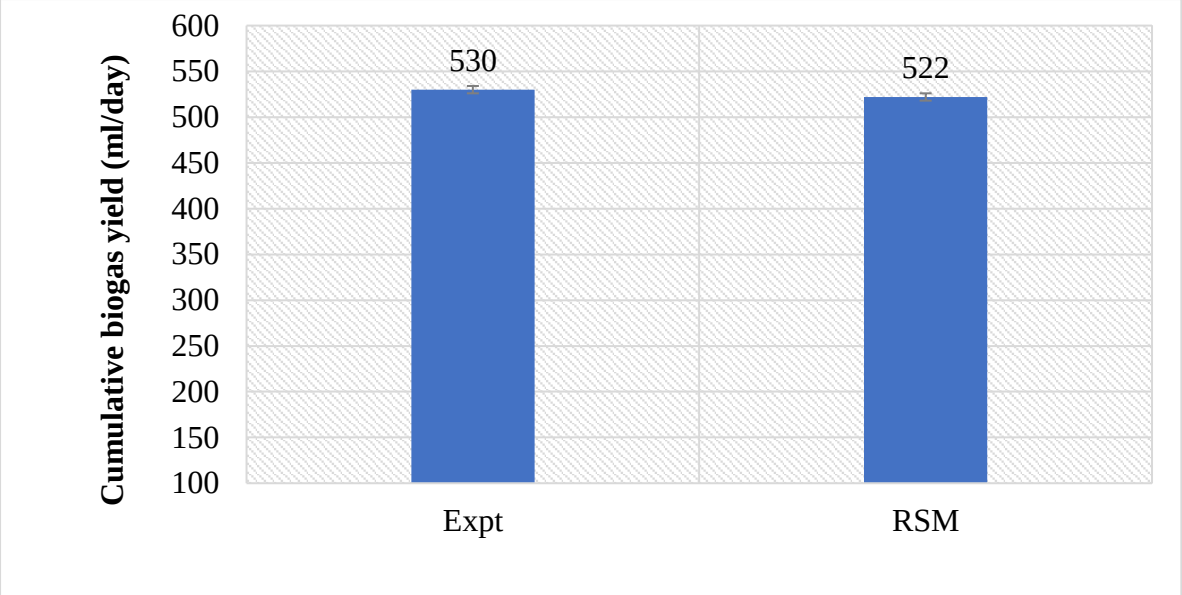

Figure 4-29 Comparing the RSM predicted response value to the experimented response value of biogas yield at MNP load of 0.5 g, temp of 35ºC, inoculum load of 500 ml and retention time of 45 days

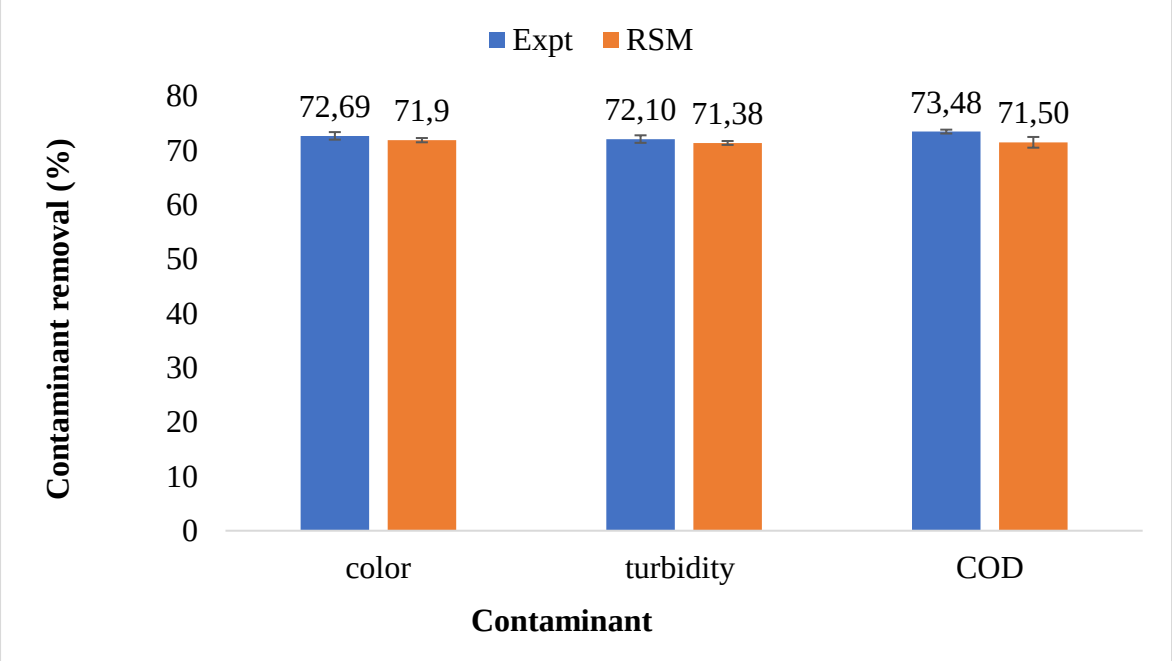

Figure 4-30 Comparing the RSM predicted response value to the experimented response values of COD, colour and turbidity at MNP load of 0.5 g, temp of 35ºC, inoculum load of 500 ml and retention time of 45 days

4.4.8 Summary

Many process engineers consider the requirement to minimize input materials while maximizing output when designing a process. The best-performing MNP was used in this study for an RSM optimisation study using Design Expert's Box-Behnken design. The BBD created 27 experimental runs based on four operational factors: MNP load (0.5–1.5 g), temperature (25–45°C), inoculum load (300–500 ml), and retention duration (15–45 days), with four responses: biogas yield (ml/day), COD reduction, colour, and turbidity removal efficiency (%). For the four responses, the outcomes of the experimental investigation were modelled of which reduced quadratic and 2FI regression models were obtained. For each response model, the analysis of variance revealed a high coefficient of determination of about 90% and low standard deviations. The P-value and F-value were found to be within the acceptable range, indicating that the model is significant. For all of the response models, the adequate precision was larger than 4. With a desirability of 96.6%, optimum values of MNP loading of 0.5 g, temperature of 35°C, inoculum loading of 500 ml, and retention time of 45 days were established after optimisation at 95% confidence level. The findings were then validated, revealing that the regression model had acceptable applicability, with a modest deviation of less than 2%.

4.5 Comparative study of magnetised and non-magnetised BMP

The application of magnetic field in anaerobic digestion has been explored and the influence of the magnetism on the microbial activities was found to greatly impact the performance of the AD system (Łebkowska, Narożniak-Rutkowska and Pajor 2013; de Souza Matos *et al.* 2020; Zieliński *et al.* 2021). In this present research study, the possibility of the biostimulation of both MNP and constant magnetic field of 20 mT were evaluated on a BMP system for biogas production from wastewater and the results were compared to a BMP system coupled with only MNPs.

4.5.1 Effect of magnetic field and magnetic nanoparticles on water quality

The study evaluated the BMP treatability performance for both bioreactors to determine their contaminant removal efficiency. COD, colour, and turbidity were the water parameters that were assessed in this study and the results are presented in Figure 4-31. The result showed more than 80% bioreactor removal efficiency for bioreactor MB which had both the MNP and 20 mT magnetic field exposure of 3 hours. Though bioreactor NMB had about 80% removal

efficiency for COD and turbidity, the colour removal efficiency was less than 70%. The removal efficiency for bioreactor MB was 84.78% COD, 83.07% colour, and 95.19% turbidity removal while bioreactor NMB recorded 79.33%, 60.46%, and 85.89% of COD, colour, and turbidity removal, respectively. The exposure of the BMP bioreactor with MNP additives to the magnetic field was found to improve the magnetic susceptibility of both the microbes and the MNP additives which led to the improvement in its degradation of the contaminants (Fang *et al.* 2010; Zaidi *et al.* 2014; de Souza Matos *et al.* 2020; Zieliński *et al.* 2021).

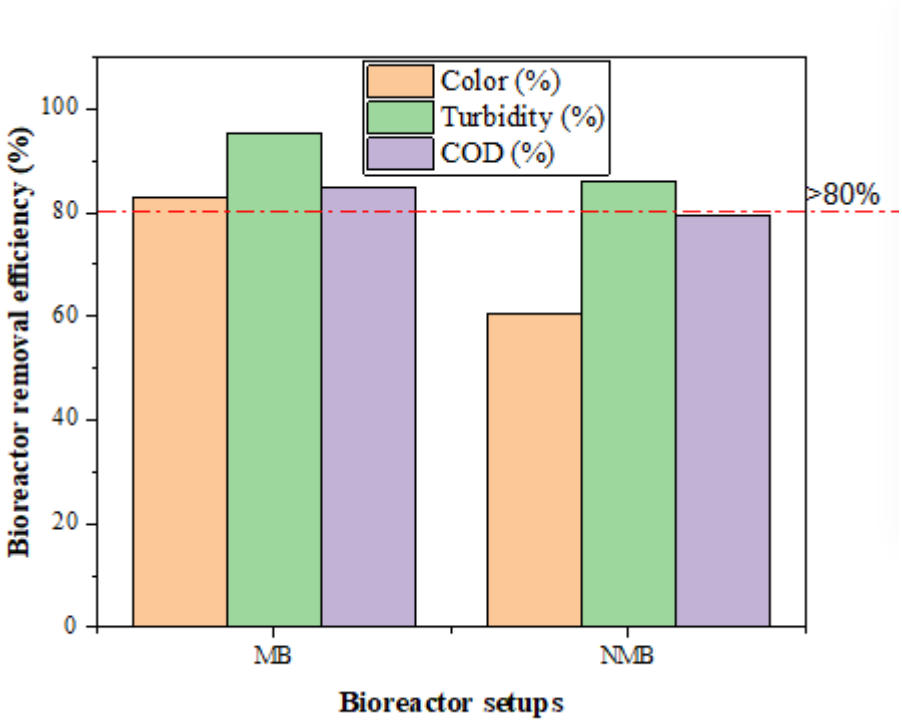

Figure 4-31 Bioreactor contaminant removal efficiency for BMP set-ups MB and NMB over 45 days digestion.

4.5.2 Effect of magnetic field and magnetic nanoparticles on biogas and methane yield

The daily biogas yield of each set-up (MB and NMB) was monitored, and the cumulative biogas yield is presented in Figure 4-32. Bioreactor MB recorded the highest biogas yield of mL/day after 45 days of digestion with a methane composition of 99.94% and the remaining 0.06% being the content of CO_2. While bioreactor NMB showed a biogas yield of mL/day with 98.85% methane and 1.15% CO_2 composition as presented in Figure 4-33 and Table 4-27. Though both BMP set-ups had over 90% methane yield, there was an increase in methane yield for the bioreactor MB which had a magnetic field exposure and MNP seeding. There was also about 40% increase in the biogas yield. The study has already established that MNP does have

a significant impact on the microbial activities of the AD system, however, its performance to stimulate methanogens to further produce more methane and also improve the hydrogenation of CO_2 to CH_4 was also found to improve (Niu *et al.* 2013; de Souza Matos *et al.* 2020; Kweinor Tetteh and Rathilal 2021b, 2021a; Tetteh and Rathilal 2021; Zieliński *et al.* 2021).

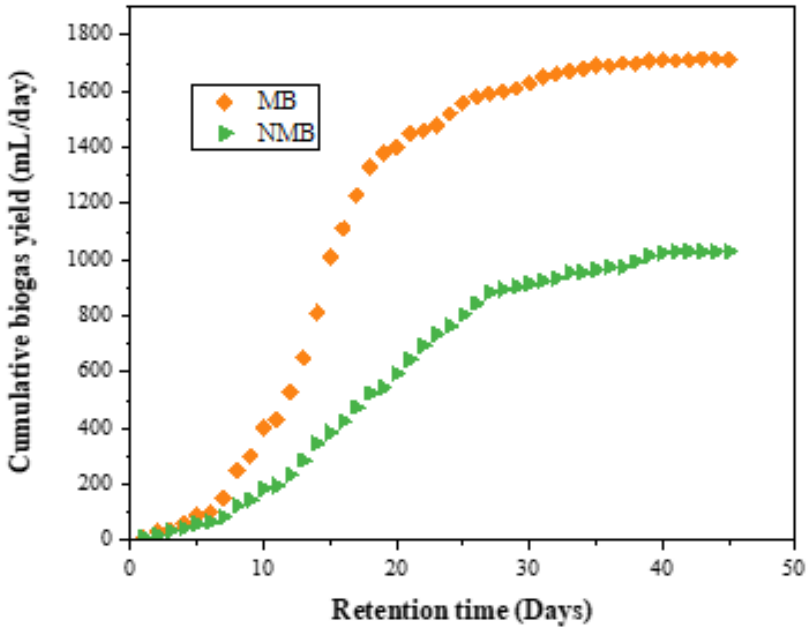

Figure 4-32 Cumulative biogas yield for BMP bioreactors MB & NMB over 45-days digestion

Table 4-26 shows the characteristic of the digestate for each set-up and the results obtained showed low digestate for bioreactor MB 12 mg TS/L and 10 mg VS/L as compared to NMB (16.6 mg TS/L and 15 mg VS/L). This indicated a higher microbial activity which resulted in higher degradation of the solids in the system (Kavitha *et al.* 2014; Niu *et al.* 2014; Liu *et al.* 2015; Tetteh, Amo-Duodu and Rathilal 2021). These results corresponded to the high biogas yield as shown in Figure 4-31. A VS/TS of 97% and 89% was recorded for bioreactors MB and NMB, respectively.

Table 4-26: Digestate characteristics of the BMP bioreactors MB & NMB after 45-days digestion.

Set-up	MB	NMB
pH	7.13	7.07
COD (mg/L)	350.00	475.33
Biogas yield (mL/day)	1715	1030
Methane yield (%)	1713.97	1018.155
TS (mg TS/L)	12	16.5
VS (mg VS/L)	10	15
TS (%)	70.97	60.08
VS (%)	69.07	53.61
VS/TS	0.97	0.89

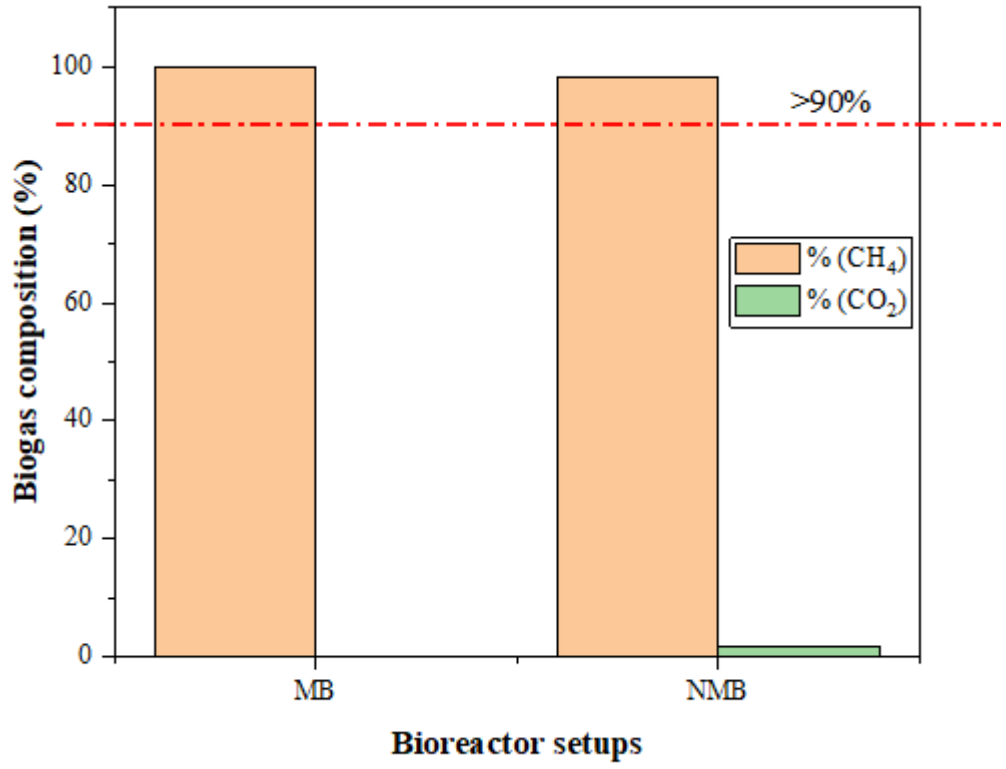

Figure 4-33 Biogas compositions of BMP bioreactors MB & NMB after 45-days digestion

4.5.3 Comparing the magnetised and non-magnetised BMP systems.

The study evaluated the synergistic impact of MNP and magnetic field exposure on a BMP for biogas production and wastewater treatment. The results as aforementioned and discussed showed a significant impact of the magnetic field and MNP of the BMP performance. About 40% increase in biogas yield and 2% increase in methane yield were observed for the BMP set-up MB with MNP seeding and 20 mT magnetic field exposure of 3 hours. In terms of treatability of the wastewater, there was a great increase in the removal efficiency for bioreactor MB as compared to NMB showing above 80% efficiency for contaminant removal. The bioreactor MB with MNP additives and magnetic field exposure was found to have higher degradability of organic matters which lead to higher biogas and methane yield as well as contaminant removal as shown in Table 4-27. The induction of magnetic field had stimulated the metabolic activities of the microbes, also magnetic field increased and improved the magnetic susceptibility of the microbes and the MNP which improved the interactions between the intracellular enzymes and metal ions (Niu *et al.* 2014; Zaidi *et al.* 2014; Dębowski *et al.* 2016; de Souza Matos *et al.* 2020; Abbas *et al.* 2021; Zieliński *et al.* 2021). Though the impact of magnetic field on the AD system had been proven, limited information is found in its application in biogas production from wastewater which necessitated this study. Herein, there is the need to further carry out transcriptomic analysis to understand the microbial community.

Table 4-27: Comparing the performance of magnetised and non-magnetised BMP systems

Set-up	**MB**	**NMB**
pH	7.13	7.07
Colour (%)	83.07	60.46
Turbidity	95.19	85.89
COD (%)	84.78	79.33
Biogas Yield (mL/day)	1715	1030
Methane yield (mL/day)	1713.97	1018.16
COD (mg/L)	350	475.33

4.5.4 Kinetic study of magnetised and non-magnetised BMP systems.

The kinetics of the system to understand the anaerobic digestion pathway was also evaluated for both set-ups by fitting the cumulative yield (Figure 4-32) on the first-order model (eqn.3.6)

and modified Gompertz model (eqn.3.7) and the results obtained (constants) are presented in Table 4-28. The kinetics of the system was found to fit best on Gompertz (Figure 4-34) with a correlation coefficient (R^2) value of 0.9969 and 0.9987 for bioreactors MB and NMB, respectively with an error margin of 0.0013- 0.0031. The lag phase for 6 days was found for the bioreactor MB and 8 days for NMB. Though the first-order model predicted higher biogas yield than the modified Gompertz, it was observed that the modified Gompertz predicted biogas yield was closer to the measured. The summary of the kinetic study is presented in Table 4-28.

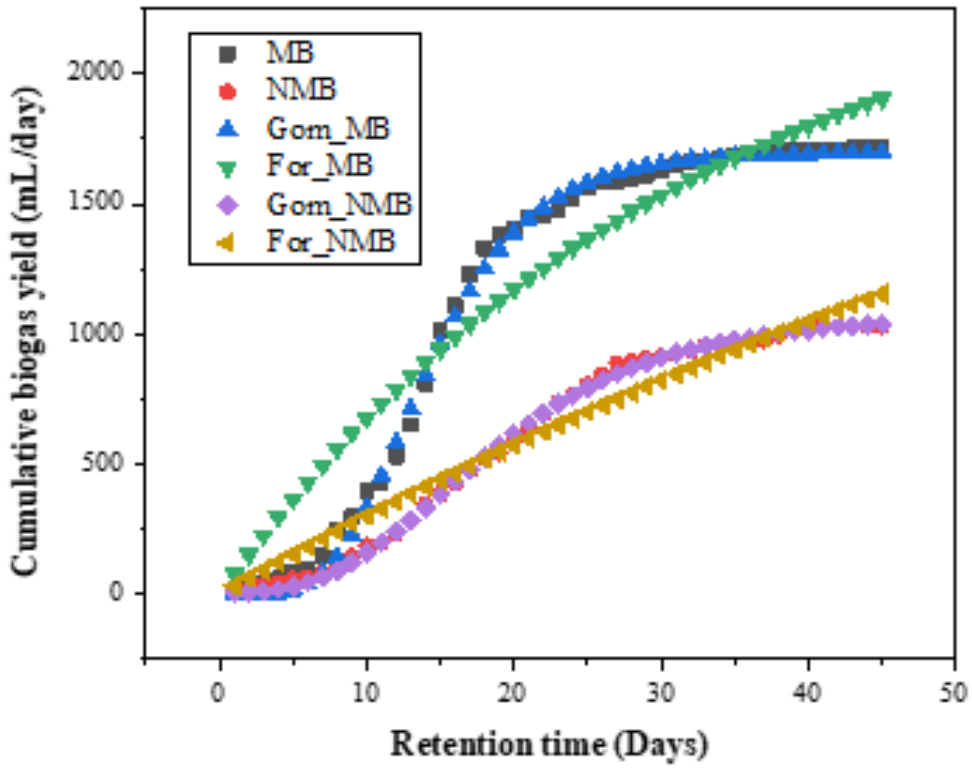

Figure 4-34 Fitting of Cumulative biogas yield on First order (FOR) and modified Gompertz (GOM) kinetic models for BS wastewater.

Table 4-28: Summary of the kinetic study for BMP bioreactors MB & NMB over 45-days digestion

Set-up	MB		NMB	
Model	First order model	Modified Gompertz model	First order model	Modified Gompertz model
St (mL/day)	1715	1715	1030	1030
Sp (mL/day)	1904.87	1695.92	1154.72	1038.53
Sp-St (mL/day)	189.87	-19.08	124.72	8.53
Sm (mL/day)	2529.45	1697.73	3332.22	1063.97
SSR	1566643	78444.76	1566643	11331.42
R^2	0.9277	0.9969	0.9592	0.9987
k (1/day)	0.0311	0.2094	0.0095	0.1248
ʎ (Day)	-	6.32	-	8.18

* R^2 = correlation coefficient, ʎ = lag phase, SSR= sum of square error, Sp = model predicted cumulative biogas yield, St= measure cumulative biogas yield, and Sm = Maximum cumulative yield predicted by the models and k= rate constant*

4.5.5 Summary.

To increase the performance of BMP for both biogas production from wastewater as well as its treatability of the wastewater, a comparative study was done to evaluate magnetised BMP and non-magnetised BMP systems. The results showed good degradability of organic matter which resulted in higher biogas and methane yield for the magnetised BMP system as compared to the non-magnetised BMP system. About 40% increase in biogas yield and 2% increase in methane yield was obtained for the magnetised BMP system which showed above 80% bioreactor efficiency. An induction of BMP system with 0.5 g MNP additives with 20 mT magnetic field intensity for 3 hours was found to improve the BMP system significantly, and further studies are recommended for a better understanding of the microbial communities and the magnetic impact.

Chapter Five

CONCLUSION AND RECOMMENDATION

The important findings and deduction made from the research study is presented in this chapter. Some recommendations were made for additional research and understanding of the work in order to make smart decisions in energy and wastewater treatment. A biochemical methane potential test was carried out for biogas production from industrial and municipal wastewater collected from a local sugar refinery, Umbilo water works, and Umgeni water in South Africa's KwaZulu-Natal province. The specific objectives of the study were as follows;

- To synthesize and characterise the magnetised nanoparticles.
- To evaluate the AD treatability performance in terms of water quality.
- To evaluate and optimise the anaerobic magnetised system for methane enhancement for biogas production.
- To compare the performance of magnetised biochemical methane potential to non-magnetised biochemical methane potential.
- To study the kinetics of the anaerobic magnetised system using modified Gompertz and first-order kinetic models.

5.1 Conclusion

The following findings were obtained from the observations made from the different MNPs on BMP systems understudied; the RSM optimisation of the best MNP and the comparative study between magnetised BMP and non-magnetised BMP systems.

- The feasibility of the MNPs in the BMP system for biogas production from wastewater was possible as a high yield of biogas was observed for all systems with NPs with methane composition above 80%. These results showed about 20% increase in methane as compared to the control system with no NPs. The key finding in this feasibility study was that the addition of NPs had little impact on colour removal and that the dose is within an allowable limit.

- The results reveal that the co-precipitation synthesis procedure was successful; the elemental compositions show that magnetite (Fe and O) is present in each of the MNPs, with particle sizes ranging from 3.2 to 5.42 nm. Face-centred and monoclinic crystal structures were discovered in all MNPs, with O-H stretching and Fe-O vibrations functional groups being common. Magnetite's surface area (27.59 m^2/g) was found to be bigger than that of hybridized NPs (less than 20 m^2/g but greater than 9 m^2/g). When the co-precipitation method was successfully used to magnetise all of the NPs, the synthesis goal was achieved.
- The AD process was shown to be more efficient when magnetic nanoparticles were used on the two samples. The results suggest that the BMP systems with MNP additions have good COD and turbidity degradation. The performance of the MNPs were magnate (mFe) > copper ferrite (CmFe) > nickel ferrite (NmFe) > magnesium ferrite (MmFe) > aluminium ferrite (AmFe).
- With the addition of MNPs, the biogas and methane yields increased by approximately 100% and 20%, respectively, for BMP systems. It was also discovered that adding MNPs to the AD process enhanced not only the biogas and methane yield but also the treatability of the AD systems. When compared to the control bioreactors (with no MNPs), the efficiency of the BMP bioreactors with MNPs was enhanced and was shown to be approximately 20-30%.
- After optimisation at 95% confidence level, optimum parameters were MNP loading of 0.5 g, temperature of 35°C, inoculum loading of 500 ml, and retention time of 45 days were established with a desirability of 96.6%. A biogas yield of 530 ml/day, COD reduction of 73.48%, colour removal of 72.69%, and turbidity removal of 71.38% were obtained at the optimal conditions, and the validation test results revealed similar performance to the predicted response values with a deviation of less than 2%.
- The comparative study was done to evaluate magnetised BMP and non-magnetised BMP systems and showed good degradability of organic matter which resulted in higher biogas and methane yield for the magnetised BMP system as compared to the non-magnetised BMP system.
- About 40% increase in biogas yield and 2% increase in methane yield was obtained for the magnetised BMP system which showed over 80% bioreactor efficiency. An induction of BMP system with 0.5 g MNP additives with 20 mT magnetic field intensity for 3 hours was found to improve the BMP system significantly for colour removal as compared to the non-magnetised BMP system.

It can therefore be concluded that the addition of synthesized magnetic nanoparticles to anaerobic digestion process for biogas production from wastewater is highly viable which will increase the performance of the AD. It will also enhance the biogas production as well as increase the methane yield. Incorporation of a magnetic field to the AD system with MNP additives was also found to be viable with a high-performance rate.

5.2 Recommendation

Based on the research findings the followings recommendations were made for better understanding and decision making.

- Though the results obtained are promising and can be used, in-depth research on a large-scale of the work is needed to determine the optimum conditions on a large scale and to verify if similar performance can be reached at the optimum conditions. Parameters such as the MNP loading is key in this and needs much attention.
- There is a need to research on the microbial community of the system's microorganisms. It is necessary to have a thorough understanding of the microorganisms as well as the substantial impact of MNP on the microbial community and its activities.
- Technoeconomic analysis is highly recommended to further attest the economic viability of this process developed.

Reference

Abbas, Y., Yun, S., Wang, K., Shah, F. A., Xing, T. and Li, B. 2021. Static-magnetic-field coupled with fly-ash accelerant: A powerful strategy to significantly enhance the mesophilic anaerobic-co-digestion. *Bioresource Technology*, 327: 124793.

Abdelsalam, E., Samer, M., Attia, Y., Abdel-Hadi, M., Hassan, H. and Badr, Y. 2016. Comparison of nanoparticles effects on biogas and methane production from anaerobic digestion of cattle dung slurry. *Renewable Energy*, 87: 592-598.

Abdelsalam, E., Samer, M., Attia, Y., Abdel-Hadi, M., Hassan, H. and Badr, Y. 2017. Influence of zero valent iron nanoparticles and magnetic iron oxide nanoparticles on biogas and methane production from anaerobic digestion of manure. *Energy*, 120: 842-853.

Abdelsalam, E. M. and Samer, M. 2019. Biostimulation of anaerobic digestion using nanomaterials for increasing biogas production. *Reviews in Environmental Science and Bio/Technology*, 18 (3): 525-541.

Abdelwahab, T. A. M., Mohanty, M. K., Sahoo, P. K. and Behera, D. 2020. Application of nanoparticles for biogas production: Current status and perspectives. *Energy sources, part a: recovery, utilization, and environmental Effects*, Article ID: 1-13.

Abu-Reesh, I. M. 2014. Kinetics of anaerobic digestion of labaneh whey in a batch reactor. *African Journal of Biotechnology*, 13 (16).

Abubakar, B. and Ismail, N. 2012. Anaerobic digestion of cow dung for biogas production. *ARPN journal of engineering and applied sciences*, 7 (2): 169-172.

Adefarati, T., Papy, N. B., Thopil, M. and Tazvinga, H. 2017. Non-renewable distributed generation technologies: a review. In: *Handbook of Distributed Generation*. Springer, 69-105.

Adewumi, J., Ilemobade, A. and Van Zyl, J. 2010. Treated wastewater reuse in South Africa: Overview, potential and challenges. *Resources, Conservation and Recycling*, 55 (2): 221-231.

Affairs, D. o. E. 2014. *National Guideline for the Discharge of Effluent from Land based Sources into the Coastal Environment.* Pretoria, South Africa.: 28 June 2021).

Afgan, N. H. and Carvalho, M. G. 2002. Multi-criteria assessment of new and renewable energy power plants. *Energy*, 27 (8): 739-755.

Ağbulut, Ü. and Sarıdemir, S. 2021. A general view to converting fossil fuels to cleaner energy source by adding nanoparticles. *International Journal of Ambient Energy*, 42 (13): 1569-1574.

Ahmed, M. B., Zhou, J. L., Ngo, H. H., Guo, W., Thomaidis, N. S. and Xu, J. 2017. Progress in the biological and chemical treatment technologies for emerging contaminant removal from wastewater: a critical review. *Journal of hazardous materials*, 323: 274-298.

AHPA, A. 2007. WEF (2005) Standard methods for the examination of water and wastewater. *American Public Health Association, American Water Works Association, and Water Environment Federation*, Article ID.

AHPA, A. P. H. A., ,. 2012. *Standard Methods for the Examination of Water and Wastewater.* , Article ID. Washington, DC.: 11 August 2021).

Ajay, C., Mohan, S., Dinesha, P. and Rosen, M. A. 2020. Review of impact of nanoparticle additives on anaerobic digestion and methane generation. *Fuel*, 277: 118234.

Allured, B., DelaCruz, S., Darling, T., Huda, M. N. and Subramanian, V. R. 2014. Enhancing the visible light absorbance of Bi2Ti2O7 through Fe-substitution and its effects on photocatalytic hydrogen evolution. *Applied Catalysis B: Environmental*, 144: 261-268.

Ambashta, R. D. and Sillanpää, M. 2010. Water purification using magnetic assistance: A review. *Journal of Hazardous Materials*, 180 (1): 38-49.

Amen, T. W. M., Eljamal, O., Khalil, A. M. E., Sugihara, Y. and Matsunaga, N. 2018. Methane yield enhancement by the addition of new novel of iron and copper-iron bimetallic nanoparticles. *Chemical Engineering and Processing - Process Intensification*, 130: 253-261.

Amo-Duodu, G., Kweinor Tetteh, E., Rathilal, S. and Chollom, M. N. 2022. Synthesis and characterization of magnetic nanoparticles: Biocatalytic effects on wastewater treatment. *Materials Today: Proceedings*, Article ID.

Amo-Duodu, G., Rathilal, S., Chollom, M. N. and Kweinor Tetteh, E. 2021a. Application of metallic nanoparticles for biogas enhancement using the biomethane potential test. *Scientific African*, 12: e00728.

Amo-Duodu, G., Tetteh, E. K., Rathilal, S., Armah, E. K., Adedeji, J., Chollom, M. N. and Chetty, M. 2021b. Effect of Engineered Biomaterials and Magnetite on Wastewater Treatment: Biogas and Kinetic Evaluation. *Polymers*, 13 (24): 4323.

APHA, A., WEF. 2012. Standard methods for examination of water and wastewater, APHA, AWWA, WEF. Standard methods exam. *Water Wastewater*, Article ID.

Appels, L., Baeyens, J., Degrève, J. and Dewil, R. 2008. Principles and potential of the anaerobic digestion of waste-activated sludge. *Progress in energy and combustion science*, 34 (6): 755-781.

Arun, K. 2016. *Wastewater Treatment Process*. Available: http://web.iitd.ac.in/~arunku/files/CVL100_Y16/LecSep1220.pdf (Accessed 29 August 2021)

aus der Beek, T., Weber, F. A., Bergmann, A., Hickmann, S., Ebert, I., Hein, A. and Küster, A. 2016. Pharmaceuticals in the environment—Global occurrences and perspectives. *Environmental toxicology and chemistry*, 35 (4): 823-835.

Azizan, N. A. Z., Yuzir, A. and Abdullah, N. 2021. Pharmaceutical compounds in anaerobic digestion: A review on the removals and effect to the process performance. *Journal of Environmental Chemical Engineering*, 9 (5): 105926.

Bachmann, N., la Cour Jansen, J., Bochmann, G. and Montpart, N. 2015. *Sustainable biogas production in municipal wastewater treatment plants*. IEA Bioenergy Massongex, Switzerland.

Bahadur, N. M., Chowdhury, F., Obaidullah, M., Hossain, M. S., Rashid, R., Akter, Y., Furusawa, T., Sato, M. and Suzuki, N. 2019. Ultrasonic-Assisted Synthesis, Characterization, and Photocatalytic Application of SiO₂@TiO₂ Core-Shell Nanocomposite Particles. *Journal of Nanomaterials*, 2019: 6368789.

Baniamerian, H., Isfahani, P. G., Tsapekos, P., Alvarado-Morales, M., Shahrokhi, M., Vossoughi, M. and Angelidaki, I. 2019. Application of nano-structured materials in anaerobic digestion: Current status and perspectives. *Chemosphere*, 229: 188-199.

Bar-On, Y. M., Phillips, R. and Milo, R. 2018. The biomass distribution on Earth. *Proceedings of the National Academy of Sciences*, 115 (25): 6506.

Begum, R. A., Sohag, K., Abdullah, S. M. S. and Jaafar, M. 2015. CO2 emissions, energy consumption, economic and population growth in Malaysia. *Renewable and Sustainable Energy Reviews*, 41: 594-601.

Bekun, F. V., Alola, A. A. and Sarkodie, S. A. 2019. Toward a sustainable environment: Nexus between CO2 emissions, resource rent, renewable and nonrenewable energy in 16-EU countries. *Science of The Total Environment*, 657: 1023-1029.

Bilecka, I. and Niederberger, M. 2010. Microwave chemistry for inorganic nanomaterials synthesis. *Nanoscale*, 2 (8): 1358-1374.

Bochmann, G. and Montgomery, L. F. 2013. Storage and pre-treatment of substrates for biogas production. In: *The biogas handbook*. Elsevier, 85-103.

Bosque-Sendra, J. M., Pescarolo, S., Cuadros-Rodríguez, L., García-Campaña, A. M. and Almansa-López, E. M. 2001. Optimizing analytical methods using sequential response surface

methodology. Application to the pararosaniline determination of formaldehyde. *Fresenius' journal of analytical chemistry*, 369 (7): 715-718.

BP, p. I. c. 2021. *Statistical Review of World Ennergy* Available: https://www.bp.com/content/dam/bp/business-sites/en/global/corporate/pdfs/energy-economics/statistical-review/bp-stats-review-2021-full-report.pdf (Accessed 26 January 2022).

Brar, S. K., Verma, M., Tyagi, R. and Surampalli, R. 2010. Engineered nanoparticles in wastewater and wastewater sludge–Evidence and impacts. *Waste management*, 30 (3): 504-520.

Brollo, M. E. F., Veintemillas-Verdaguer, S., Salván, C. M. and Morales, M. d. P. 2017. Key Parameters on the Microwave Assisted Synthesis of Magnetic Nanoparticles for MRI Contrast Agents. *Contrast Media & Molecular Imaging*, 2017: 8902424.

Budiyono, I. S. and Sumardiono, S. 2014. Kinetic model of biogas yield production from vinasse at various initial pH: comparison between modified Gompertz model and first order kinetic model. *Research Journal of Applied Sciences, Engineering and Technology*, 7 (13): 2798-2805.

Bull, S. R. 2001. Renewable energy today and tomorrow. *Proceedings of the IEEE*, 89 (8): 1216-1226.

Cao, L.-y., Zhang, C.-b. and Huang, J.-f. 2005. Synthesis of hydroxyapatite nanoparticles in ultrasonic precipitation. *Ceramics International*, 31 (8): 1041-1044.

CarbonBrief. 2018. *The Carbon Brief Profile: South Africa.* . Available: https://www.carbonbrief.org/the-carbon-brief-profile-south-africa (Accessed 19 July 2021)

Casadonte, D. J., Li, Z. and Mingos, D. M. P. 2007. 1.12 - Applications of Sonochemistry and Microwaves in Organometallic Chemistry. In: Mingos, D. M. P. and Crabtree, R. H. eds. *Comprehensive Organometallic Chemistry III*. Oxford: Elsevier, 307-339. Available: http://www.sciencedirect.com/science/article/pii/B0080450474000133 (Accessed 12 October 2021)

Cervadoro, A., Coclite, A., Di Mascolo, D., Ferreira, M., Palange, A., Palomba, R., Pereira, R. C. and Decuzzi, P. 2018. 10 - Smart nanoconstructs for theranostics in cancer and cardiovascular diseases. In: Focarete, M. L. and Tampieri, A. eds. *Core-Shell Nanostructures for Drug Delivery and Theranostics*. Woodhead Publishing, 297-321. Available: https://www.sciencedirect.com/science/article/pii/B9780081021989000107 (Accessed 17 September 2021)

Chan, Y. J., Chong, M. F., Law, C. L. and Hassell, D. G. 2009. A review on anaerobic–aerobic treatment of industrial and municipal wastewater. *Chemical Engineering Journal*, 155 (1): 1-18.

Change, I. P. O. C. 2006. 2006 IPCC guidelines for national greenhouse gas inventories. *Institute for Global Environmental Strategies, Hayama, Kanagawa, Japan*, Article ID.

Chaudhary, P. P., Brablcová, L., Buriánková, I. and Rulík, M. 2013. Molecular diversity and tools for deciphering the methanogen community structure and diversity in freshwater sediments. *Applied Microbiology and Biotechnology*, 97 (17): 7553-7562.

Chen, H. H. and Lee, A. H. 2014a. Comprehensive overview of renewable energy development in Taiwan. *Renewable and Sustainable Energy Reviews*, 37: 215-228.

Chen, H. H. and Lee, A. H. I. 2014b. Comprehensive overview of renewable energy development in Taiwan. *Renewable and Sustainable Energy Reviews*, 37: 215-228.

Chen, J. L., Steele, T. W. and Stuckey, D. C. 2018. The effect of Fe2NiO4 and Fe4NiO4Zn magnetic nanoparticles on anaerobic digestion activity. *Science of the total environment*, 642: 276-284.

Chen, L. and Neibling, H. 2014. Anaerobic digestion basics. *University of Idaho Extension*, 6.

Chen, Y.-R. and Hashimoto, A. G. 1978. *Kinetics of methane fermentation*. Science and Education Administration, Clay Center, NE (USA). Meat Animal ….

Chetty, S. and Pillay, L. 2019. Assessing the influence of human activities on river health: a case for two South African rivers with differing pollutant sources. *Environmental monitoring and assessment*, 191 (3): 1-11.

Chiu, H.-C. and Yeh, C.-S. 2007. Hydrothermal Synthesis of SnO2 Nanoparticles and Their Gas-Sensing of Alcohol. *The Journal of Physical Chemistry C*, 111 (20): 7256-7259.

Cho, E. J., Holback, H., Liu, K. C., Abouelmagd, S. A., Park, J. and Yeo, Y. 2013. Nanoparticle characterization: state of the art, challenges, and emerging technologies. *Molecular pharmaceutics*, 10 (6): 2093-2110.

Chollom, M. N., Rathilal, S., Swalaha, F. M., Bakare, B. F. and Tetteh, E. K. 2020. Removal of antibiotics during the anaerobic digestion of slaughterhouse wastewater. *Planning*, 15 (3): 335-343.

Choorit, W. and Wisarnwan, P. 2007. Effect of temperature on the anaerobic digestion of palm oil mill effluent. *Electronic Journal of Biotechnology*, 10 (3): 376-385.

Christou, M., Vasileiadis, S., Karpouzas, D. G., Angelidaki, I. and Kotsopoulos, T. 2021. Effects of organic loading rate and hydraulic retention time on bioaugmentation performance to tackle ammonia inhibition in anaerobic digestion. *Bioresource Technology*, 334: 125246.

Chum, H., Faaij, A., Moreira, J., Berndes, G., Dhamija, P., Dong, H., Gabrielle, B., Eng, A. G., Lucht, W. and Mapako, M. 2011. Bioenergy. In: *Renewable energy sources and climate change mitigation: Special report of the Intergovernmental Panel on Climate Change*. Cambridge University Press, 209-332.

Chum, H. F., A. ; Moreira, J. ; Berndes, G. ; Dhamija, P. ; Dong, H. ; Gabrielle, B. ; Goss Eng, A. ; Lucht, W. ; Mapako, M. ; Masera Cerutti, O. ; McIntyre, T. ; Minowa, T. ; Pingoud, Kim. 2011. *Bioenergy. Renewable Energy Sources and Climate Change Mitigation: Special Report of the Intergovernmental Panel on Climate Change*

Cioabla, A. E., Ionel, I., Dumitrel, G.-A. and Popescu, F. 2012. Comparative study on factors affecting anaerobic digestion of agricultural vegetal residues. *Biotechnology for biofuels*, 5 (1): 1-9.

Corbett, J. F. 1972. Pseudo first-order kinetics. *Journal of Chemical Education*, 49 (10): 663.

Danso-Boateng, E., Mohammed, A. S., Sander, G., Wheatley, A. D., Nyktari, E. and Usen, I. C. 2021. Production and characterisation of adsorbents synthesised by hydrothermal carbonisation of biomass wastes. *SN Applied Sciences*, 3 (2): 257.

Daou, T., Pourroy, G., Bégin-Colin, S., Greneche, J.-M., Ulhaq-Bouillet, C., Legaré, P., Bernhardt, P., Leuvrey, C. and Rogez, G. 2006. Hydrothermal synthesis of monodisperse magnetite nanoparticles. *Chemistry of Materials*, 18 (18): 4399-4404.

Das, S., Mukherjee, A., Sengupta, G. and Singh, V. K. 2020. Chapter 18 - Overview of nanomaterials synthesis methods, characterization techniques and effect on seed germination. In: Singh, P., Borthakur, A., Mishra, P. K. and Tiwary, D. eds. *Nano-Materials as Photocatalysts for Degradation of Environmental Pollutants*. Elsevier, 371-401. Available: http://www.sciencedirect.com/science/article/pii/B9780128185988000183 (Accessed 5 August 2021)

de Souza Matos, J. C., Rozenský, L., Vrba, Z., Hansen, J. M., Hájek, M., Lípa, J., Rodrigues, C. V., Luz, F. G. F., de Castro, M. C. A. A. and Maintinguer, S. I. 2020. Application of electromagnetic field in anaerobic biodigestion in batch reactors. *BioResources*, 15 (3): 4972-4981.

Dębowski, M., Zieliński, M., Kisielewska, M. and Hajduk, A. 2016. Effect of constant magnetic field on anaerobic digestion of algal biomass. *Environmental technology*, 37 (13): 1656-1663.

Deepanraj, B., Sivasubramanian, V. and Jayaraj, S. 2017. Effect of substrate pretreatment on biogas production through anaerobic digestion of food waste. *International Journal of Hydrogen Energy*, 42 (42): 26522-26528.

Dennehy, C., Lawlor, P. G., Croize, T., Jiang, Y., Morrison, L., Gardiner, G. E. and Zhan, X. 2016. Synergism and effect of high initial volatile fatty acid concentrations during food waste and pig manure anaerobic co-digestion. *Waste Management*, 56: 173-180.

Deublein, D. and Steinhauser, A. 2011. *Biogas from waste and renewable resources: an introduction*. John Wiley & Sons.

Dhinakar, K. G. and Sundar, S. M. 2017. Structural & Optical Properties of Co DOPED SnO2 Nanoparticles Synthesised By Microwave Assisted Solvothermal Method. *IOSR J. Appl. Phys.*, 3: 92.

Dhungana, A., Dutta, A. and Basu, P. 2012. Torrefaction of non-lignocellulose biomass waste. *The Canadian Journal of Chemical Engineering*, 90 (1): 186-195.

Ding, Y., Jiang, Y., Xu, F., Yin, J., Ren, H., Zhuo, Q., Long, Z. and Zhang, P. 2010. Preparation of nano-structured LiFePO4/graphene composites by co-precipitation method. *Electrochemistry Communications*, 12 (1): 10-13.

Dobre, P., Nicolae, F. and Matei, F. 2014. Main factors affecting biogas production-an overview. *Romanian Biotechnological Letters*, 19 (3): 9283-9296.

Ealias, A. M. and Saravanakumar, M. 2017. A review on the classification, characterisation, synthesis of nanoparticles and their application. In: Proceedings of *IOP Conf. Ser. Mater. Sci. Eng.* 032019.

Edokpayi, J. N., Odiyo, J. O. and Durowoju, O. S. 2017. Impact of wastewater on surface water quality in developing countries: a case study of South Africa. *Water quality*, Article ID: 401-416.

El-Mashad, H. M., Zeeman, G., Van Loon, W. K., Bot, G. P. and Lettinga, G. 2004. Effect of temperature and temperature fluctuation on thermophilic anaerobic digestion of cattle manure. *Bioresource technology*, 95 (2): 191-201.

El Ghandoor, H., Zidan, H., Khalil, M. M. and Ismail, M. 2012. Synthesis and some physical properties of magnetite (Fe3O4) nanoparticles. *Int. J. Electrochem. Sci*, 7 (6): 5734-5745.

Elhambakhsh, A., Zaeri, M. R., Mehdipour, M. and Keshavarz, P. 2020. Synthesis of different modified magnetic nanoparticles for selective physical/chemical absorption of CO2 in a bubble column reactor. *Journal of Environmental Chemical Engineering*, 8 (5): 104195.

Energy, E. 2020. *Energy Wise*. Available: https://www.edfenergy.com/terms-conditions/accessibility-statement (Accessed 21 June 2021)

Enitan, A. M., Adeyemo, J., Kumari, S. K., Swalaha, F. M. and Bux, F. 2015. Characterization of brewery wastewater composition. *International Journal of Environmental and Ecological Engineering*, Article ID.

Esakkimuthu, T., Sivakumar, D. and Akila, S. 2014. Application of nanoparticles in wastewater treatment. *Pollut. Res*, 33 (03): 567-571.

Esfandiari, N., Kashefi, M., Afsharnezhad, S. and Mirjalili, M. 2020. Insight into enhanced visible light photocatalytic activity of Fe3O4–SiO2–TiO2 core-multishell nanoparticles on the elimination of Escherichia coli. *Materials Chemistry and Physics*, 244: 122633.

Evans, T. D. 2016. *Sewage sludge: operational and environmental issues*. Foundation for Water Research.

Fang, M., Mishima, F., Akiyama, Y. and Nishijima, S. 2010. Fundamental study on magnetic separation of organic dyes in wastewater. *Physica C: Superconductivity and its applications*, 470 (20): 1827-1830.

Fayazzadeh, S., Khodaei, M., Arani, M., Mahdavi, S., Nizamov, T. and Majouga, A. 2020. Magnetic properties and magnetic hyperthermia of cobalt ferrite nanoparticles synthesized by hydrothermal method. *Journal of Superconductivity and Novel Magnetism*, 33 (7): 2227-2233.

Fedailaine, M., Moussi, K., Khitous, M., Abada, S., Saber, M. and Tirichine, N. 2015. Modeling of the anaerobic digestion of organic waste for biogas production. *Procedia Computer Science*, 52: 730-737.

Feng, Y., Zhang, Y., Quan, X. and Chen, S. 2014. Enhanced anaerobic digestion of waste activated sludge digestion by the addition of zero valent iron. *Water research*, 52: 242-250.

Ferreira, S. C., Bruns, R., Ferreira, H., Matos, G., David, J., Brandão, G., da Silva, E. P., Portugal, L., Dos Reis, P. and Souza, A. 2007. Box-Behnken design: an alternative for the optimization of analytical methods. *Analytica chimica acta*, 597 (2): 179-186.

Fito, J., Tefera, N. and Van Hulle, S. W. 2019. Sugarcane biorefineries wastewater: bioremediation technologies for environmental sustainability. *Chemical and Biological Technologies in Agriculture*, 6 (1): 1-13.

Fytili, D. and Zabaniotou, A. 2008. Utilization of sewage sludge in EU application of old and new methods—a review. *Renewable and sustainable energy reviews*, 12 (1): 116-140.

Gan, Y. X., Jayatissa, A. H., Yu, Z., Chen, X. and Li, M. 2020. Hydrothermal Synthesis of Nanomaterials. *Journal of Nanomaterials*, 2020: 8917013.

Ghaleb, A., Kutty, S., Ho, Y., Jagaba, A., Noor, A., Al-Sabaeei, A., Kumar, V. and Saeed, A. 2020a. Anaerobic co-digestion for oily-biological sludge with sugarcane bagasse for biogas production under mesophilic condition. In: Proceedings of *IOP Conference Series: Materials Science and Engineering*. IOP Publishing, 012084.

Ghaleb, A. A. S., Kutty, S. R. M., Ho, Y.-C., Jagaba, A. H., Noor, A., Al-Sabaeei, A. M. and Almahbashi, N. M. Y. 2020b. Response surface methodology to optimize methane production from mesophilic anaerobic co-digestion of oily-biological sludge and sugarcane bagasse. *Sustainability*, 12 (5): 2116.

Ghassemi, M., Andersen, P. K., Ghassemi, A. and Chianelli, R. R. 2004. Hazardous Waste from Fossil Fuels. In: Cleveland, C. J. ed. *Encyclopedia of Energy*. New York: Elsevier, 119-131. Available: http://www.sciencedirect.com/science/article/pii/B012176480X003958 (Accessed 13 July 2021)

Goli, J. and Sahu, O. 2018. Development of heterogeneous alkali catalyst from waste chicken eggshell for biodiesel production. *Renewable Energy*, 128: 142-154.

Gray, N. 2005. Pathogens and their removal. *Water technology, an introduction for environmental scientists and engineers. Elsevier Butterworth-Heinemann, Oxford, UK*, Article ID.

Guermazi-Toumi, S., Chouari, R. and Sghir, A. 2019. Molecular analysis of methanogen populations and their interactions within anaerobic sludge digesters. *Environmental technology*, 40 (22): 2864-2879.

Gumbi, N. 2020. The effectiveness of domestic water treatment processes, North West Province, South Africa. Article IDNorth-West University (South Africa).

Gutierrez, M. P. R., Mendez, V. M. J. and Vazquez, A. I. 2017. Chapter 2: A novel approach to oral delivery of bionanostructures for systemic disease. Article ID.

Hannah, R. a. M., Roser. 2020. *Energy* 2022. Available: https://ourworldindata.org/energy (Accessed 5 November 2021)

Hasan, S. 2015. A review on nanoparticles: their synthesis and types. *Res. J. Recent Sci*, 2277: 2502.

Hassanein, A., Lansing, S. and Tikekar, R. 2019. Impact of metal nanoparticles on biogas production from poultry litter. *Bioresource technology*, 275: 200-206.

Hayashi, H. and Hakuta, Y. 2010. Hydrothermal Synthesis of Metal Oxide Nanoparticles in Supercritical Water. *Materials*, 3 (7): 3794-3817.

Henze, M., van Loosdrecht, M. C., Ekama, G. A. and Brdjanovic, D. 2008. *Biological wastewater treatment*. IWA publishing.

Houshiar, M., Zebhi, F., Razi, Z. J., Alidoust, A. and Askari, Z. 2014. Synthesis of cobalt ferrite (CoFe2O4) nanoparticles using combustion, coprecipitation, and precipitation methods: A comparison study of size, structural, and magnetic properties. *Journal of Magnetism and Magnetic Materials*, 371: 43-48.

Hülsemann, B., Zhou, L., Merkle, W., Hassa, J., Müller, J. and Oechsner, H. 2020. Biomethane potential test: Influence of inoculum and the digestion system. *Applied Sciences*, 10 (7): 2589.

Husain, A. 1998. Mathematical models of the kinetics of anaerobic digestion—a selected review. *Biomass and Bioenergy*, 14 (5-6): 561-571.

Igbinosa, E. and Okoh, A. 2009. Impact of discharge wastewater effluents on the physico-chemical qualities of a receiving watershed in a typical rural community. *International Journal of Environmental Science & Technology*, 6 (2): 175-182.

Iloms, E., Ololade, O. O., Ogola, H. J. and Selvarajan, R. 2020. Investigating industrial effluent impact on municipal wastewater treatment plant in Vaal, South Africa. *International journal of environmental research and public health*, 17 (3): 1096.

Isiaka, A. A. and Olaniran, A. O. 2021. Treatment of industrial oily wastewater by advanced technologies: a review. *Applied Water Science*, 11 (6).

Jain, S., Jain, S., Wolf, I. T., Lee, J. and Tong, Y. W. 2015. A comprehensive review on operating parameters and different pretreatment methodologies for anaerobic digestion of municipal solid waste. *Renewable and Sustainable Energy Reviews*, 52: 142-154.

Jalilpour, M. and Fathalilou, M. 2012. Effect of aging time and calcination temperature on the cerium oxide nanoparticles synthesis via reverse co-precipitation method. *International Journal of Physical Sciences*, 7 (6): 944-948.

Jetten, M. S., Horn, S. J. and van Loosdrecht, M. C. 1997. Towards a more sustainable municipal wastewater treatment system. *Water science and technology*, 35 (9): 171-180.

Jia, B., Yun, S., Shi, J., Han, F., Wang, Z., Chen, J., Abbas, Y., Xu, H., Wang, K. and Xing, T. 2020. Enhanced anaerobic mono-and co-digestion under mesophilic condition: Focusing on the magnetic field and Ti-sphere core–shell structured additives. *Bioresource technology*, 310: 123450.

Jia, W., Zhang, J., Lu, Y., Li, G., Yang, W. and Wang, Q. 2018. Response of nitrite accumulation and microbial characteristics to low-intensity static magnetic field during partial nitrification. *Bioresource technology*, 259: 214-220.

Joshi, M., Bhattacharyya, A. and Ali, S. W. 2008. Characterization techniques for nanotechnology applications in textiles. Article ID.

Joss, A., Zabczynski, S., Göbel, A., Hoffmann, B., Löffler, D., McArdell, C. S., Ternes, T. A., Thomsen, A. and Siegrist, H. 2006. Biological degradation of pharmaceuticals in municipal wastewater treatment: proposing a classification scheme. *Water research*, 40 (8): 1686-1696.

K'Oreje, K. O., Okoth, M., Van Langenhove, H. and Demeestere, K. 2020. Occurrence and treatment of contaminants of emerging concern in the African aquatic environment: Literature review and a look ahead. *Journal of Environmental Management*, 254: 109752.

Kacprzak, M., Neczaj, E., Fijałkowski, K., Grobelak, A., Grosser, A., Worwag, M., Rorat, A., Brattebo, H., Almås, Å. and Singh, B. R. 2017. Sewage sludge disposal strategies for sustainable development. *Environmental research*, 156: 39-46.

Kahan, A. 2019. *TODAY IN ENERGY* 2020. Available: https://www.eia.gov/todayinenergy/detail.php?id=41433 (Accessed 26 May 2021)

Kalloum, S., Bouabdessalem, H., Touzi, A., Iddou, A. and Ouali, M. S. 2011. Biogas production from the sludge of the municipal wastewater treatment plant of Adrar city (southwest of Algeria). *Biomass and Bioenergy*, 35 (7): 2554-2560.

Kamyab, H., Yuzir, M. A., Al-Qaim, F. F., Purba, L. D. A. and Riyadi, F. A. 2021. Application of Box-Behnken design to mineralization and color removal of palm oil mill effluent by electrocoagulation process. *Environmental Science and Pollution Research*, Article ID: 1-13.

Kandpal, N., Sah, N., Loshali, R., Joshi, R. and Prasad, J. 2014. Co-precipitation method of synthesis and characterization of iron oxide nanoparticles. Article ID.

Kavitha, S., Jayashree, C., Kumar, S. A., Yeom, I. T. and Banu, J. R. 2014. The enhancement of anaerobic biodegradability of waste activated sludge by surfactant mediated biological pretreatment. *Bioresource technology*, 168: 159-166.

Kefeni, K. K., Msagati, T. A. and Mamba, B. B. 2017. Ferrite nanoparticles: synthesis, characterisation and applications in electronic device. *Materials Science and Engineering: B*, 215: 37-55.

Kudr, J., Haddad, Y., Richtera, L., Heger, Z., Cernak, M., Adam, V. and Zitka, O. 2017. Magnetic nanoparticles: From design and synthesis to real world applications. *Nanomaterials*, 7 (9): 243.

Kushwaha, J. P. 2015. A review on sugar industry wastewater: sources, treatment technologies, and reuse. *Desalination and Water Treatment*, 53 (2): 309-318.

Kweinor Tetteh, E. and Rathilal, S. 2020. Kinetics and Nanoparticle Catalytic Enhancement of Biogas Production from Wastewater Using a Magnetized Biochemical Methane Potential (MBMP) System. *Catalysts*, 10 (10): 1200.

Kweinor Tetteh, E. and Rathilal, S. 2021a. Application of biomagnetic nanoparticles for biostimulation of biogas production from wastewater treatment. *Materials Today: Proceedings*, 45: 5214-5220.

Kweinor Tetteh, E. and Rathilal, S. 2021b. Biogas production from wastewater treatment-evaluating anaerobic and biomagnetic systems. *Water-Energy Nexus*, 4: 165-173.

Laiq Ur Rehman, M., Iqbal, A., Chang, C. C., Li, W. and Ju, M. 2019. Anaerobic digestion. *Water Environment Research*, 91 (10): 1253-1271.

Łebkowska, M., Narożniak-Rutkowska, A. and Pajor, E. 2013. Effect of a static magnetic field of 7 mT on formaldehyde biodegradation in industrial wastewater from urea–formaldehyde resin production by activated sludge. *Bioresource technology*, 132: 78-83.

Lee, J., Jin, S., Hwang, Y., Park, J.-G., Park, H. M. and Hyeon, T. 2005. Simple synthesis of mesoporous carbon with magnetic nanoparticles embedded in carbon rods. *Carbon*, 43 (12): 2536-2543.

Li, J., Luo, G., He, L., Xu, J. and Lyu, J. 2018. Analytical approaches for determining chemical oxygen demand in water bodies: a review. *Critical reviews in analytical chemistry*, 48 (1): 47-65.

Li, X.-M., Xu, G., Liu, Y. and He, T. 2011. Magnetic Fe3O4 nanoparticles: Synthesis and application in water treatment. *Nanoscience & Nanotechnology-Asia*, 1 (1): 14-24.

Liu, D. H. and Lipták, B. G. 2020. *Wastewater treatment*. CRC Press.

Liu, W., Zhang, J., Liu, H., Guo, X., Zhang, X., Yao, X., Cao, Z. and Zhang, T. 2021. A review of the removal of microplastics in global wastewater treatment plants: Characteristics and mechanisms. *Environment International*, 146: 106277.

Liu, Y., Wang, Q., Zhang, Y. and Ni, B.-J. 2015. Zero valent iron significantly enhances methane production from waste activated sludge by improving biochemical methane potential rather than hydrolysis rate. *Scientific reports*, 5 (1): 1-6.

Lohani, S. P. and Havukainen, J. 2018. Anaerobic digestion: factors affecting anaerobic digestion process. In: *Waste Bioremediation*. Springer, 343-359.

Lu, H., Gong, Y., Areeprasert, C., Ding, L., Guo, Q., Chen, W.-H. and Yu, G. 2021. Integration of Biomass Torrefaction and Gasification based on Biomass Classification: A Review. *Energy Technology*, 9 (5): 2001108.

Maaz, K., Karim, S., Mumtaz, A., Hasanain, S., Liu, J. and Duan, J. 2009. Synthesis and magnetic characterization of nickel ferrite nanoparticles prepared by co-precipitation route. *Journal of Magnetism and Magnetic Materials*, 321 (12): 1838-1842.

Maaz, K., Mumtaz, A., Hasanain, S. and Ceylan, A. 2007. Synthesis and magnetic properties of cobalt ferrite (CoFe2O4) nanoparticles prepared by wet chemical route. *Journal of Magnetism and Magnetic Materials*, 308 (2): 289-295.

Mahmoudi, M., Sant, S., Wang, B., Laurent, S. and Sen, T. 2011. Superparamagnetic iron oxide nanoparticles (SPIONs): development, surface modification and applications in chemotherapy. *Advanced drug delivery reviews*, 63 (1-2): 24-46.

Majidi, S., Zeinali Sehrig, F., Farkhani, S. M., Soleymani Goloujeh, M. and Akbarzadeh, A. 2016a. Current methods for synthesis of magnetic nanoparticles. *Artificial Cells, Nanomedicine, and Biotechnology*, 44 (2): 722-734.

Majidi, S., Zeinali Sehrig, F., Samiei, M., Milani, M., Abbasi, E., Dadashzadeh, K. and Akbarzadeh, A. 2016b. Magnetic nanoparticles: Applications in gene delivery and gene therapy. *Artificial cells, nanomedicine, and biotechnology*, 44 (4): 1186-1193.

Maksoud, M. A., Elgarahy, A. M., Farrell, C., Ala'a, H., Rooney, D. W. and Osman, A. I. 2020. Insight on water remediation application using magnetic nanomaterials and biosorbents. *Coordination Chemistry Reviews*, 403: 213096.

Mao, C., Feng, Y., Wang, X. and Ren, G. 2015. Review on research achievements of biogas from anaerobic digestion. *Renewable and Sustainable Energy Reviews*, 45: 540-555.

Mara, D. 2013. *Domestic wastewater treatment in developing countries*. Routledge.

Martinez-Boubeta, C. and Simeonidis, K. 2019. Magnetic nanoparticles for water purification. In: *Nanoscale Materials in Water Purification*. Elsevier, 521-552.

Martinez-Burgos, W. J., Sydney, E. B., Medeiros, A. B. P., Magalhães, A. I., de Carvalho, J. C., Karp, S. G., de Souza Vandenberghe, L. P., Letti, L. A. J., Soccol, V. T. and de Melo Pereira, G. V. 2021. Agro-industrial wastewater in a circular economy: Characteristics, impacts and applications for bioenergy and biochemicals. *Bioresource technology*, 341: 125795.

Mascolo, M. C., Pei, Y. and Ring, T. A. 2013. Room Temperature Co-Precipitation Synthesis of Magnetite Nanoparticles in a Large pH Window with Different Bases. *Materials*, 6 (12): 5549-5567.

McCarty, P. L., Bae, J. and Kim, J. 2011. *Domestic wastewater treatment as a net energy producer–can this be achieved?* : ACS Publications.

McKendry, P. 2002. Energy production from biomass (part 1): overview of biomass. *Bioresource technology*, 83 (1): 37-46.

Meng, X., Khoso, S. A., Jiang, F., Zhang, Y., Yue, T., Gao, J., Lin, S., Liu, R., Gao, Z. and Chen, P. 2020. Removal of chemical oxygen demand and ammonia nitrogen from lead smelting wastewater with high salts content using electrochemical oxidation combined with coagulation–flocculation treatment. *Separation and Purification Technology*, 235: 116233.

Menyah, K. and Wolde-Rufael, Y. 2010. Energy consumption, pollutant emissions and economic growth in South Africa. *Energy Economics*, 32 (6): 1374-1382.

Merlin Christy, P., Gopinath, L. R. and Divya, D. 2014. A review on anaerobic decomposition and enhancement of biogas production through enzymes and microorganisms. *Renewable and Sustainable Energy Reviews*, 34: 167-173.

Mitchell, S. A., De Wit, M., Blignaut, J. N. and Crookes, D. 2014. *Waste Water Treatment Plants: The Financing Mechanisms Associated with Achieving Green Drop Rating*.

Mohan, D., Pittman Jr, C. U. and Steele, P. H. 2006. Pyrolysis of wood/biomass for bio-oil: a critical review. *Energy & fuels*, 20 (3): 848-889.

Mohanraj, V. and Chen, Y. 2006. Nanoparticles-a review. *Tropical journal of pharmaceutical research*, 5 (1): 561-573.

Mohr, S., Wang, J., Ellem, G., Ward, J. and Giurco, D. 2015. Projection of world fossil fuels by country. *Fuel*, 141: 120-135.

Möller, J., Kuchemüller, K. B., Steinmetz, T., Koopmann, K. S. and Pörtner, R. 2019. Model-assisted design of experiments as a concept for knowledge-based bioprocess development. *Bioprocess and biosystems engineering*, 42 (5): 867-882.

Montgomery, D. C. 2017. *Design and analysis of experiments*. John wiley & sons.

Montwedi, M., Munyaradzi, M., Pinoy, L., Dutta, A., Ikumi, D. S., Motoasca, E. and Van der Bruggen, B. 2021. Resource recovery from and management of wastewater in rural South Africa: Possibilities and practices. *Journal of Water Process Engineering*, 40: 101978.

Motjoadi, V., Bokoro, P. N. and Onibonoje, M. O. 2020. A review of microgrid-based approach to rural electrification in South Africa: Architecture and policy framework. *Energies*, 13 (9): 2193.

Mu, H., Chen, Y. and Xiao, N. 2011. Effects of metal oxide nanoparticles (TiO2, Al2O3, SiO2 and ZnO) on waste activated sludge anaerobic digestion. *Bioresource technology*, 102 (22): 10305-10311.

Mustafa, A. M., Li, H., Radwan, A. A., Sheng, K. and Chen, X. 2018. Effect of hydrothermal and Ca (OH) 2 pretreatments on anaerobic digestion of sugarcane bagasse for biogas production. *Bioresource technology*, 259: 54-60.

Mustafa, N., Elbeshbishy, E., Nakhla, G. and Zhu, J. 2014. Anaerobic digestion of municipal wastewater sludges using anaerobic fluidized bed bioreactor. *Bioresource technology*, 172: 461-466.

Muttamara, S. 1996. Wastewater characteristics. *Resources, conservation and recycling*, 16 (1-4): 145-159.

N. Politis, S., Colombo, P., Colombo, G. and M. Rekkas, D. 2017. Design of experiments (DoE) in pharmaceutical development. *Drug development and industrial pharmacy*, 43 (6): 889-901.

Nabaterega, R., Kumar, V., Khoei, S. and Eskicioglu, C. 2021. A review on two-stage anaerobic digestion options for optimizing municipal wastewater sludge treatment process. *Journal of environmental chemical engineering*, 9 (4): 105502.

Nasrabadi, M. R. N. and Razavi, S. H. 2010. Use of response surface methodology in a fed-batch process for optimization of tricarboxylic acid cycle intermediates to achieve high levels of canthaxanthin from Dietzia natronolimnaea HS-1. *Journal of bioscience and bioengineering*, 109 (4): 361-368.

Nassar, N. N. 2013. The application of nanoparticles for wastewater remediation. In. Future Medicine.

Negwamba, T. and Dinka, M. O. 2019. Assessing the performance of Trichardt Wastewater Treatment Plant (South Africa). *Physics and Chemistry of the Earth, Parts A/B/C*, 114: 102784.

Nguyen, D. D., Chang, S. W., Jeong, S. Y., Jeung, J., Kim, S., Guo, W. and Ngo, H. H. 2016. Dry thermophilic semi-continuous anaerobic digestion of food waste: Performance evaluation, modified Gompertz model analysis, and energy balance. *Energy Conversion and Management*, 128: 203-210.

Niu, C., Geng, J., Ren, H., Ding, L., Xu, K. and Liang, W. 2013. The strengthening effect of a static magnetic field on activated sludge activity at low temperature. *Bioresource technology*, 150: 156-162.

Niu, C., Liang, W., Ren, H., Geng, J., Ding, L. and Xu, K. 2014. Enhancement of activated sludge activity by 10–50 mT static magnetic field intensity at low temperature. *Bioresource technology*, 159: 48-54.

Nzila, A. 2017. Mini review: Update on bioaugmentation in anaerobic processes for biogas production. *Anaerobe*, 46: 3-12.

Obotey Ezugbe, E. and Rathilal, S. 2020. Membrane technologies in wastewater treatment: a review. *Membranes*, 10 (5): 89.

Okoli, C., Fornara, A., Qin, J., Toprak, M. S., Dalhammar, G., Muhammed, M. and Rajarao, G. K. 2011. Characterization of Superparamagnetic Iron Oxide Nanoparticles and Its Application in Protein Purification. *Journal of Nanoscience and Nanotechnology*, 11 (11): 10201-10206.

Ololade, O. O. 2018. Understanding the nexus between energy and water: A basis for human survival in South Africa. *Development Southern Africa*, 35 (2): 194-209.

Ondari, J. M. 2015. Anaerobic co-digestion of abattoir and textile industry wastewater in a UASB reactor. Article ID.

Oruko, R., Selvarajan, R., Ogola, H., Edokpayi, J. and Odiyo, J. 2020. Contemporary and future direction of chromium tanning and management in sub Saharan Africa tanneries. *Process Safety and Environmental Protection*, 133: 369-386.

Osaka, T., Matsunaga, T., Nakanishi, T., Arakaki, A., Niwa, D. and Iida, H. 2006. Synthesis of magnetic nanoparticles and their application to bioassays. *Analytical and bioanalytical chemistry*, 384 (3): 593-600.

Owusu, P. A. and Asumadu-Sarkodie, S. 2016. A review of renewable energy sources, sustainability issues and climate change mitigation. *Cogent Engineering*, 3 (1).

Paritosh, K., Kushwaha, S. K., Yadav, M., Pareek, N., Chawade, A. and Vivekanand, V. 2017. Food waste to energy: an overview of sustainable approaches for food waste management and nutrient recycling. *BioMed Research International*, 2017.

Patil, J. H., AntonyRaj, M., Shankar, B., Shetty, M. K. and Kumar, B. P. 2014. Anaerobic co-digestion of water hyacinth and sheep waste. *Energy Procedia*, 52: 572-578.

Peeters, K., Lespes, G., Zuliani, T., Ščančar, J. and Milačič, R. 2016. The fate of iron nanoparticles in environmental waters treated with nanoscale zero-valent iron, FeONPs and Fe3O4NPs. *Water research*, 94: 315-327.

Pérez-Lombard, L., Ortiz, J. and Pout, C. 2008. A review on buildings energy consumption information. *Energy and Buildings*, 40 (3): 394-398.

Petcharoen, K. and Sirivat, A. 2012. Synthesis and characterization of magnetite nanoparticles via the chemical co-precipitation method. *Materials Science and Engineering: B*, 177 (5): 421-427.

Pisarevsky, A., Polozova, I. and Hockridge, P. 2005. Chemical oxygen demand. *Russian Journal of applied chemistry*, 78 (1): 101-107.

Politis N., S., Colombo, P., Colombo, G. and M. Rekkas, D. 2017. Design of experiments (DoE) in pharmaceutical development. *Drug development and industrial pharmacy*, 43 (6): 889-901.

Ponce-Robles, L., Masdemont-Hernández, B., Munuera-Pérez, T., Pagán-Muñoz, A., Lara-Guillén, A. J., García-García, A. J., Pedrero-Salcedo, F., Nortes-Tortosa, P. A. and Alarcón-Cabañero, J. J. 2020. WWTP effluent quality improvement for agricultural reuse using an autonomous prototype. *Water*, 12 (8): 2240.

Pramanik, S. K., Suja, F. B., Porhemmat, M. and Pramanik, B. K. 2019. Performance and Kinetic Model of a Single-Stage Anaerobic Digestion System Operated at Different Successive Operating Stages for the Treatment of Food Waste. *Processes*, 7 (9): 600.

Qasim, S. R. 2017. *Wastewater treatment plants: planning, design, and operation*. Routledge.

Qu, J., Wang, H., Wang, K., Yu, G., Ke, B., Yu, H.-Q., Ren, H., Zheng, X., Li, J. and Li, W.-W. 2019. Municipal wastewater treatment in China: Development history and future perspectives. *Frontiers of Environmental Science & Engineering*, 13 (6): 1-7.

Rane, A. V., Kanny, K., Abitha, V. K. and Thomas, S. 2018. Chapter 5 - Methods for Synthesis of Nanoparticles and Fabrication of Nanocomposites. In: Mohan Bhagyaraj, S., Oluwafemi, O. S., Kalarikkal, N. and Thomas, S. eds. *Synthesis of Inorganic Nanomaterials*. Woodhead Publishing, 121-139. Available:

https://www.sciencedirect.com/science/article/pii/B9780081019757000051 (Accessed 30 May 2021)

Rani, S., Gunjyal, N., Ojha, C. and Singh, R. P. 2021. Review of Challenges for Algae-Based Wastewater Treatment: Strain Selection, Wastewater Characteristics, Abiotic, and Biotic Factors. *Journal of Hazardous, Toxic, and Radioactive Waste*, 25 (2): 03120004.

Rao, B. G., Mukherjee, D. and Reddy, B. M. 2017. Chapter 1 - Novel approaches for preparation of nanoparticles. In: Ficai, D. and Grumezescu, A. M. eds. *Nanostructures for Novel Therapy*. Elsevier, 1-36. Available: http://www.sciencedirect.com/science/article/pii/B9780323461429000013 (Accessed 15 July 2021)

Ratshomo, K. R. A. K. 2018. *SOUTH AFRICAN ENERGY SECTOR REPORT, DIRECTORATE: ENERGY DATA COLLECTION, MANAGEMENT AND ANALYSIS.* . Available: http://www.energy.gov.za/files/media/explained/2018-South-African-Energy-Sector-Report.pdf (Accessed 4 August 2021).

Rea, J. 2014. Kinetic Modeling and experimentation of anaerobic digestion. Article IDMassachusetts Institute of Technology.

Rodda, N. 2012. *Wastewater Production, Treatment, and Use in South Africa*. Durban: University of KwaZulu-Nata. Available: https://www.ais.unwater.org/ais/pluginfile.php/231/mod_page/content/188/Session3a_CountryReport_Rodda_South%20Africa.pdf (Accessed 4 August 2021).

Safoniuk, M. 2004. Wastewater engineering: Treatment and reuse. *Chemical Engineering*, 111 (7): 10-12.

Sakka, S. 2013. Chapter 11.1.2 - Sol–Gel Process and Applications. In: Somiya, S. ed. *Handbook of Advanced Ceramics (Second Edition)*. Oxford: Academic Press, 883-910. Available: http://www.sciencedirect.com/science/article/pii/B9780123854698000484 (Accessed 26 March 2021)

Samer, M. 2015. Biological and chemical wastewater treatment processes. *Wastewater Treatment Engineering*, 150.

Sanchez, E., Borja, R., Weiland, P., Travieso, L. and Martin, A. 2000. Effect of temperature and pH on the kinetics of methane production, organic nitrogen and phosphorus removal in the batch anaerobic digestion process of cattle manure. *Bioprocess Engineering*, 22 (3): 247-252.

Sandeep Kumar, V. 2013. Magnetic nanoparticles-based biomedical and bioanalytical applications. *J Nanomed Nanotechol*, 4: e130.

SANS-SABS. 2007. *SANS 3696/ISO 3696, South African National Standard Water*. South Africa: 11 August 2021).

Scarlat, N., Dallemand, J.-F. and Fahl, F. 2018. Biogas: Developments and perspectives in Europe. *Renewable Energy*, 129: 457-472.

Schmidt, T., McCabe, B. and Harris, P. 2018. Process monitoring and control for an anaerobic covered lagoon treating abattoir wastewater. *Chemical Engineering & Technology*, 41 (4): 755-760.

Seno, J. 2010. The kinetic of biogas production rate from cattle manure in batch mode. *International Journal of chemical and biological Engineering*, 3 (1): 39-45.

Shah, A. and Shah, M. 2020. Characterisation and bioremediation of wastewater: A review exploring bioremediation as a sustainable technique for pharmaceutical wastewater. *Groundwater for Sustainable Development*, 11: 100383.

Shen, L., Qiao, Y., Guo, Y., Meng, S., Yang, G., Wu, M. and Zhao, J. 2014. Facile co-precipitation synthesis of shape-controlled magnetite nanoparticles. *Ceramics International*, 40 (1): 1519-1524.

Shu, Z. and Wang, S. 2009. Synthesis and Characterization of Magnetic Nanosized F e 3 O 4/M n O 2 Composite Particles. *Journal of Nanomaterials*, 2009.

Sikosana, M. L., Sikhwivhilu, K., Moutloali, R. and Madyira, D. M. 2019. Municipal wastewater treatment technologies: A review. *Procedia Manufacturing*, 35: 1018-1024.

Silva, G. A. 2004. Introduction to nanotechnology and its applications to medicine. *Surgical neurology*, 61 (3): 216-220.

Singh, S., Kumar, V., Romero, R., Sharma, K. and Singh, J. 2019. Applications of nanoparticles in wastewater treatment. In: *Nanobiotechnology in bioformulations*. Springer, 395-418.

Sonune, A. and Ghate, R. 2004. Developments in wastewater treatment methods. *Desalination*, 167: 55-63.

Sorensen, J., Lapworth, D., Nkhuwa, D., Stuart, M., Gooddy, D., Bell, R., Chirwa, M., Kabika, J., Liemisa, M. and Chibesa, M. 2015. Emerging contaminants in urban groundwater sources in Africa. *Water Research*, 72: 51-63.

Sreekrishnan, T., Kohli, S. and Rana, V. 2004. Enhancement of biogas production from solid substrates using different techniques—a review. *Bioresource Technology*, 95 (1): 1-10.

Stafford, W., Cohen, B., Pather-Elias, S., Von Blottnitz, H., Van Hille, R., Harrison, S. T. and Burton, S. G. 2013. Technologies for recovery of energy from wastewaters: Applicability and potential in South Africa. *Journal of Energy in Southern Africa*, 24 (1): 00-00.

Stronach, S. M., Rudd, T. and Lester, J. N. 2012. *Anaerobic digestion processes in industrial wastewater treatment*. Springer Science & Business Media.

Stuart, P. 2006. The advantages and disadvantages of anaerobic digestion as a renewable energy source. *Loughborough University*, Article ID.

Sun, W., Qian, X., Gu, J., Wang, X.-J. and Duan, M.-L. 2016. Mechanism and effect of temperature on variations in antibiotic resistance genes during anaerobic digestion of dairy manure. *Scientific reports*, 6 (1): 1-9.

Tchobanoglous, G., Burton, F. L. and Stensel, H. 1991. Wastewater engineering. *Management*, 7 (1): 4.

Tchobanoglus, G., Burton, F. and Stensel, H. D. 2003. Wastewater engineering: Treatment and reuse. *American Water Works Association. Journal*, 95 (5): 201.

Tebbutt, T. H. Y. 1997. *Principles of water quality control*. Elsevier.

Tebbutt, T. H. Y. 2013. *Principles of water quality control*. Elsevier.

Templeton, M. R. and Butler, D. 2011. *Introduction to wastewater treatment*. Bookboon.

Tena, M., Perez, M. and Solera, R. 2021. Effect of hydraulic retention time on the methanogenic step of a two-stage anaerobic digestion system from sewage sludge and wine vinasse: Microbial and kinetic evaluation. *Fuel*, 296: 120674.

Tetteh, E. K., Amo-Duodu, G. and Rathilal, S. 2021. Synergistic Effects of Magnetic Nanomaterials on Post-Digestate for Biogas Production. *Molecules*, 26 (21): 6434.

Tetteh, E. K. and Rathilal, S. 2021. Application of biomagnetic nanoparticles for biostimulation of biogas production from wastewater treatment. *Materials Today: Proceedings*, 45: 5214-5220.

Tetteh, E. K., Rathilal, S., Chetty, M., Armah, E. K. and Asante-Sackey, D. 2019. Treatment of water and wastewater for reuse and energy generation-emerging technologies. In: *Water and Wastewater Treatment*. IntechOpen, 53-80.

Tian, R., Li, F., Yang, Y., Huang, J. and Zhu, M. Multivariate Parameter Optimization of PAM Wastewater Treatment by Ti/Ir–Ta Electrocatalysis via the Box-Behnken Design. *Polish Journal of Environmental Studies*, Article ID.

University Of Pretoria, S. A. L. I. I. 2013. *National Water Act 36 0f 1998 [Online]*. . Available: https://cer.org.za/wp-content/uploads/2014/02/Revision-of-General-Authorisations-2013 (Accessed 14 February 2022)

Vaghari, H., Jafarizadeh-Malmiri, H., Mohammadlou, M., Berenjian, A., Anarjan, N., Jafari, N. and Nasiri, S. 2016. Application of magnetic nanoparticles in smart enzyme immobilization. *Biotechnology letters*, 38 (2): 223-233.

Valijanian, E., Tabatabaei, M., Aghbashlo, M., Sulaiman, A. and Chisti, Y. 2018. Biogas production systems. In: *Biogas*. Springer, 95-116.

Vaona, A. 2012. Granger non-causality tests between (non) renewable energy consumption and output in Italy since 1861: the (ir) relevance of structural breaks. *Energy Policy*, 45: 226-236.

Verbruggen, Fischedick, Moomaw, Weir, Nadaï, Nilsson and Sathaye. 2010. Renewable energy costs, potentials, barriers: Conceptual issues. *Energy Policy*, 38: 850-861.

Vollath, D. 2008. Nanomaterials an introduction to synthesis, properties and application. *Environmental Engineering and Management Journal*, 7 (6): 865-870.

Von Sperling, M. 2007. *Wastewater characteristics, treatment and disposal*. IWA publishing.

Wainaina, S., Awasthi, M. K., Horváth, I. S. and Taherzadeh, M. J. 2020. Anaerobic digestion of food waste to volatile fatty acids and hydrogen at high organic loading rates in immersed membrane bioreactors. *Renewable Energy*, 152: 1140-1148.

Wang, X., Li, H. and Chen, G. 2018. 6 - Core-shell nanoparticles for cancer imaging and therapy. In: Focarete, M. L. and Tampieri, A. eds. *Core-Shell Nanostructures for Drug Delivery and Theranostics*. Woodhead Publishing, 143-175. Available: https://www.sciencedirect.com/science/article/pii/B9780081021989000065 (Accessed 26 January 2021)

Ward, A. J., Hobbs, P. J., Holliman, P. J. and Jones, D. L. 2008. Optimisation of the anaerobic digestion of agricultural resources. *Bioresource technology*, 99 (17): 7928-7940.

Willard, M., Kurihara, L., Carpenter, E., Calvin, S. and Harris, V. 2004. Chemically prepared magnetic nanoparticles. *International materials reviews*, 49 (3-4): 125-170.

Wilson, C. A., Murthy, S., Fang, Y. and Novak, J. 2008. The effect of temperature on the performance and stability of thermophilic anaerobic digestion. *Water science and technology*, 57 (2): 297-304.

Xia, H. and Wang, Q. 2002. Ultrasonic Irradiation: A Novel Approach To Prepare Conductive Polyaniline/Nanocrystalline Titanium Oxide Composites. *Chemistry of Materials*, 14 (5): 2158-2165.

Xie, S., Hai, F. I., Zhan, X., Guo, W., Ngo, H. H., Price, W. E. and Nghiem, L. D. 2016. Anaerobic co-digestion: A critical review of mathematical modelling for performance optimization. *Bioresource Technology*, 222: 498-512.

Yadav, T. P., Yadav, R. M. and Singh, D. P. 2012. Mechanical milling: a top down approach for the synthesis of nanomaterials and nanocomposites. *Nanoscience and Nanotechnology*, 2 (3): 22-48.

Yadollahpour, A. 2015. Magnetic nanoparticles in medicine: a review of synthesis methods and important characteristics. *Orient. J. Chem*, 31: 271-277.

Yadvika, Santosh, Sreekrishnan, T. R., Kohli, S. and Rana, V. 2004. Enhancement of biogas production from solid substrates using different techniques—a review. *Bioresource technology*, 95 (1): 1-10.

Yang, H., Zhang, K., Shi, R., Li, X., Dong, X. and Yu, Y. 2006. Sol–gel synthesis of TiO2 nanoparticles and photocatalytic degradation of methyl orange in aqueous TiO2 suspensions. *Journal of Alloys and Compounds*, 413 (1): 302-306.

Yazdani, M., Ebrahimi-Nik, M., Heidari, A. and Abbaspour-Fard, M. H. 2019. Improvement of biogas production from slaughterhouse wastewater using biosynthesized iron nanoparticles from water treatment sludge. *Renewable Energy*, 135: 496-501.

Yu, Q., Liu, R., Li, K. and Ma, R. 2019. A review of crop straw pretreatment methods for biogas production by anaerobic digestion in China. *Renewable and Sustainable Energy Reviews*, 107: 51-58.

Yue, D., You, F. and Snyder, S. W. 2014. Biomass-to-bioenergy and biofuel supply chain optimization: Overview, key issues and challenges. *Computers & Chemical Engineering*, 66: 36-56.

Yusuf, M., Debora, A. and Ogheneruona, D. 2011. Ambient temperature kinetic assessment of biogas production from co-digestion of horse and cow dung. *Research in Agricultural Engineering*, 57 (3): 97-104.

Zaidi, A. A., RuiZhe, F., Shi, Y., Khan, S. Z. and Mushtaq, K. 2018. Nanoparticles augmentation on biogas yield from microalgal biomass anaerobic digestion. *International Journal of Hydrogen Energy*, 43 (31): 14202-14213.

Zaidi, N. S., Sohaili, J., Muda, K. and Sillanpää, M. 2014. Magnetic field application and its potential in water and wastewater treatment systems. *Separation & Purification Reviews*, 43 (3): 206-240.

Zamri, M., Hasmady, S., Akhiar, A., Ideris, F., Shamsuddin, A., Mofijur, M., Fattah, I. R. and Mahlia, T. 2021. A comprehensive review on anaerobic digestion of organic fraction of municipal solid waste. *Renewable and Sustainable Energy Reviews*, 137: 110637.

Zhang, J. and Lu, Y. 2016. Conductive Fe3O4 nanoparticles accelerate syntrophic methane production from butyrate oxidation in two different lake sediments. *Frontiers in microbiology*, 7: 1316.

Zhao, H.-x. and Magoulès, F. 2012. A review on the prediction of building energy consumption. *Renewable and Sustainable Energy Reviews*, 16 (6): 3586-3592.

Zhao, Q., Arhin, S. G., Yang, Z., Liu, H., Li, Z., Anwar, N., Papadakis, V. G., Liu, G. and Wang, W. 2021. pH regulation of the first phase could enhance the energy recovery from two-phase anaerobic digestion of food waste. *Water Environment Research*, 93 (8): 1370-1380.

Zhou, H., Li, X., Xu, G. and Yu, H. 2018. Overview of strategies for enhanced treatment of municipal/domestic wastewater at low temperature. *Science of the Total Environment*, 643: 225-237.

Zhou, X., Lu, Y., Huang, L., Zhang, Q., Wang, X. and Zhu, J. 2021. Effect of pH on volatile fatty acid production and the microbial community during anaerobic digestion of Chinese cabbage waste. *Bioresource technology*, 336: 125338.

Zhu, K., Ju, Y., Xu, J., Yang, Z., Gao, S. and Hou, Y. 2018. Magnetic nanomaterials: Chemical design, synthesis, and potential applications. *Accounts of chemical research*, 51 (2): 404-413.

Zieliński, M., Zielińska, M., Cydzik-Kwiatkowska, A., Rusanowska, P. and Dębowski, M. 2021. Effect of static magnetic field on microbial community during anaerobic digestion. *Bioresource Technology*, 323: 124600.

Appendix A

SAMPLE CALCULATIONS AND TABLES

In this section all the calculations of removal efficiency for the BMP set-up, total and volatile solids and percentage composition of the biogas have been presented. Tables for the daily biogas yield, water parameters have also been displayed in this section.

Water quality analysis for sugar refinery wastewater sample

$$Removal\ efficiency\ (\%) = \frac{Initial\ concentration - final\ concentration}{initial\ concentration} \times 100$$

Table A-1: Concentration of water quality parameters for BMP set-up Asw – Fsw

BMP bioreactor	Colour (Pt.Co)			Turbidity (NTU)			COD (mg/L)		
Asw	600	585	563	97.75	65.7	10.1	593	568	345
Bsw	589	550	512	78.75	46.8	14.8	579	456	432
Csw	465	345	305	17.6	13.45	7	260	220	171
Dsw	530	512	505	62.75	45.7	10.3	410	356	300
Esw	520	467	417	60.25	34.7	9.9	405	387	335
Fsw	692.5	667	654	148.25	124.78	7.8	1679	1545	1460
Feed avg	1340			200			3570		

Table A-2: Average concentration of water quality parameters

BMP bioreactor	Avg_Colour (Pt.Co)	Avg_Turbidity (NTU)	Avg_COD (mg/L)
Asw	582.67	57.85	502.00
Bsw	550.33	46.78	489.00
Csw	371.67	12.68	217.00
Dsw	515.67	39.58	355.33
Esw	468.00	34.95	375.67
Fsw	671.17	93.61	1561.33

COD removal efficiency for BMP bioreactor Asw using average values in Table A-2

$$COD\ removal\ efficiency\ (\%) = \frac{COD\ Feed - CODavg}{COD\ Feed} \times 100$$

$$COD\ removal\ efficiency\ (\%) = \frac{3570 - 502}{3570} \times 100$$

COD removal efficiency (%) for BMP bioreactor Asw

$$= 85.93\%$$

Colours removal efficiency for BMP bioreactor Asw using average values in Table A-2

$$Color\ removal\ efficiency\ (\%) = \frac{Color\ Feed - Color\ avg}{Color\ Feed} \times 100$$

$$Color\ removal\ efficiency\ (\%) = \frac{1340 - 582.67}{1340} \times 100$$

Colour removal efficiency (%) for BMP bioreactor Asw

$$= 56.72\%$$

Turbidity removal efficiency for BMP bioreactor Asw using average values in Table A-2

$$Turbidity\ removal\ efficiency\ (\%) = \frac{Turbidity\ Feed - Turbidity\ avg}{Turbidity\ Feed} \times 100$$

$$Turbidity\ removal\ efficiency\ (\%) = \frac{200 - 57.85}{200} \times 100$$

Turbidity removal efficiency (%) for BMP bioreactor Asw

$$= 71.08\%$$

Using the same procedure, the removal efficiency (%) for each BMP bioreactor was calculated.

Total and volatile solids analysis for sugar refinery wastewater sample

$$Total\ solid\ (TS), mg\ TS/L = \frac{(Mass\ of\ sample\ after\ drying\ (C), g - mass\ of\ crucible\ (A), g)\ \times 1000}{Volume\ of\ sample\ (Vs), L}$$

$$Volatile\ solid\ (TS), mg\ TS/L = \frac{(Mass\ of\ sample\ after\ drying\ (C), g - mass\ of\ sample\ after\ calcination\ (D), g)\ \times 1000}{Volume\ of\ sample\ (Vs), L}$$

Table A-3: Sludge characteristics for BMP bioreactors Asw – Fsw.

BMP bioreactor	Mass of crucible (g), A	mass of A + 20 mL of sample (g), B	Mass of B after oven drying (g), C	Mass of C after calcination (g), D
Asw	38.49	57.27	50.39	45.01
Bsw	44.85	63.56	57.6	53.31
Csw	49.67	60.87	56.05	53.63
Dsw	48.61	62.60	55.56	50.17
Esw	49.78	67.32	58.33	53.98
Fsw	34.56	55.87	50.32	40.82
Feed	39.28	71.67	58.18	47.2

Total solids for BMP bioreactor Asw

$$Total\ solid\ (mg\ TS/\ L) = \frac{C - A\ \times 1000}{Vs}$$

$$Total\ solid\ (mg\ TS/\ L) = \frac{(50.39 - 38.49) \times 1000}{20}$$

$$= 585\ mg\ TS/L$$

Volatile solids for BMP bioreactor Asw

$$Volatile\ solid\ (mg\ VS/\ L) = \frac{C - D \times 1000}{Vs}$$

$$Total\ solid\ (mg\ VS/\ L) = \frac{(50.39 - 45.01) \times 1000}{20}$$

$$= 269\ mg\ VS/L$$

Following the same calculation procedure, the total and volatile solids for the rest of the BMP bioreactors were calculated. The removal efficiency of total and volatiles for each bioreactor was also determined using the sample calculations used for the removal efficiency.

Table A-4: Daily biogas yield from sugar refinery wastewater sample (industrial wastewater) for BMP bioreactors Asw - Fsw

BMP	**Days**																				
bioreactors	**1**	**2**	**3**	**4**	**5**	**6**	**7**	**8**	**9**	**10**	**11**	**12**	**13**	**14**	**15**	**16**	**17**	**18**	**19**	**20**	**21**
Asw	5	5	5	10	10	5	5	5	5	5	5	5	5	0	0	0	5	0	0	0	0
Bsw	5	5	5	5	10	5	5	10	10	10	5	10	10	15	10	5	5	5	0	0	0
Csw	10	10	15	20	10	20	15	15	15	15	10	20	20	15	15	15	10	10	5	10	5
Dsw	5	10	5	10	15	10	10	5	10	10	10	15	10	10	5	5	10	5	5	5	5
Esw	5	5	10	15	15	10	10	5	10	10	5	10	5	5	5	10	5	5	0	0	0
Fsw	0	0	2.5	5	5	5	10	5	0	0	5	0	0	0	5	0	0	5	0	0	0

Table A-5: Cumulative biogas yield from sugar refinery wastewater (industrial wastewater) sample for BMP bioreactors Asw - Fsw

BMP	**Days**																				
bioreactors	**1**	**2**	**3**	**4**	**5**	**6**	**7**	**8**	**9**	**10**	**11**	**12**	**13**	**14**	**15**	**16**	**17**	**18**	**19**	**20**	**21**
Asw	5	10	15	25	35	40	45	50	55	60	65	70	75	75	75	75	80	80	80	80	80
Bsw	5	10	15	20	30	35	40	50	60	70	75	85	95	110	120	125	130	135	135	135	135
Csw	10	20	35	55	65	85	100	115	130	145	155	175	195	210	225	240	250	260	265	275	280
Dsw	5	15	20	30	45	55	65	70	80	90	100	115	125	135	140	145	155	160	165	170	175
Esw	5	10	20	35	50	60	70	75	85	95	100	110	115	120	125	135	140	145	145	145	145
Fsw	0	0	0	5	10	15	25	30	30	30	35	35	35	35	40	40	40	45	45	45	45

Table A-6: Daily biogas yield from Umbilo Aeration and biofiltration system wastewater sample (Municipal wastewater) for BMP bioreactors Cas - Fbs

	Days																														
Set-up	**1**	**2**	**3**	**4**	**5**	**6**	**7**	**8**	**9**	**10**	**11**	**12**	**13**	**14**	**15**	**16**	**17**	**18**	**19**	**20**	**21**	**22**	**23**	**24**	**25**	**26**	**27**	**28**	**29**	**30**	**31**
Cas	0	10	12	15	20	25	25	30	35	40	40	45	50	50	55	60	62	65	70	75	78	85	85	55	40	20	10	10	5	0	0
Das	0	5	10	12	15	20	22	25	30	32	35	35	40	45	50	52	55	55	60	60	65	70	65	60	50	40	15	5	0	0	0
Eas	0	10	11	13	15	20	25	30	35	37	40	45	45	50	55	60	60	55	60	50	48	45	40	40	35	30	25	15	10	0	0
Fas	0	0	0	5	9	10	12	15	20	20	25	30	40	50	55	40	32	32	30	20	20	15	15	10	5	5	5	5	0	0	0
Cbs	0	10	14	15	20	25	30	35	40	45	48	50	50	55	60	62	65	70	70	75	80	75	70	50	40	20	15	15	10	0	0
Dbs	0	5	7	10	15	20	25	28	30	35	35	40	45	50	55	60	60	65	60	55	55	50	40	35	20	15	10	10	5	0	0
Ebs	0	5	8	13	15	20	25	30	35	35	40	45	50	60	60	68	69	70	75	60	60	50	45	30	25	10	10	5	5	0	0
Fbs	0	0	5	7	10	12	15	15	20	20	25	26	28	30	35	35	36	40	35	30	25	20	15	15	5	5	0	0	0	0	0

Table A-7: Cumulative biogas yield from Umbilo Aeration and biofiltration system wastewater sample (Municipal wastewater) for BMP bioreactors Cas - Fbs

	Days																														
Set-up	**1**	**2**	**3**	**4**	**5**	**6**	**7**	**8**	**9**	**10**	**11**	**12**	**13**	**14**	**15**	**16**	**17**	**18**	**19**	**20**	**21**	**22**	**23**	**24**	**25**	**26**	**27**	**28**	**29**	**30**	**31**
Cas	0	10	22	37	57	82	107	137	172	212	252	297	347	397	452	512	574	639	709	784	862	947	1032	1087	1127	1147	1157	1167	1172	1172	1172
Das	0	5	15	27	42	62	84	109	139	171	206	241	281	326	376	428	483	538	598	658	723	793	858	918	968	1008	1023	1028	1028	1028	1028
Eas	0	10	21	34	49	69	94	124	159	196	236	281	326	376	431	491	551	606	666	716	764	809	849	889	924	954	979	994	1004	1004	1004
Fas	0	0	0	5	14	24	36	51	71	91	116	146	186	236	291	331	363	395	425	445	465	480	495	505	510	515	520	525	525	525	525
Cbs	0	10	24	39	59	84	114	149	189	234	282	332	382	437	497	559	624	694	764	839	919	994	1064	1114	1154	1174	1189	1204	1214	1214	1214
Dbs	0	5	12	22	37	57	82	110	140	175	210	250	295	345	400	460	520	585	645	700	755	805	845	880	900	915	925	935	940	940	940
Ebs	0	5	13	26	41	61	86	116	151	186	226	271	321	381	441	509	578	648	723	783	843	893	938	968	993	1003	1013	1018	1023	1023	1023
Fbs	0	0	5	12	22	34	49	64	84	104	129	155	183	213	248	283	319	359	394	424	449	469	484	499	504	509	509	509	509	509	509

Table A-8: The XRD characteristics results obtained for the physical and chemical properties of the MNPs.

2θ (degree)	Miller indices (hkl) plane	dhkl (nm)	Crystal structure	Nanostructure	JCPDS pattern
24.865	(62)	3.549	Orthohombic	β-$FeSO_4$	00-033-0682
28.294	(0)	2.297	Monoclinic	Calcium sulfite	00-038-0701
14.686	(0)	0.233	Monoclinic	Calcium sulfate hydrate	00-047-0964
24.482	(225)	1.988	Face-centred cubic	Sylvite	00-41-1476
46.8	(148)	3.157	Rhombohedral	Mikasaite	00-047-1774
83.568	(15)	6.505	Base-centred monoclinic	Tenorite (CuO)	00-048-1548
21.398	(14)	3.202	Monoclinic	ferrimagnetite	00-070-2091
25.432	(63)	2.961	Base-centred orthohombic	Calcium sulfate ($CaSO_4$)	01-070-0909
74.365	(227)	4.498	Face-centred cubic	Magnessium -iron oxide	01-071-1254
48.491	(12)	2.106	Monoclinic	Clinoptilolite	01-071-1425
76.561	(59)	3.606	Orthohombic	Iron oxide chloride	01-072-0619
47.197	(63)	3.654	Base-centred orthohombic	Iron sulfate	01-073-1057
36.989	(15)	3.102	Base-centred monoclinic	Szomolnokite	01-074-1332
51.44	(44)	2.162	Base-centred orthohombic	Sodium nitrate	01-075-2073
65.976	(227)	5.42	Face-centred cubic	Cupper iron oxide	01-077-0010
84.582	(148)	2.856	Rhombohedral	Aluminium sulfate	01-077-0385
53.755	(227)	5.547	Face-centred cubic	Nickel iron oxide	01-080-0072
22.337	(12)	2.174	Monoclinic	Heulandite	01-082-1228
40.224	(152)	2.635	Hexagonal	Quartz	01-083-0539
27.589	(15)	1.572	Monoclinic	Sodium oxide hydrate	01-083-0597
69.934	(139)	3.232	Body-centred tetragonal	Calcium oxide	00-003-0865
29.406	(167)	2.711	Rhombohedral	Calcite	00-005-0586
27.335	(225)	2.163	Face-centred cubic	Halite	00-005-0628
32.497	(29)	2.263	Orthohombic	Thermonatrite	00-008-0448
20.212	(13)	1.96	Monoclinic	Iron chloride hydrate	00-016-0123
35.525	(227)	4.523	Face-centred cubic	Magnesioferrite	00-017-0464
35.423	(227)	5.197	Face-centred cubic	Magnetite (Fe_3O_4)	00-019-0629
27.335	(53)	3.336	Orthohombic	Iron sulfate	00-021-0428
25.281	(141)	3.893	Body -centred tetragonal	Anatase (TiO_2)	00-021-1272
14.63	(0)	2.613	Hexagonal	Calcium sulfate hydrate	00-023-0128
41.806	(150)	1.712	Hexagonal	Antarcticite	00-026-1053
33.837	(15)	2.124	Monoclinic	Trona	00-029-1447
17.374	(160)	3.065	Rhombohedral	Hydroniumjarosite	00-031-0650
33.153	(167)	5.27	Rhombohedral	Hematite (α-Fe_2O_3)	00-033-0664
24.717	(148)	3.06	Rhombohedral	Mikasaite	00-033-0679
35.631	(213)	4.858	Cubic	Maghemite (□-Fe_2O_3)	00-039-1346

Appendix B

The RSM diagnostics plots and reports table for each response are shown in this section. The RSM projected values and the actual experimental values are included in the reports, as well as the deviations and other diagnostic values that validate the 1model. Each diagnostic report has been accompanied by normality and residual plots.

The residual vs expected plots are used to test the constant variance assumptions. This indicates how well the projected values match the actual values. The normality plots illustrate whether the residual follows a straight line, which is the normal distribution. As a result, having the aligned to the diagonal plots reveals an equal distribution of residuals.

Table B-1: Diagnostic report for Response 1: Biogas yield

Run	Actual	Predicted	Residual	Leverage	Internally	Externally	Cook's	Influence on	Standard
1	355.4879	365.944	-10.4562	0.453704	-1.74888	-1.84649	0.423363	-1.68275	5
2	472.1545	482.6107	-10.4562	0.453704	-1.74888	-1.84649	0.423363	-1.68275	8
3	355.4879	358.085	-2.59711	0.203704	-0.35979	-0.35221	0.005519	-0.17814	17
4	413.8212	408.5592	5.261977	0.203704	0.728974	0.720581	0.022657	0.364456	9
5	432.7522	427.4902	5.261977	0.203704	0.728974	0.720581	0.022657	0.364456	16
6	425	451.1744	-26.1744	0.453704	-4.37787	-14.4558	2.652881	-13.1739	6
7	355.4879	350.2259	5.261977	0.453704	0.880106	0.875188	0.107217	0.797579	7
8	413.8212	408.5592	5.261977	0.203704	0.728974	0.720581	0.022657	0.364456	10
9	413.8212	416.4183	-2.59711	0.203704	-0.35979	-0.35221	0.005519	-0.17814	11
10	355.4879	358.085	-2.59711	0.203704	-0.35979	-0.35221	0.005519	-0.17814	18
11	374.4189	377.016	-2.59711	0.203704	-0.35979	-0.35221	0.005519	-0.17814	24
12	413.8212	412.4888	1.332433	0.037037	0.167858	0.163922	0.000181	0.032148	26
13	425	412.4888	12.51125	0.037037	1.576145	1.6381	0.015925	0.321258	25
14	394.8902	397.4873	-2.59711	0.203704	-0.35979	-0.35221	0.005519	-0.17814	13
15	316.0855	318.6826	-2.59711	0.203704	-0.35979	-0.35221	0.005519	-0.17814	14
16	453.2235	447.9615	5.261977	0.203704	0.728974	0.720581	0.022657	0.364456	21
17	453.2235	451.8911	1.332433	0.203704	0.18459	0.180288	0.001453	0.091186	2
18	472.1545	466.8925	5.261977	0.203704	0.728974	0.720581	0.022657	0.364456	20
19	374.4189	369.1569	5.261977	0.203704	0.728974	0.720581	0.022657	0.364456	22
20	374.4189	373.0864	1.332433	0.203704	0.18459	0.180288	0.001453	0.091186	4
21	413.8212	416.4183	-2.59711	0.203704	-0.35979	-0.35221	0.005519	-0.17814	12
22	413.8212	412.4888	1.332433	0.037037	0.167858	0.163922	0.000181	0.032148	27
23	511.5569	506.2949	5.261977	0.203704	0.728974	0.720581	0.022657	0.364456	15
24	472.1545	466.8925	5.261977	0.203704	0.728974	0.720581	0.022657	0.364456	19
25	453.2235	455.8206	-2.59711	0.203704	-0.35979	-0.35221	0.005519	-0.17814	23
26	453.2235	451.8911	1.332433	0.203704	0.18459	0.180288	0.001453	0.091186	1
27	374.4189	373.0864	1.332433	0.203704	0.18459	0.180288	0.001453	0.091186	3

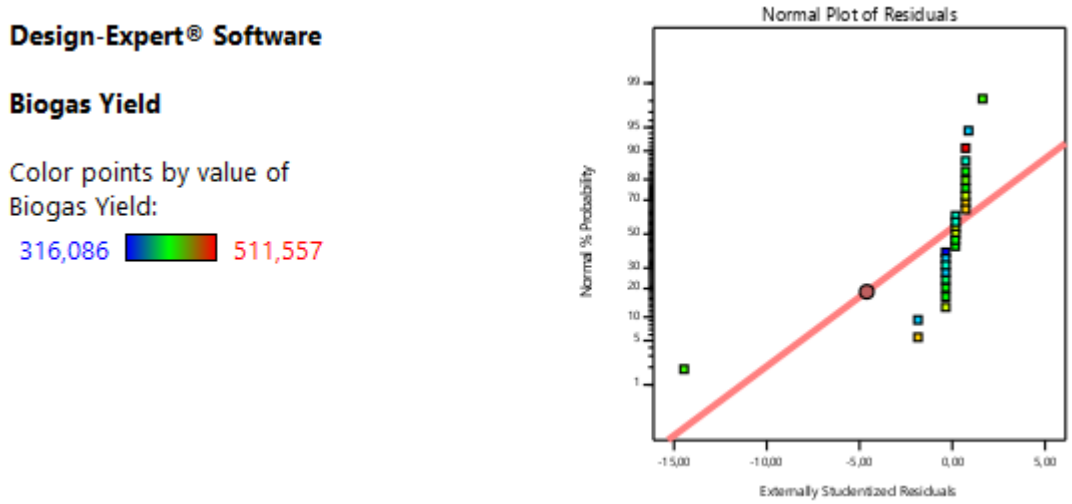

Figure B-1 Plot of normal probability vs residual

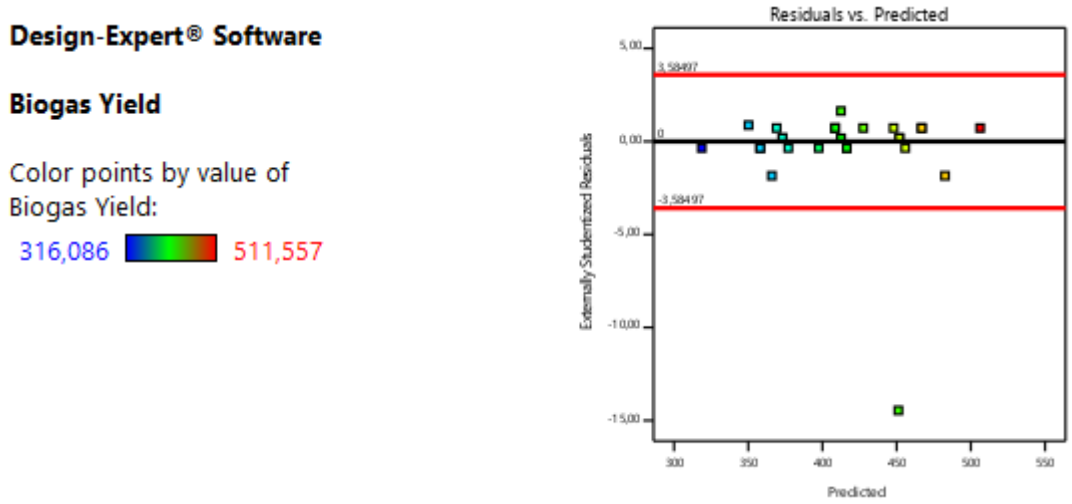

Figure B-2 Plot of residual vs predicted

Table B-2: Diagnostic report for Response 2: COD reduction

Run	Actual	Predicted	Residual	Leverage	Internally	Externally	Cook's	Influence on	Standard
1	68.71643	68.81155	-0.09512	0.277778	-0.48718	-0.47718	0.011411	-0.29593	5
2	71.20574	71.36181	-0.15607	0.277778	-0.79934	-0.79144	0.030719	-0.49083	8
3	69.44249	69.46246	-0.01997	0.267361	-0.10156	-0.09887	0.00047	-0.05973	17
4	70.69458	70.68407	0.010503	0.267361	0.053411	0.05199	0.00013	0.031407	9
5	70.88641	70.98256	-0.09615	0.267361	-0.48897	-0.47895	0.010907	-0.28933	16
6	71.21318	71.3083	-0.09512	0.277778	-0.48718	-0.47718	0.011411	-0.29593	6
7	68.709	68.86506	-0.15607	0.277778	-0.79934	-0.79144	0.030719	-0.49083	7
8	69.23503	69.22453	0.010503	0.267361	0.053411	0.05199	0.00013	0.031407	10
9	70.68714	70.73758	-0.05044	0.267361	-0.25652	-0.25011	0.003002	-0.15109	11
10	67.98294	68.00291	-0.01997	0.267361	-0.10156	-0.09887	0.00047	-0.05973	18

11	70	69.85237	0.147634	0.517361	0.924986	0.921298	0.114644	0.953862	24
12	71	70.08668	0.913321	0.111111	4.216564	16.19237	0.277803	5.724869	26
13	69.96109	70.08668	-0.12559	0.111111	-0.57983	-0.56942	0.005253	-0.20132	25
14	69.03577	69.07097	-0.03521	0.267361	-0.17904	-0.17441	0.001462	-0.10536	13
15	68.38966	68.48582	-0.09615	0.267361	-0.48897	-0.47895	0.010907	-0.28933	14
16	70.28786	70.38401	-0.09615	0.517361	-0.60245	-0.59206	0.048631	-0.61299	21
17	69.55437	69.48395	0.070415	0.319444	0.371527	0.362939	0.008099	0.248656	2
18	70.47969	70.49966	-0.01997	0.267361	-0.10156	-0.09887	0.00047	-0.05973	20
19	69.64175	69.61601	0.02574	0.517361	0.16127	0.157076	0.003485	0.162628	22
20	68.90826	68.8988	0.009468	0.319444	0.049953	0.048624	0.000146	0.033313	4
21	69.2276	69.27804	-0.05044	0.267361	-0.25652	-0.25011	0.003002	-0.15109	12
22	69.96109	70.08668	-0.12559	0.111111	-0.57983	-0.56942	0.005253	-0.20132	27
23	71.53251	71.56772	-0.03521	0.267361	-0.17904	-0.17441	0.001462	-0.10536	15
24	71.93923	71.9592	-0.01997	0.267361	-0.10156	-0.09887	0.00047	-0.05973	19
25	70.28042	70.25468	0.02574	0.517361	0.16127	0.157076	0.003485	0.162628	23
26	71.01391	70.9435	0.070415	0.319444	0.371527	0.362939	0.008099	0.248656	1
27	70.36781	70.35834	0.009468	0.319444	0.049953	0.048624	0.000146	0.033313	3

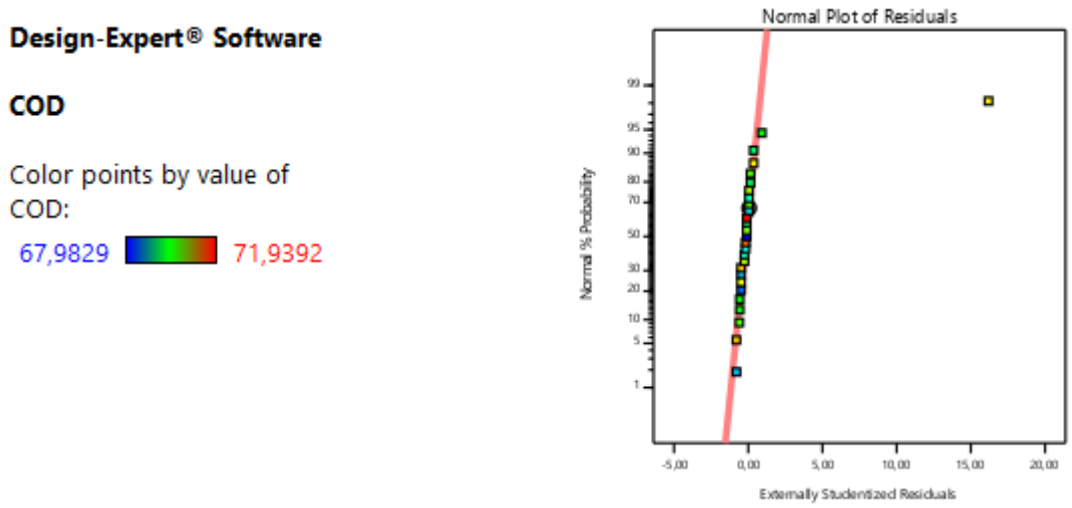

Figure B-3 Plot of normal probability vs residual

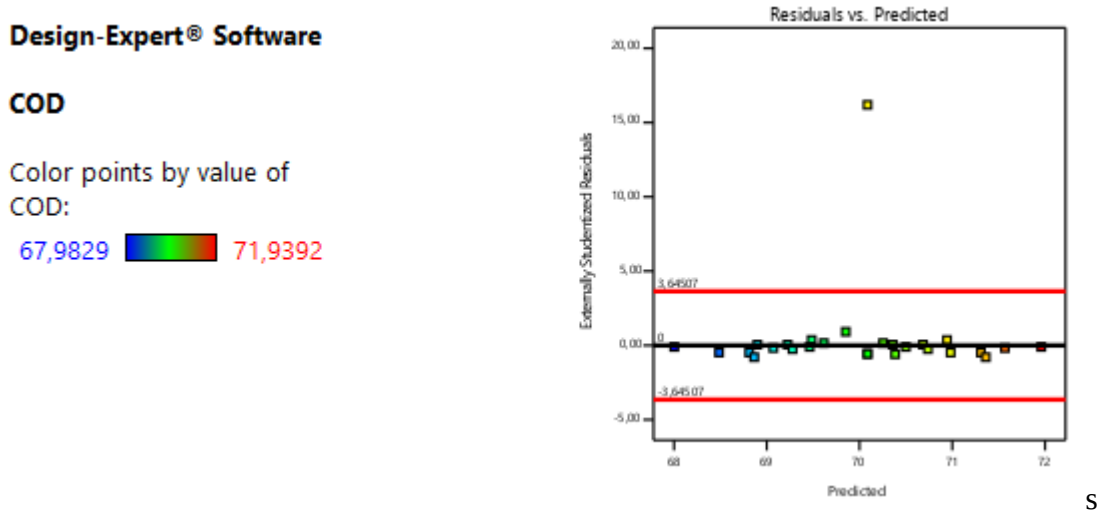

s

Figure B-4 Plot of residual vs predicted

Table B-3: Diagnostic report for Response 3: Turbidity removal

Run	Actual	Predicted	Residual	Leverage	Internally	Externally	Cook's	Influence on	Standard
1	68.71157	68.88017	-0.1686	0.203704	-0.6386	-0.62935	0.017387	-0.31831	5
2	70.92849	70.92415	0.004334	0.203704	0.016417	0.016021	1.15E-05	0.008103	8
3	69.56919	69.56486	0.004334	0.203704	0.016417	0.016021	1.15E-05	0.008103	17
4	70.42195	70.24468	0.177267	0.453704	0.810634	0.803774	0.090958	0.732497	9
5	70.34139	70.42352	-0.08213	0.203704	-0.31109	-0.3043	0.004126	-0.15391	16
6	70.67278	70.84138	-0.1686	0.203704	-0.6386	-0.62935	0.017387	-0.31831	6
7	68.96727	68.96294	0.004334	0.203704	0.016417	0.016021	1.15E-05	0.008103	7
8	70	69.47687	0.523133	0.453704	2.392262	2.737181	0.792155	2.494454	10
9	70.67765	70.84625	-0.1686	0.453704	-0.77099	-0.76329	0.08228	-0.69561	11
10	68.10965	68.27825	-0.1686	0.203704	-0.6386	-0.62935	0.017387	-0.31831	18
11	69.48864	69.4843	0.004334	0.203704	0.016417	0.016021	1.15E-05	0.008103	24

12	71	69.90216	1.09784	0.037037	3.781332	6.532404	0.091657	1.28111	26
13	69.82003	69.90216	-0.08213	0.037037	-0.28289	-0.2766	0.000513	-0.05425	25
14	69.29867	69.3808	-0.08213	0.203704	-0.31109	-0.3043	0.004126	-0.15391	13
15	68.38018	68.46231	-0.08213	0.203704	-0.31109	-0.3043	0.004126	-0.15391	14
16	70.15142	70.32002	-0.1686	0.203704	-0.6386	-0.62935	0.017387	-0.31831	21
17	69.5495	69.7181	-0.1686	0.203704	-0.6386	-0.62935	0.017387	-0.31831	2
18	70.07086	70.23946	-0.1686	0.203704	-0.6386	-0.62935	0.017387	-0.31831	20
19	69.23293	69.40153	-0.1686	0.203704	-0.6386	-0.62935	0.017387	-0.31831	22
20	68.63101	68.79961	-0.1686	0.203704	-0.6386	-0.62935	0.017387	-0.31831	4
21	69.21811	69.04084	0.177267	0.453704	0.810634	0.803774	0.090958	0.732497	12
22	69.82003	69.90216	-0.08213	0.037037	-0.28289	-0.2766	0.000513	-0.05425	27
23	71.25988	71.34201	-0.08213	0.203704	-0.31109	-0.3043	0.004126	-0.15391	15
24	71.53041	71.52607	0.004334	0.203704	0.016417	0.016021	1.15E-05	0.008103	19
25	70.40713	70.40279	0.004334	0.203704	0.016417	0.016021	1.15E-05	0.008103	23
26	71.00904	71.00471	0.004334	0.203704	0.016417	0.016021	1.15E-05	0.008103	1
27	70.09055	70.08622	0.004334	0.203704	0.016417	0.016021	1.15E-05	0.008103	3

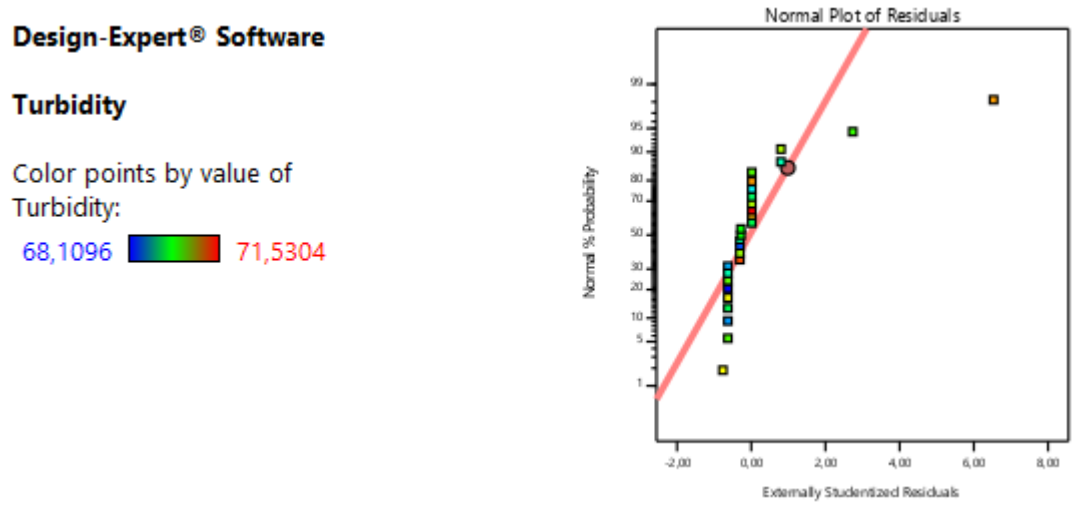

Figure B-5 Plot of normal probability vs residual

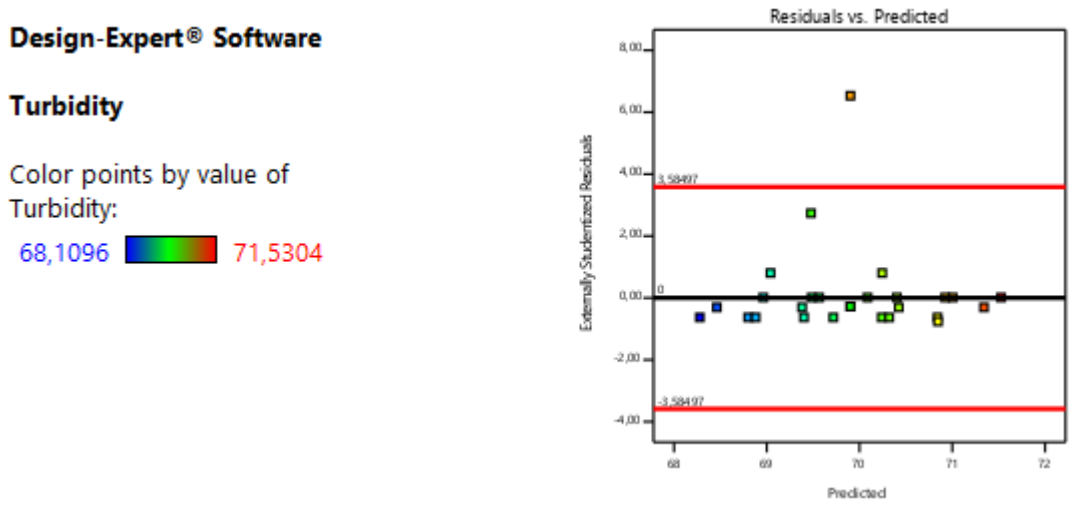

Figure B-6 Plot of residual vs predicted

Table B-4: Diagnostic report for Response 4: Colour removal

Run	Actual	Predicted	Residual	Leverage	Internally	Externally	Cook's	Influence on	Standard
1	68.71643	68.7012	0.015237	0.333333	0.048607	0.047241	0.000131	0.033404	5
2	71.20574	71.25145	-0.04571	0.333333	-0.14582	-0.1418	0.001181	-0.10027	8
3	69.44249	69.41201	0.030474	0.333333	0.097215	0.094501	0.000525	0.066822	17
4	70.69458	70.67934	0.015237	0.333333	0.048607	0.047241	0.000131	0.033404	9
5	70.88641	70.93212	-0.04571	0.333333	-0.14582	-0.1418	0.001181	-0.10027	16
6	71.21318	71.19794	0.015237	0.333333	0.048607	0.047241	0.000131	0.033404	6
7	68.709	68.75471	-0.04571	0.333333	-0.14582	-0.1418	0.001181	-0.10027	7
8	69.23503	69.2198	0.015237	0.333333	0.048607	0.047241	0.000131	0.033404	10
9	70.68714	70.73285	-0.04571	0.333333	-0.14582	-0.1418	0.001181	-0.10027	11
10	67.98294	67.95247	0.030474	0.333333	0.097215	0.094501	0.000525	0.066822	18

11	70	69.75621	0.243789	0.333333	0.777719	0.768835	0.033603	0.543648	24
12	68	69.30739	-1.30739	0.333333	-4.17075	-22.1114	0.966397	-15.6351	26
13	69.96109	69.30739	0.653695	0.333333	2.085375	2.327143	0.241599	1.645538	25
14	69.03577	69.02053	0.015237	0.333333	0.048607	0.047241	0.000131	0.033404	13
15	68.38966	68.43537	-0.04571	0.333333	-0.14582	-0.1418	0.001181	-0.10027	14
16	70.28786	70.28786	0	0.333333	0	0	0	0	21
17	69.55437	69.53913	0.015237	0.333333	0.048607	0.047241	0.000131	0.033404	2
18	70.47969	70.44921	0.030474	0.333333	0.097215	0.094501	0.000525	0.066822	20
19	69.64175	69.7027	-0.06095	0.333333	-0.19443	-0.18915	0.0021	-0.13375	22
20	68.90826	68.95397	-0.04571	0.333333	-0.14582	-0.1418	0.001181	-0.10027	4
21	69.2276	69.27331	-0.04571	0.333333	-0.14582	-0.1418	0.001181	-0.10027	12
22	69.96109	69.30739	0.653695	0.333333	2.085375	2.327143	0.241599	1.645538	27
23	71.53251	71.51727	0.015237	0.333333	0.048607	0.047241	0.000131	0.033404	15
24	71.93923	71.90876	0.030474	0.333333	0.097215	0.094501	0.000525	0.066822	19
25	70.28042	70.34137	-0.06095	0.333333	-0.19443	-0.18915	0.0021	-0.13375	23
26	71.01391	70.99867	0.015237	0.333333	0.048607	0.047241	0.000131	0.033404	1
27	70.36781	70.41352	-0.04571	0.333333	-0.14582	-0.1418	0.001181	-0.10027	3

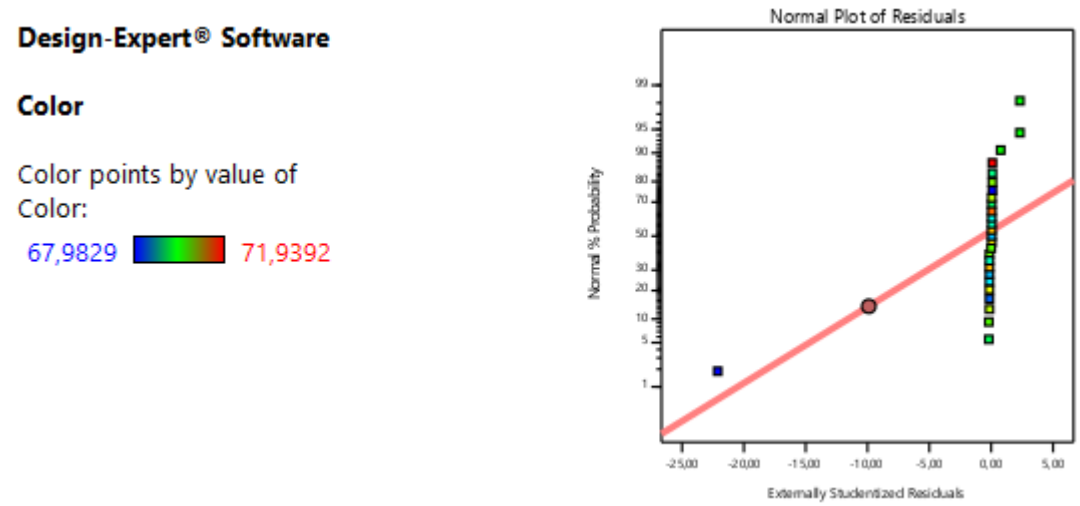

Figure B-7 Plot of normal probability vs residual

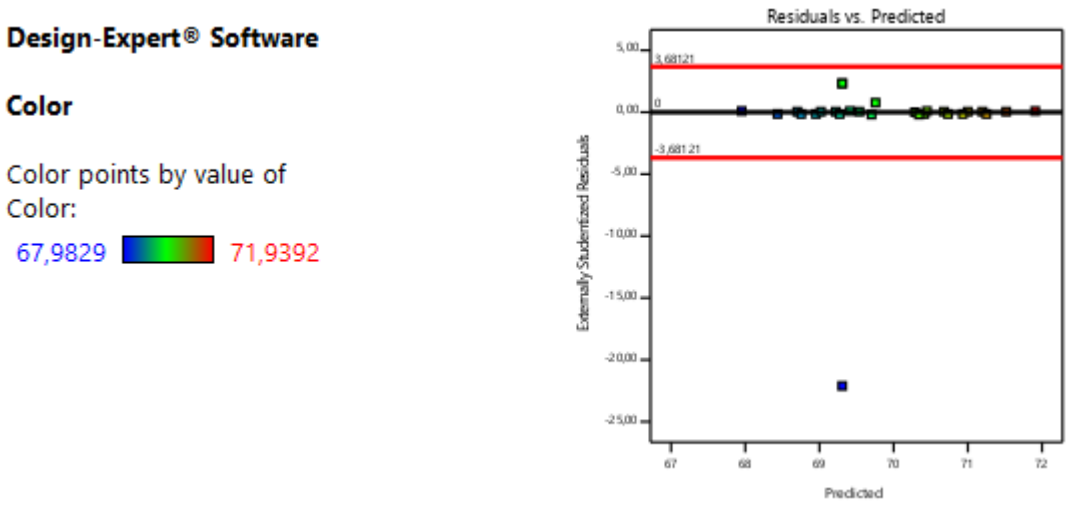

Figure B-8 Plot of residual vs predicted

Appendix C

BIOCHEMICAL METHANE POTENTIAL SET-UP COMPONENTS

Pictures of the components of the BMP set-up decrsibed and labelled has been presented in this section. Some relevant equipment used during the rsearch study has also been presented here.

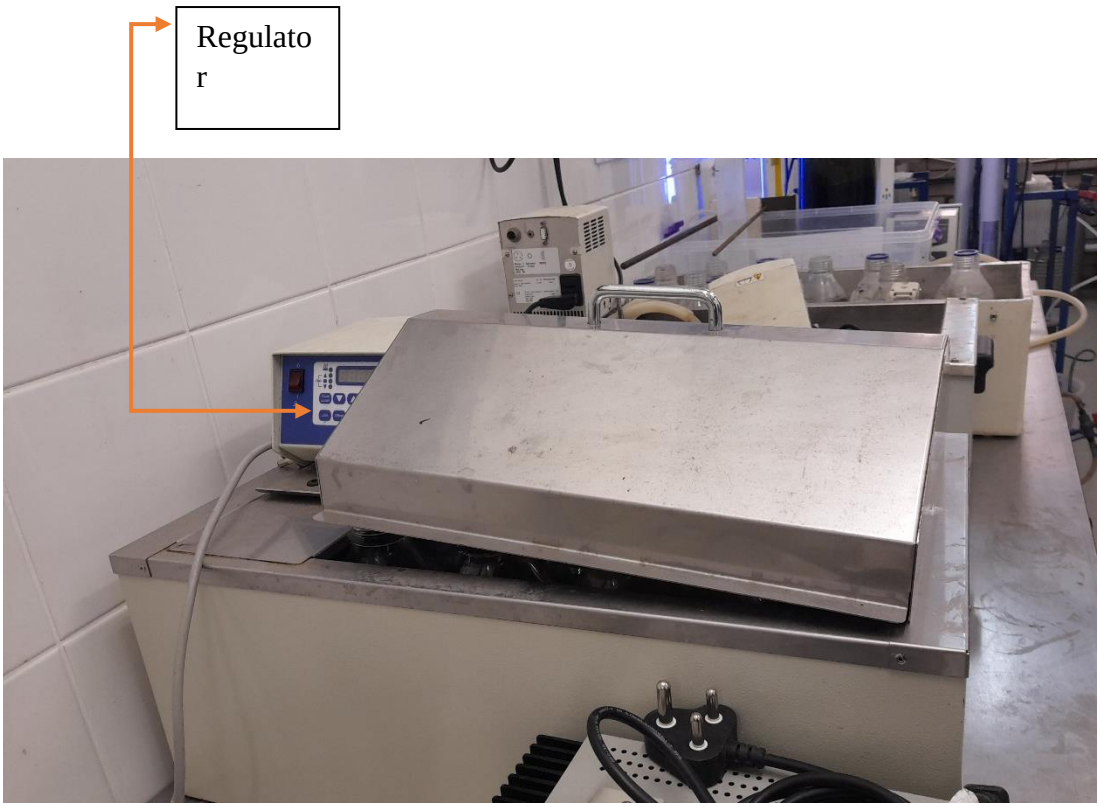

Figure C-1 Thermostatic Water used for the BMP process to regulate and maintain temperature at the required set-point.

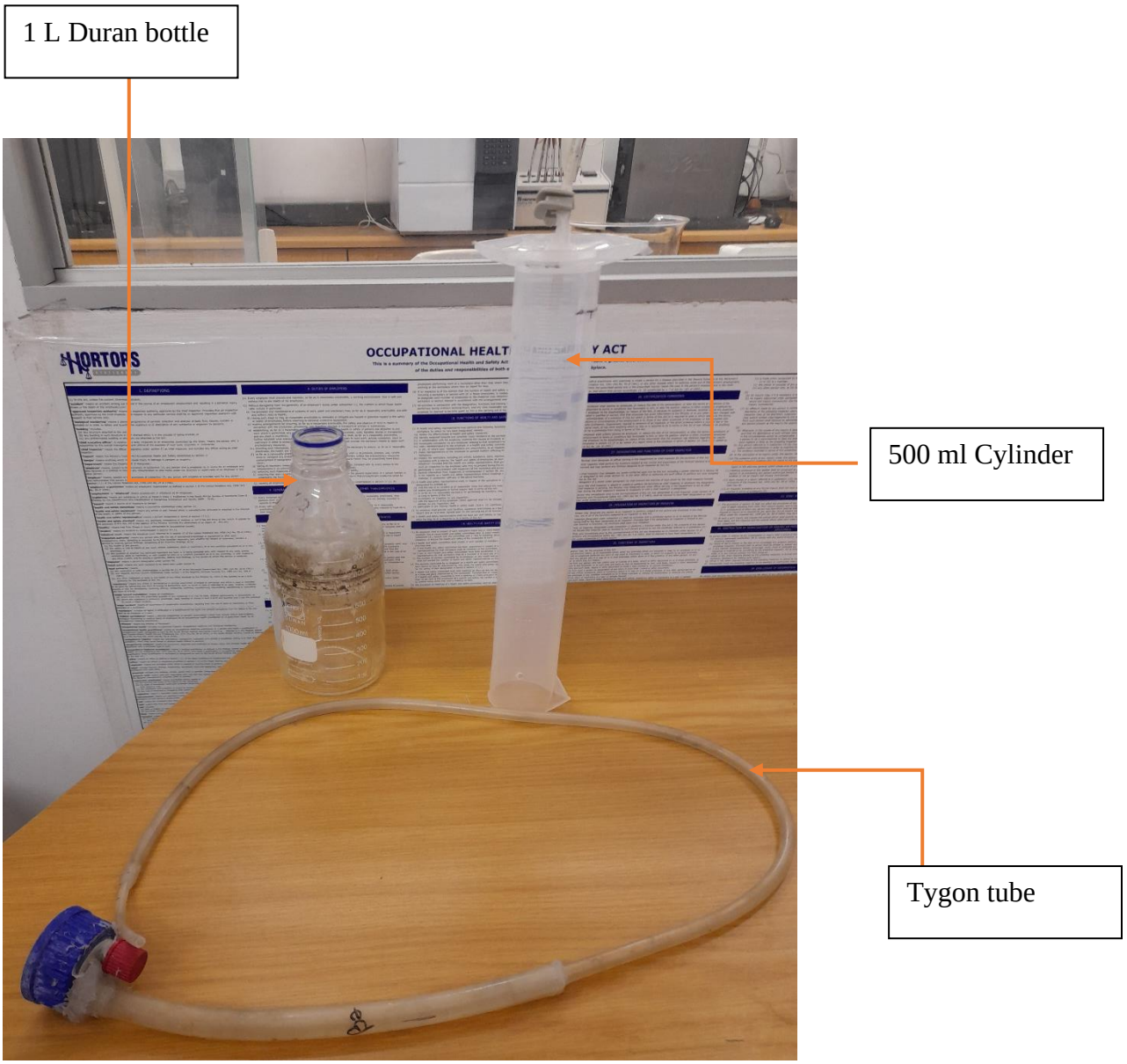

Figure C-2 The separate parts of the bioreactors showing the 1 L Duran bottle, 500 ml Cylinder and tygon tube

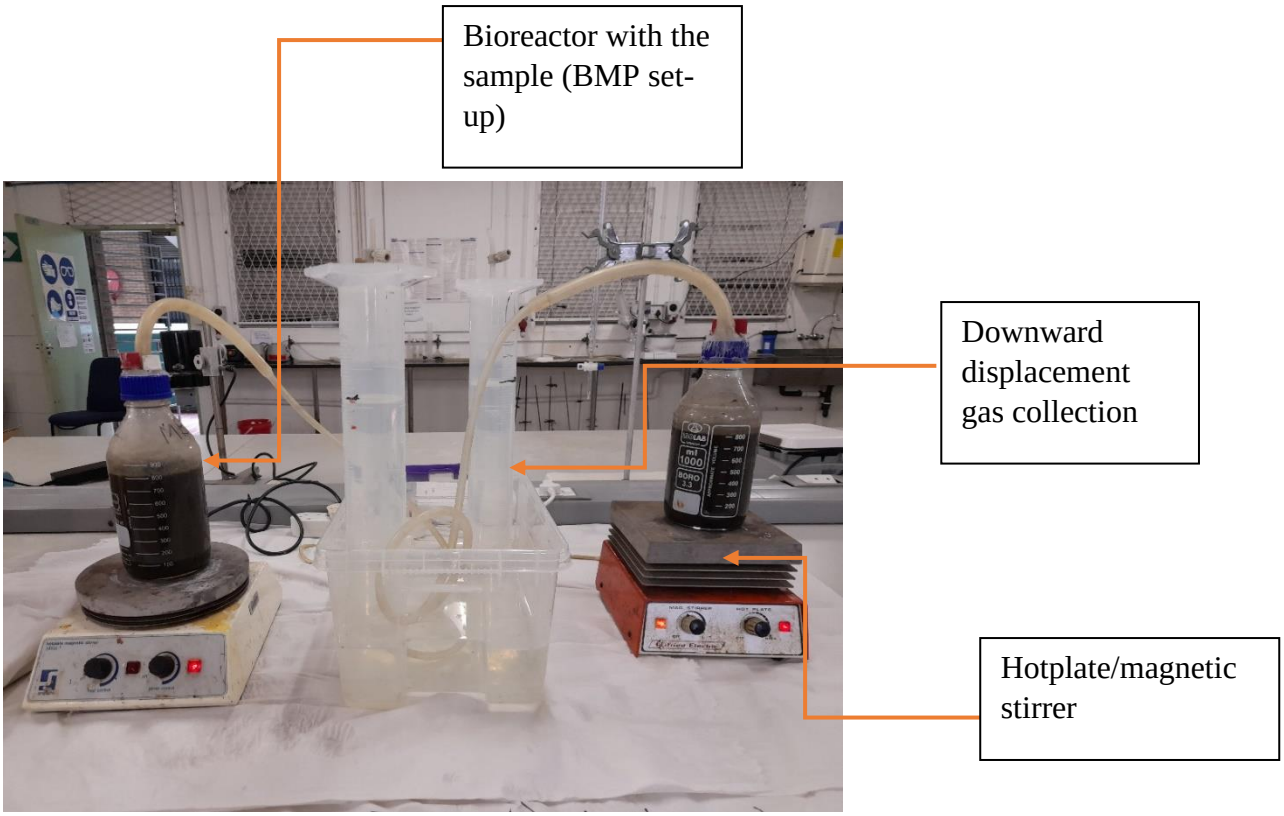

Figure C-3 BMP set-up using a magnetic/hotplate for stirring and heating to keep the temperature at the desire set-point.

Photographs of some relevant equipment and materials used in the study

Figure C-4 The Furnace used

Figure C-5 GMX Model 800 magnets

Figure C-6 HACH CRB 200 digestors

Figure C-7 HACH DR3900 Spectrophotometer

Figure C-8: ELGA PURELAB Option-Q water deionizer